Chitosan-Based Scaffolds for Stem Cell Renewal and Differentiation

Matthew Chi-hang Leung

A dissertation
submitted in partial fulfillment of the
requirements for the degree of

Doctor of Philosophy

University of Washington
2013

Reading Committee:
Professor Miqin Zhang, Chair
Professor Candan Tamerler-Behar
Professor James Park

Program Authorized to Offer Degree:
Materials Science and Engineering

University of Washington

Abstract

Chitosan-Based Microenvironments for Biomedical Applications

Matthew Chi-hang Leung

Chair of the Supervisory Committee:
Professor Miqin Zhang
Materials Science and Engineering

Tissue engineering aims to restore function and treat disease through the fabrication of a suitable microenvironmental niche to facilitate recovery and repair. Often, a scaffold is necessary to provide the appropriate spatial, chemical, and mechanical cues in place of the native extracellular matrix. The cellular microenvironment determines cellular behavior and cell fate via contact, nutrient and waste concentration gradients, soluble signaling factors and cell–cell signaling. Thus, an effective tissue engineering scaffold must recapitulate the native extracellular microenvironment to promote the appropriate cellular behavior, and in turn, restoration of function. Chitosan-based materials are an attractive candidate for tissue engineering scaffolds on account of the inherent biocompatibility, biodegradability, availability, and range of processing techniques available. We first fabricated a porous, 3D chitosan-alginate scaffold, which we determined is an effective microenvironment for human embryonic stem cell (hESC) renewal to confluency without the use of feeder cells or conditioned media. Additionally, a technique was developed to dissolve the scaffold and recover hESCs while maintaining pluripotency. Thus, we developed an

effective system for the high-density propagation of hESCs, which will be necessary for translation to future clinical applications. Subsequently, we developed an *in vitro* cell culture system for the myogenic induction of hESCs that integrates soluble factors with aligned chitosan-PCL fibrous ECM . In the course of this combinatorial study, it was determined that aligned chitosan-PCL fibers convey unique microenvironmental stimuli that guide cell differentiation. Finally, the aligned chitosan-PCL fibrous ECM was used to address the limitations of existing tendon grafts. Tenogenic differentiation was induced in human bone marrow stem cells more rapidly and with a greater purity than possible with current techniques. These findings demonstrate the potential use of chitosan-based materials for tissue engineering applications, and that specific microenvironmental cues can be conveyed by rational design of the scaffold to maximize the biological performance of a tissue-engineered construct.

Table of Contents

List of Figures

List of Tables

Acknowledgments

I sincerely thank my advisor, Professor Miqin Zhang, for her guidance, support, and encouragement throughout the course of my program. I would also like to thank the members of my PhD supervisory committee: Professor James O. Park and Professor Candan Tamerler for their commitment to this process and their feedback on my work. I would like to thank my collaborators, Professor Randy Moon, Professor Rich Ellenbogen, and Professor Richard Hopper. I also acknowledge the financial support from the UW TGF, UW UWEB, the Kyocera Endowment, Seattle Children's Hospital, and gift funding from the Washington Research Foundation.

I would also like to thank all members of the research group, as each person has helped to shape my learning in their own way, and my program could not have been as successful without each one of them. Thank you Dr. Zhensheng Li, Dr. Narayan Bhattarai, Dr. Ashleigh Cooper, Dr. Steve Florczyk, Dr. Soumen Jana, Dennis Edmondson, David Wood, Dr. Jonathan Gunn Esq., Dr. Forrest Kievet, Dr. Omid Veiseh, Dr. Conroy Sun, Dr. Chen Fang, Kui Wang, Professor Julia Chang, Dr. Fiona Tsao, Professor Tao Lou, and Dr. Jonathan Sham for supporting me in the lab, night and day. Finally, thank you to the Materials Science and Engineering faculty and staff, in particular Professor Fumio Ohuchi, Bichtien Thach, Kathleen Elkins, Dr. Hanson Fong, Tuesday Kuykendall, Jay Montague, and Karen Wetterhahn for always being available to support me to the fullest of their abilities.

I also thank my family and friends for their dedication and support throughout my life. Each of them have helped me to become the person that I am today, and they encourage me to accomplish yet more.

Chapter 1: Introduction

1.1 TISSUE ENGINEERING APPROACH

Tissue engineering is a rapidly developing, interdisciplinary field that draws heavily from the field of materials science and engineering to develop means to replace and restore failing tissue and organs[1]. Traditional transplantation surgeries with either autologous or allogenic tissue are unable to address all circumstances. Autologous transplants are limited by the availability of healthy donor tissue and the loss of function resulting from donor site morbidity[2,3]. Allogenic transplants increase the availability of donor tissue, but are accompanied by a significant risk of disease transmission[4] and chronic immune rejection[5]. Potentially, tissue engineering will address the current limitations accompanying transplant therapy by generating replacement tissues and organs as needed to address the specific needs of the patient.

Most commonly, tissue-engineered constructs combine living cells, signaling factors, and a scaffolding material[1]. The living cells in the construct perform the functions of the diseased or damaged tissues, while the combination of signaling factors and scaffold morphology create a suitable microenvironment to facilitate proper cell function[6]. Additionally, the scaffold may bridge native tissues, provide structural support, and contribute to the controlled release of signaling factors. Thus, the following design criteria apply to all tissue engineering scaffolds[7]:

1. biologically conductive and inductive to target cell types
2. biodegradation rate corresponding to the rate of new tissue formation
3. non-toxicity and non-immunogenicity
4. mechanical performance matching the target tissue
5. adequate mass transfer between the construct and the local environment

As these criteria in turn dictate the success or failure of the entire tissue-engineered construct, the significance of proper scaffold design for a given tissue engineering application cannot be underestimated. The appropriate biological performance of a tissue engineering scaffold is a necessity for the success of any tissue-engineered construct, and is thus central to the central to the rational design of a tissue engineering device.

The potential benefits to health and quality of life that may result from repair and replacement of diseased tissues and organs via tissue engineering approaches have generated tremendous interest and development in this field. The engineering of a wide range of tissue types has been explored including bone[8], cartilage[9], tendon[10], skin[11], cardiac muscle[12], blood vessels[13], nervous tissue[14], skeletal muscle [15], and liver[16]. Significantly, tissue engineering methodology has been recently applied to the *in vitro* modeling of diseased tissue, notably cancer[17-20], with the aim of creating an accurate *in vitro* model to facilitate the development of therapeutics and to understand the underlying mechanisms of the disease. Overall, the field of tissue engineering presents tremendous promise for the improvement of health and as a tool for understanding cellular behavior.

1.2 SCAFFOLDS AS INSTRUCTIVE MICROENVIRONMENTS

The cellular microenvironment is known to have an essential role is determining cell behavior and fate[6,21-27]. In a multicellular tissue, cells are subject to a range of endocrine, paracrine, autocrine, and contact signaling cues from remote cells via the circulation, and from adjacent cells in the form of signaling molecules and cell–cell interactions[6,25,28-33]. *In vivo*, the extracellular matrix (ECM) is a combination of biological scaffold materials comprised of structural and functional molecules that provide support, organization, and direction for cell and tissue function[34]. Figure 1-1 illustrates the complex coordination of spatial and temporal cues that direct cell behavior from the cellular microenvironment. The "choice" of a cell to differentiate, proliferate, migrate, apoptose, or perform other specific functions is a coordinated response to the microenvironment, and is under continuous reassessment as the behavior of the cell modifies the soluble and ECM microenvironment, feeding back once again into the cell.

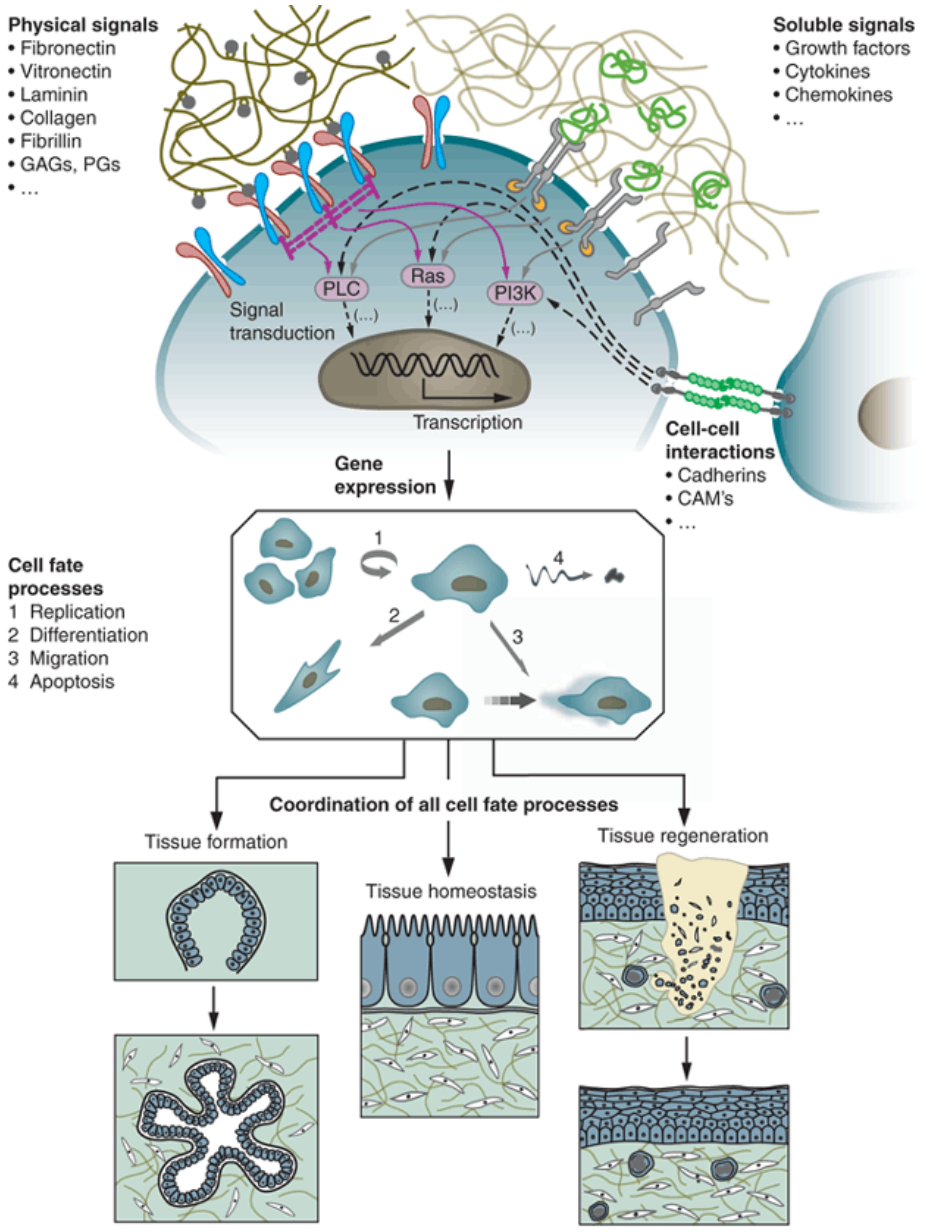

Figure 1-1: Microenvironmental cues direct cell function and fate. Binding of signaling cues with cell-surface receptors induces intracellular signaling that in turn alters gene expression, cell fate, and tissue function. Reprinted with permission[6], see APPENDIX A for a copy of the copyright transfer agreement.

The use of biomaterials to tailor the microenvironment is a key tissue engineering strategy; the scaffold is a proxy for the natural ECM and must convey the appropriate physical and chemical signals for the intended tissue function. The microenvironmental cues provided by the scaffold will influence the function of cells cultured *in vitro* to generate the tissue-engineered device, and will also govern the interaction and integration of the implanted device with host tissues, impacting the effectiveness of the tissue engineering therapy and the quality of the patient outcome[3,9,15,35-37].

In vivo, organized cellular geometry is strongly correlated to the alignment and organization of the ECM in contact with the cells, suggesting that the ECM influences cellular organization[22,25,38-41]. At the single cell scale, cell shape regulates many aspects of cellular behavior and stem cell commitment and differentiation[42]. Altering the overall 2D and 3D geometry of the tissue engineering scaffold over a tissue-sized scale creates a controlled microenvironment with long-range order and alters cell–cell interactions, local concentrations of soluble factors, and chemical gradients such as oxygen concentration, pH[26,39,43,44]. Furthermore, cells cultured in 2D or 3D microenvironments vary drastically in overall morphology and phenotype[45]. In 3D microenvironments, porosity (including the geometry, connectivity, and density) is a critical consideration[46]. Vascularization of scaffolds is critical for the long-term survival of the implant *in vivo*, and favors decreasing pore size[47], but diffusion of nutrients, wastes, and signaling factors, which are critical *in vitro* and during the short-term *in vivo,* favors increasing pore sizes[46]. Porosity must be balanced for the effects on cell signaling and thus biological performance, as well as *in vitro* and *in vivo* survival of the tissue-engineered construct. The Young's modulus of the ECM also plays a defining role in the cell behavior. Physiologically, the Young's modulus of ECMs in the body varies over three orders of magnitude from bone to soft tissues[22]. Mechanosensing structures including integrins and focal adhesions regulate the mechanotransduction process that influences cell function[34]. Indeed, ECM elasticity alone can dictate stem cell differentiation[48]. The geometric, morphological, and mechanical properties of a tissue engineering scaffold are a significant consideration for the design of the microenvironment.

The native ECM is also capable of conveying chemical signals to the cell, via membrane-associated signal transduction molecules like cell surface receptors, which also influence cell function[22]. The ECM comprises adhesion ligands and adsorbed signaling factors. ECM composition, in the absence of other topological cues, regulates cell behavior and fate[49]. Integrins link the epitopes of the ECM to the cell's cytoskeleton, transmitting information about the microenvironment to the inside of the cell, and influencing cell phenotype via mechanostransduction to the nucleus and activation of numerous signaling pathways[34]. During the design of a tissue engineering scaffold, the choice of material that directly interfaces with the cell must be carefully considered.

Growth factors, hormones, and chemicals have classically been directly added into the culture medium. These biomolecules also can be directly incorporated within the scaffold structure or encapsulated into the scaffold biomaterials in a variety of ways during the scaffold manufacturing process. Morphogenesis during tissue development is regulated by a number of protein families including hedgehog proteins (Hhgs), Wnt proteins, Notch ligands, members of the transforming growth factor beta (TGF) superfamily such as bone morphogenetic proteins (BMPs) or fibroblast growth factors (FGFs) and fibronectin. These morphogens control self-renewal, migration, and differentiation, plus other cell fate processes of uncommitted stem or progenitor cells. The question of how the right quantity of a signaling molecule is detected by the right cells at the right time is the subject of extensive investigation. Once differentiation by the interpretation of morphogenetic signals and gradients has occurred, local cell–cell interactions establish boundaries between different populations of cells.

This dissertation documents the use of chitosan-based materials to generate tissue-engineered, microenvironmental niches to direct cell function. Chitosan-based scaffolds and fibers were prepared with controlled morphologies and combined with soluble signaling factors to develop three distinct systems: for human embryonic stem cell renewal, directing differentiation of human embryonic stem cells into the myogenic lineage, and directing the differentiation of human bone marrow stem cells into the tenogenic lineage.

1.3 DISSERTATION OVERVIEW

Chapter 1 describes the field of tissue engineering and general microenvironmental design considerations including ECM topology and physical and soluble signals necessary for directing cell fate.

Chapter 2 reviews the structure and function relationships in chitosan polymers in a tissue engineering context, along with current biomedical applications of chitosan. The rationale for using chitosan as a tissue engineering material is introduced, along with the method used to synthesize chitosan-alginate 3D scaffolds with relevant variables.

Chapter 3 introduces the use of nanofibrous scaffolds for tissue engineering applications along with nanotopologial design considerations made accessible by this material system. It also presents an overview of nanofiber synthesis parameters relevant to tissue engineering, along with the method to generate chitosan-based nanofibers.

Chapter 4 reviews the potential role of hESC as a cell source for tissue engineering applications and the challenge of maintaining clinically relevant cell populations. The rationale for using 3D chitosan scaffold to facilitate hESC renewal is introduced.

Chapter 5 reviews the field of muscle tissue engineering. hESC are proposed as a potential source of myogenic progenitor cells, and the rationale for inducing myogenic differentiation with chitosan based aligned nanofibers is introduced.

Chapter 6 reviews the field of tendon tissue engineering. Adult bone marrow stem cells are proposed as a potential source of tenogenic progenitor cells, and the rationale for inducing tenogenic differentiation with chitosan based aligned nanofibers is introduced.

Chapter 7 describes the application of 3D chitosan scaffolds for the proliferation of pluripotent hESCs.

Chapter 8 describes the development of myogenic differentiation conditions and application of chitosan-based aligned nanofibers for the myogenic differentiation of hESCs.

Chapter 9 describes the use of chitosan-based aligned nanofibers as a scaffold for the tenogenic differentiation of bone marrow stem cells.

Chapter 10 summarizes the results and conclusions presented in this dissertation.

Chapter 2: 3D Chitosan-based Scaffolds for Tissue Engineering Applications

2.1 Structure and Biocompatibility

Chitosan is the deacetylated form of the second most abundant natural polymer, chitin (Figure 2-1) and is comprised of copolymers of glucosamine (β(1–4)-linked 2-amino-2-deoxy-d-glucose) and N-acetylglucosamine (2-acetamido-2-deoxy-d-glucose)[7]. Chitin is commonly found in the exoskeletons of crustaceans and insects and in the cell walls of fungi[50]. Chitosan has been approved by the US Food and Drug Administration[1,51] and is routinely used in drug delivery and hemostatic wound dressings. In physiological conditions, chitosan with a pKa of ~6.5 is can be protonated at the amino group and positively charged (Figure 2-1), which facilitates interactions with native ECM proteins including glycosaminoglycan (GAG) and proteoglycans[51]. The content of glucosamine is referred to as the degree of deacetylation, and depending on source and preparation, the molecular weight of natural chitosan may range from 300 to over 1000 kD, with degree of deacetylation ranging from 30% to 95%[7]. Notably, in its crystalline form, chitosan is normally insoluble in aqueous solution above pH 7; however, in dilute acids (pH < 6.0) the protonated free amino groups on glucosamine facilitate solubility of the molecule[7]. Significantly, anionic growth factors also may become complexed with cationic chitosan, increasing local concentrations of growth factors and stimulating additional cell signaling near the surface of the scaffold[51]. The ability of chitosan to form polyionic complexes with other charged molecules is a key strategy for the generation of chitosan biomaterials that will be discussed in the following chapter.

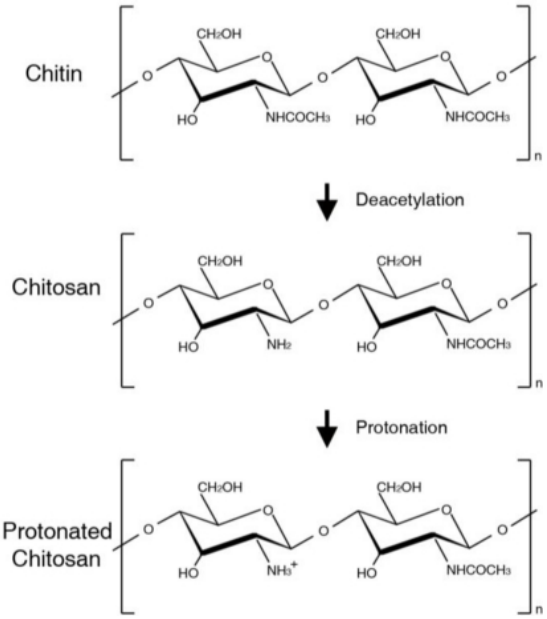

Figure 2-1: Chitin, chitosan, and protonated chitosan. Reprinted with permission[51]; see APPENDIX B for the copyright transfer agreement.

Significant study has focused on the applications of chitosan in medical applications. Chitosan bears a structural resemblance to GAG, a common ECM protein with a key role in modulating cell morphology, differentiation, and function[52]. Typically, chitosan-based materials have been found to evoke a minimal foreign body reaction, with little or no fibrous encapsulation[7]. *In vivo*, chitosan can be biodegraded by human enzymes, primarily lysozyme that breaks the linkage between acetylated units and degrades chitosan to biocompatible oligosaccharides[53]. The degree of deacetylation influences the rate of degradation, as the highly deacetylated chitosan exhibits a greater degree of crystallinity and accordingly a slower degradation rate[7]. Thus, by careful selection of chitosan polymers, the enzymatic degradation rate of the chitosan scaffolds can be tuned to match tissue remodeling rates.

The fate of chitosan degradation products after *in vivo* implantation has been well characterized in numerous studies. Subcutaneous chitosan implantation in rats showed no accumulation in distant organs over 30 days[54], and no immune response after 84 days[55]. Intraperitoneal injection of chitosan into mice resulted in the excretion of most the chitosan via the urinary tract after 14 hours, without accumulation in liver, speen, abdomen, or plasma after 24 hours[56]. In humans, only oral toxicity data is available. These studies showed that daily doses of 4.5 g of chitosan per

day over 12 days[57], and 6.75 g per day over 56 days[58] had no ill effects on the study subjects. *In vivo,* chitosan is degraded by lysozyme into chitosan oligosaccharides of various lengths, and also glucosamine monomers[50]. Interestingly, the glucosamine monomers from degraded chitosan integrate into skeletal muscle and articular cartilage[59], suggesting a synergistic effect of chitosan implantation on the healing of these tissues. Chitosan is a safe, biocompatible material that has great potential as a bioengineering material.

2.2 Current Biomedical Applications

Chitosan is increasingly used in contemporary biomedical applications. The biocompatibility of chitosan has allowed it to be used in a powder coating for surgical gloves by Esteem® and Protegrity®[60]. Chitosan is the active ingredient in a wide range of hemostatic dressings including Abbott® dressings, Aquanova® dressings, Celox™ dressings, HemCon® dressings, and Scion® dressings[61]. All of these topical hemostatic products utilize the positively charged, highly hydrophilic chitosan polymer to greatly increase platelet and erythrocyte adhesion at the wound site by ionic interaction directly with the negatively charged cell membranes[60]. However, to date, no implantable resorbable chitosan hemostatic device has been approved by the FDA[61]. Thus, as only a limited range of chitosan-based biomedical devices are available on the market, rapid research and development towards chitosan-based biomedical devices may be an untapped opportunity to bring novel treatments to the marketplace.

2.3 3D Extracellular Matrix Design Considerations

The ideal tissue engineering scaffold should mimic the ECM properties of the target tissue, including surface topology, mechanical properties, functional chemical groups, and macroscale organization to direct the formation and maintenance of functional tissues. The chitosan–alginate scaffold system is a tunable method for generating 3D tissue engineering scaffolds with relevant biological features.

Intuitively, the properties of the natural ECM of the target tissue are useful guidelines for the design of an artificial tissue engineering scaffold[62]. However, the use of decellularized native ECM as a tissue engineering scaffold is limited by the risk of acute immune and chronic inflammatory responses[63]. A 3D scaffold is a natural approach to address a fundamental need for the engineering of many tissue types: the need for a 3D hierarchy and organization. The tissue engineering scaffold must provide the appropriate physical and chemical cues at the cell–material interface scale, the appropriate topological cues at the cell scale to guide cell organization and spreading, macroscale morphology and mechanical properties to match the target tissue, the appropriate mass transport properties within the scaffold, and then finally allow for cellular remodeling during the wound healing process[64]. Material chemistry together with processing determines the maximum functional properties that a scaffold can achieve, and how cells interact with the scaffold[64]. However, mass-transport requirements for cell nutrition, porous channels for cell migration, and surface features for cell attachment necessitate a porous scaffold structure[64]. Both chitosan and alginate are natural polymers and bear the proxy structure of GAG, a main component of native ECMs in tissue, which we hypothesize may provide a signaling cue for stem cell renewal. 3D porous CA scaffolds promoted cell adhesion and proliferation and tissue regeneration in our previous study[35]. Additional attributes of the CA scaffold include biocompatibility, biodegradability, structural stability, and minimal immunogenicity[27,35,36]. Thus, a rationally designed 3D tissue engineering scaffold must be fabricated from a material system that can address all these varied needs.

2.4 3D CHITOSAN SCAFFOLD SYNTHESIS

Chitosan–alginate (CA) scaffolds for this research were constructed by creating a CA solution, freezing and lyophilizing to generate porosity, and then ionically complexing the amine group of chitosan with the carboxyl group of alginate to form a polyelectrolyte complex. This method has demonstrated considerably improved mechanical strength compared to its chitosan or alginate counterparts[35,36]. Swelling in aqueous solutions, which is a challenge with pure chitosan scaffolds[65], is mitigated by the complexing with alginate. Alginate, also polysaccharide, is derived from seaweed and is composed of two repeating carboxylated monosaccharide units, guluronic acid (G) and manuronic acid (M) with a pKa of 3.5 as illustrated in Figure 2-2**a**. As

discussed earlier, chitosan polymer has many amine functional groups (n), equal to the percent deacetylation of the polymer, and a fraction of neutrally charged chitin (m) (Figure 2-2**b**); thus, in neutral to basic conditions, chitosan is positively charged. The mechanism for the ionic polyelectrolyte complexing can be elucidated from the molecular structures of chitosan and alginate.

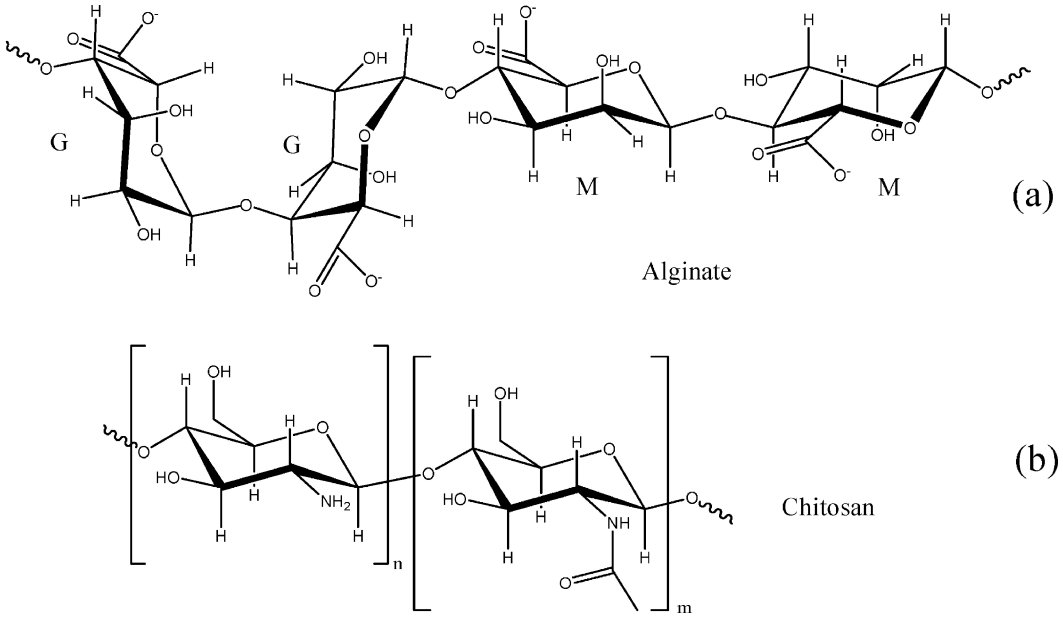

Figure 2-2: Chemical structure of (**a**) alginate consisting of guluronic acid (G) and manuronic acid (M), and (**b**) chitosan consisting of deacetylated (n) and acetylated (m) monomers. Adapted with permission[66]; see APPENDIX C for the copyright transfer agreement. Copyright 2007 American Chemical Society.

By controlling the pH of the reaction, a polyelectrolyte complex can be formed between alginate and chitosan. In the presence of alginate alone, the addition of the divalent calcium cations allows only the less sterically hindered guluronic functional groups to ionically cross-link with the calcium cations (Figure 2-3**a**)[66]. However, when alginate and chitosan polymers are in solution together, the two oppositely charged polyelectrolytes can form ionic networks via electrostatic interactions[67]. Notably, both polymers must be in ionized state, meaning that the pH of the solution must be close to the pKa of both the alginate (3.5) and the chitosan (6.5). It is believed that the carboxylate groups on alginate complex with the protonated amine groups on the chitosan ultimately form a 3D hydrogel (Figure 2-3**b)**[66]. Interestingly, the formation of the

chitosan–alginate polyelectrolyte complexes do not appear to be affected by the guluronic acid to manuronic acid ratio of the alginate[68].

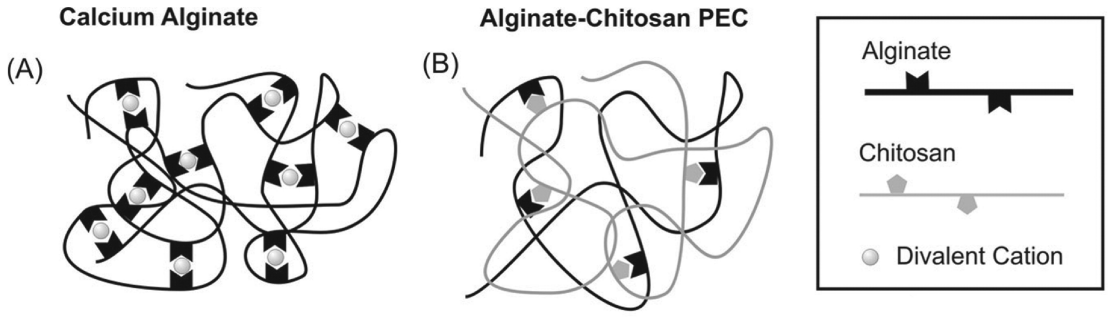

Figure 2-3: Schematic representation of the structures formed by alginate in association with (**a**) calcium ions, or (**b**) PEC with chitosan. In the PEC, the inter-associated groups are shown, but these are separated on the polymer backbone by many repeating units that are not involved in ionic associations. Adapted with permission[66], see APPENDIX C for the copyright transfer agreement. Copyright 2007 American Chemical Society.

Varying the processing conditions of the chitosan–alginate sol following complexing also has major impact on the final scaffold generated. The pore size and geometry of the CA scaffold may be varied by altering freezing temperature (effectively altering freezing rate when processing volumes are constant), with rapid nucleation favoring the formation of smaller pores. Conversely, when ice crystal growth is favored, larger pores are generated (Figure 2-4). By altering the freezing temperature, CA scaffolds can be generated with a wide range of pore sizes and morphologies. Furthermore, total CA weight percentage in the solution may also be increased to increase pore wall thickness and Young's modulus (Figure 2-5). The CA scaffold system is a promising candidate as a tunable 3D scaffold to mimic the *in vivo* ECM microenvironment.

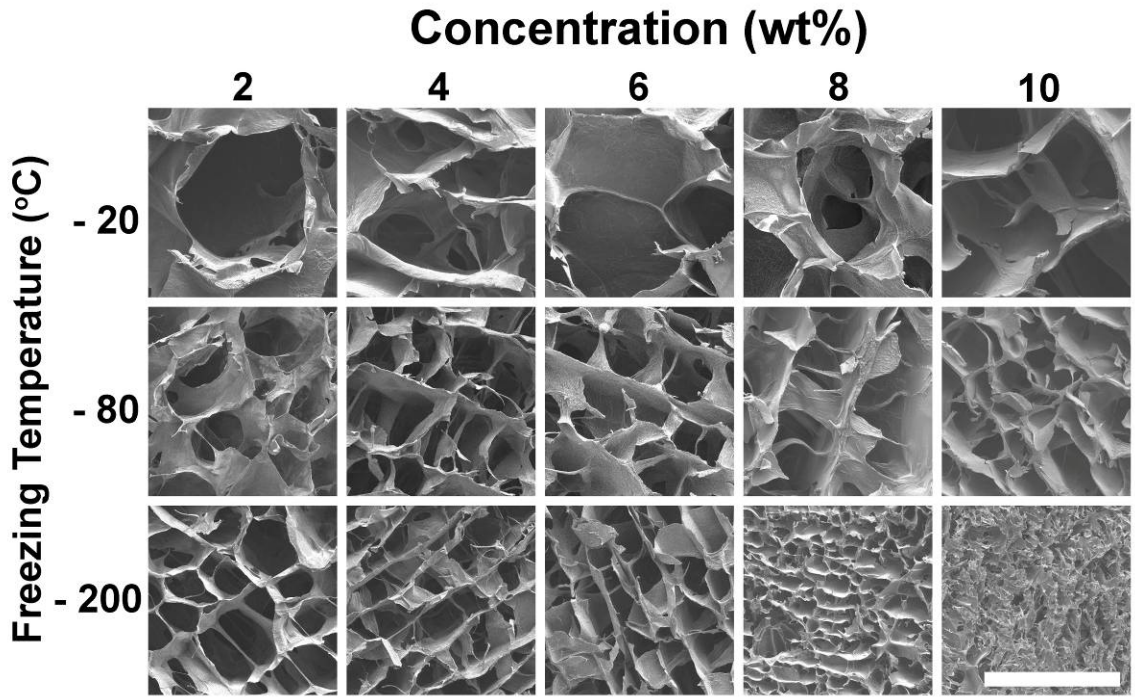

Figure 2-4: Chitosan–alginate scaffolds exhibiting a range of pore morphologies. Scale bar represents 200 μm.

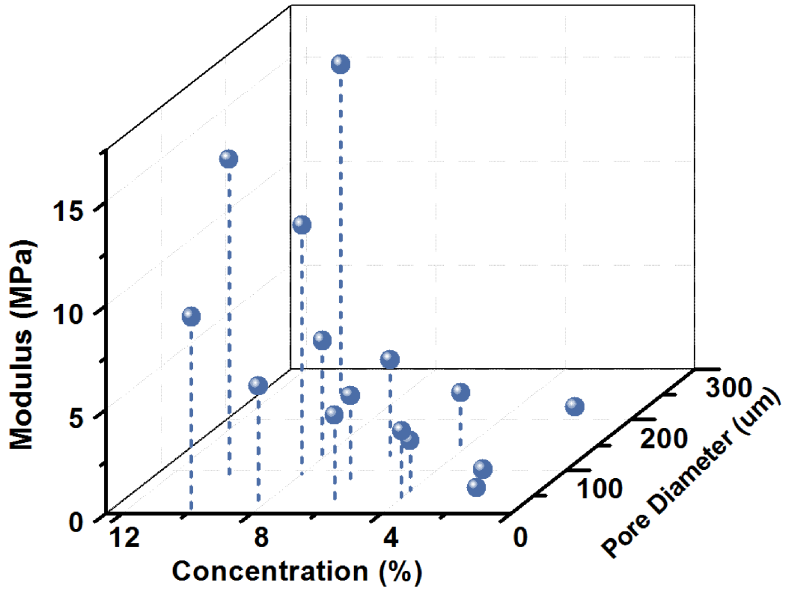

Figure 2-5: Chitosan–alginate scaffolds exhibiting a range of Young's moduli.

Chapter 3: Nanofibers for Tissue Engineering Applications

3.1 2D Nanofiber Extracellular Matrix Design Considerations

Certain tissue types are highly dependent on nanotopological extracellular matrix features to guide cell morphology and differentiation. In particular, highly aligned, parallel extracellular matrix fibers are characteristic of native muscle and tendon tissue. Nanofiber-based scaffolds are an effective way to recapitulate aligned nanotopology for tissue engineering.

The hierarchical structures of electrospun nanofibers, comprising continuous fibers with diameters on the scale of 100 nm, represent a scale of topological features smaller than a cell, and extend upwards to the overall macroscale network of nanofibers with varying degrees of alignment possible between fibers. These structuries mimic the tissue structures that surround cells in native tissue[69]. In contrast to the flat surfaces of most monolithic materials, nanofibrous networks present a large surface area of cell scale features, which facilitates cell adherence and guidance along the direction of the fibers[70]. Mechanical hindrance by small interfiber distances and fiber dimensions encourages cells cultured on electrospun scaffold to adhere to the surface of the scaffold, rather than penetrating between the fibers[71]. This property can be used to facilitate the formation of individually organized cell–scaffold layers by deliberately restricting cell mobility. Importantly, a porous nanofibrous scaffold would still allow the adhered cells to receive nutrients and soluble signals in a three-dimensional manner from all directions, allowing for potentially higher cell densities compared to impermeable 2D surfaces.

Significantly, the arrangement of ECM in certain tissues, including skeletal muscle and bone, follows highly aligned, parallel arrangements[72]. The complex arrangements of the ECM influence cell phenotype and behavior by providing direct and informational signaling cues[73]. These interactions can modulate cellular activities including migration, proliferation, differentiation, gene expression, and secretion of hormones and growth factors[73]. Therefore, an appropriately designed ECM may be the defining factor between the success or failure of a tissue-engineered construct. For example, the mechanical characteristics of aligned tissue

including muscle and tendon, which typically display high Young's modulus and tensile strength in the longitudinal direction along with alignment, are readily reproduced with aligned nanofibers. To improve bulk mechanical properties, nanofiber networks can be layered or braided[74]. However, the macroscale arrangement of the fiber bundles must be designed appropriately, as increasingly dense fiber bundles inhibit mass transfer, cell seeding, and migration[69]. Therefore, the overall 3D spatial arrangement of nanofibers and the adherent cells is an important design consideration, which may in turn dictate the overall mechanical properties of the nanofiber scaffold. The design requirements of all tissue engineering scaffolds are biocompatibility, integration, and supporting the desired cellular and tissue functions.

A chitosan–polycaprolactone (C-PCL) fibrous synthetic ECM system fabricated by electrospinning during our previous studies was applied during this research. Although PCL is not enzymatically degradable or resorbable *in vivo*, the biocompatibility of PCL has been well demonstrated[75]. Unlike most synthetic and natural polyblend nanofibers, such as collagen-PCL and gelatin-PCL, which require chemical cross-linking to retain their structure integrity and improve mechanical strength using cytotoxic cross-linking agents[76,77], polyblend C-PCL nanofibers can be produced by electrospinning without chemical cross-linking. We have previously shown that chitosan and PCL in the nanofibers were well blended and showed no apparent morphological changes or phase segregation in aqueous solutions for 30 days. Electrospun non-woven chitosan-PCL nanofiber mats demonstrated excellent mechanical properties and cellular compatibility[78]. Even in the presence of lysozyme, the primary source of chitosan degradation[55], the C-PCL fiber maintained their asprepared morphology for 30 days[78]. Additionally, in previous experiments, randomly oriented C-PCL fibers enhanced nerve regeneration compared to randomly oriented PCL fibers[39], while parallel-oriented fiber mats enhanced myogenesis of rat myoblasts cells compared to randomly oriented fibers[40]. The development of composite C-PCL nanofibers is significant, as it combines the bioactive properties of the chitosan with the mechanical strength and stability of polycaprolactone. By varying polymer ratios and processing conditions, a range of fiber diameters and fiber arrangements can be generated, which in turn results in a range of mechanical properties. Therefore, the C-PCL nanofiber scaffolds are tunable to the properties of the target tissue type and cellular response desired.

3.2 2D CHITOSAN NANOFIBER SYNTHESIS

A C-PCL fibrous synthetic ECM system fabricated by electrospinning developed during our previous studies was also used in the course of our research. We have previously demonstrated a C-PCL fibrous system that combines natural and synthetic advantages of the individual polymers[39]. When chitosan was combined with mechanically stable PCL, fibers produced by electrospinning exhibited *in vitro* stability and appropriate mechanical properties. Electrospinning is a widely used and highly flexible technique for the generation of fibers and fibrous structures of different dimensions and surface topologies via the manipulation of electrostatic forces and solvent–polymer solution properties[79].

The electrospinning process requires dedicated equipment design and processing conditions to produce fibers with a given set of physical characteristics. Figure 3-1 illustrates a schematic electrospinning setup showing the three major pieces of equipment necessary for the process: a fine nozzle to dispense the polymer–solvent solution, a high-voltage power supply, and a grounded metal collector screen. When polymer–solvent solution is electrostatically charged by the high-voltage power supply, the hemispherical surface of the fluid at the tip of the capillary tube elongates to form a conical shape known as the Taylor cone[79,80]. Increasing the strength of the electric field beyond a critical point dictated by the viscosity, surface charge, and dielectric constant of the solution overcomes the surface tension, resulting in ejection of a charged jet of fluid from the Taylor cone. The polymer solution jet elongates toward the collector, while simultaneously the solvent evaporates. Ultimately, a polymeric fiber is deposited onto the collector. The interplay of numerous variables during electrospinning dictate the properties of the resulting fiber, including length, surface morphology, diameter, and orientation.

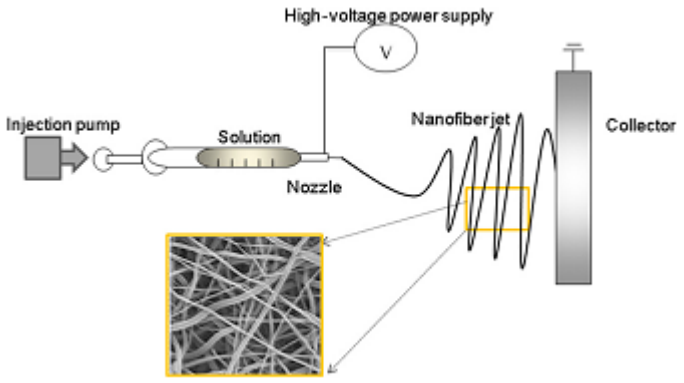

Figure 3-1: Schematic illustration of electrospinning process and key elements. Reprinted with permission[69], see APPENDIX D for copyright transfer agreement.

Many parameters can influence the transformation of polymer solutions into nanofibers through electrospinning. These parameters include (a) the solution properties such as viscosity and conductivity, (b) electric potential at the capillary tip, the distance between the tip and the collecting screen, and the overall solution flow rate, and (c) ambient parameters such as solution temperature, humidity, and air velocity in the electrospinning chamber.

Solution properties are directly correlated with fiber dimensions and morphology. One of the most significant parameters influencing the fiber diameter is the solution viscosity. A higher viscosity results in a larger fiber diameter [81]. However, when a solid polymer is dissolved in a solvent, the solution viscosity is proportional to the polymer concentration. Thus, the higher the polymer concentration the larger the resulting nanofiber diameters[69]. Interestingly, fiber diameter increases with increasing polymer concentration according to a power law relationship[82]. Increasing solution conductivity by selection of polymer or solution, or the addition of electrolytes, reduces the presence of beads or droplets on the fibers, and thus increases fiber uniformity[81]. However, increasing conductivity generally results in decreasing fiber diameter, necessitating a balance between solution viscosity and conductivity to achieve the target fiber size.

The processing variables of electric potential, the distance to the collecting screen, and the overall flow rate of polymer solution are closely interconnected and critical for ensuring the

formation of fibers. At low voltages, close to the critical voltage for polymer solution streaming, a solution droplet is suspended at the needle tip, and a jet will stream from the Taylor cone, minimizing bead formation[81]. As voltage increases, the Taylor cone recedes and eventually disappears within the nozzle, so that polymer solution streams randomly from the surface of the solution and generates beads rather than fibers. Adjusting the distance between the tip and the collector effectively alters the amount of time that the fiber is traveling through the air and evaporating solvent[81]. If the solvent is not completely evaporated prior to the polymer jet settling on the collector, the residual solvent will dissolve the fibers, again creating polymer beads rather than fibers. Similarly, a high flow rate of polymer solution tends to produce larger diameter fibers that require more time to dry. Thus, the electric potential must be tuned for the collection distance and flow rate, and vice versa to generate electrospun fibers.

Ambient parameters of solution temperature, humidity, and air velocity in the electrospinning chamber can further influence the morphology and consistency of the electrospun fibers. Decreasing temperature increases solution viscosity, with the attendant increase in fiber diameter[81]. High humidity has been observed to result in surface porosity on individual nanofibers[81]. Finally, air velocity can alter the fiber trajectory, reducing fiber network alignment. Thus, consistent environmental conditions must be maintained to generate reproducible nanofibers.

Aligned C-PCL nanofiber mats were synthesized via a novel electrospinning device with a custom fabricated collector composed of a pair of grounded parallel electrodes (separation distance ~4 cm) for the collection of parallel aligned nanofibers[40]. By changing electrospinning conditions, the same C-PCL polymer can be used to generate either random nanofiber networks (Figure 3-2**a**) or highly aligned nanofiber networks (Figure 3-2**b**). The experimental value of this technique is that the effect of surface nanotopology on cell behavior can be examined independently of the ECM composition. The unique combination of subcellular scale texture from individual C-PCL fibers, combined with the option to generate either long-range random or anisotropic arrangements, is a valuable system for the in-depth study of specific ECM microenvironmental cues. The C-PCL fiber ECM substitute system generates distinct sets of

topological cues that are capable of directly influencing cell behavior and are a promising candidate for the tissue engineering of alignment-dependent tissue types.

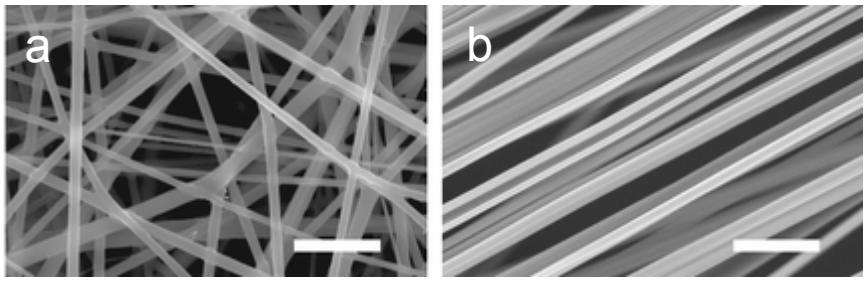

Figure 3-2: SEM images of (**a**) randomly oriented and (**b**) directionally aligned C-PCL nanofiber scaffolds. Scale bars represent 2 μm. Reprinted with permission[40], see APPENDIX E for the copyright transfer agreement.

Chapter 4: 3D Microenvironments for hESC Renewal

4.1 hESC Background

Human embryonic stem cells (hESCs) have attracted a great deal of research interest because they have the potential to produce specialized cells that may be used to regenerate any damaged tissue in the body and thus potentially treat degenerative diseases[83-88]. hESCs are pluripotent cells that can differentiate into all somatic cell types[88]; however, the signaling cues and pathways that regulate hESC self-renewal and lineage commitment are still largely unexplored. Microenvironmental conditions for the renewal and directed differentiation of hESC must be elucidated to make the idea of hESC as a universal tissue engineering cell source a reality.

hESCs are derived from the inner cell mass of 3 to 5-day-old blastocyts[89]; the use of viable human embryos for hESC cell derivation has triggered significant ethical debate. Opponents of hESC research cite that a human may be derived from the viable embryo, and equate the embryo to an individual human[90]. Typically, hESC lines are derived from embryos generated during *in vitro* fertilization treatments and that were either non-viable or unnecessary for the treatment, and subsequently were donated by the original tissue donors[91]. Alternative approaches have been developed to address these ethical concerns. Significantly, it was discovered that a single cell removed from the 8 to 10-day cell stage blastocyst, which is routinely done for pre-implantation genetic diagnosis, can be used to derive hESCs[92]. The blastocyst is unharmed by the single cell removal procedure and can develop normally to term if implanted[93]. Additionally, the pluripotency, a hallmark of hESC function, has been reproduced in adult somatic cells via the induced expression of the key pluripotency genes OCT3/4, SOX2, CMYC, and KLF4 to generate induced pluripotent stem cells (iPSCs)[94]. iPSCs are a topic of intense scientific interest, one described as heralding a new era of biological and medical study in which pluripotency can be induced as needed[95]. Emerging techniques increasingly allow for the derivation of hESC and equivalents, which are expected to address ethical concerns regarding the derivation of these cells.

hESCs are characterized by two distinct properties — the ability to self-renew (proliferate) and the capability for pluripotent differentiation. During self-renewal, the hESC may divide symmetrically and generate a daughter cell that is identical to the parent cell, or divide asymmetrically and generate a differentiated daughter cell[91]. Given the appropriate conditions, hESCs may divide symmetrically indefinitely, and are not known to undergo replicative senescense[91], which allows for the generation of the large hESC populations necessary for study and therapeutic applications. In contrast, adult stem cells have finite proliferative ability, meaning that a single patient's stem cell population may not be sufficient for therapeutic treatment either as a result of the degree of trauma or the age of the patient[91]. The mechanism that allows for hESCs to proliferate indefinitely is closely related to the maintenance of telomerase, which prevents chromosomal shortening during cellular replication, in addition to the action of transcription factors OCT4, SOX2, and NANOG [91,96].

During differentiation, pluripotent hESCs can give rise to cells from all three germ layers (ectoderm, mesoderm, endoderm), and ultimately generate all tissue types that make up the organism. Thus, hESCs are a universal stem cell for the entire organism. The pluripotent nature of hESCs and iPSCs could permit the development of novel stem cell-based regenerative therapies and drug discovery platforms[97]. Pluripotent stem cell therapy may be able to address deficiencies acquired via inherited or genetic alterations in a patient's resident adult stem cells that may lead to loss of function with aging or disease[98]. The loss of adult stem cell function is associated with numerous diseases and disorders, including hematopoietic and immune system disorders, cardiovascular diseases, diabetes, chronic hepatic injuries, gastrointestinal disorders, brain, eye, and muscular degenerative diseases, and aggressive cancers[98]. The expectation is that the transplantation of viable, tissue-specific progenitor cells into the patient may be able to induce a therapeutic response and treatment of the disorder. These prospective stem cell-based treatments are of particular interest for treating inherited and degenerative disorders for which there are no effective cures[98].

4.2 Challenges with hESC Proliferation

The success of stem cell therapy is, however, dependent on the ability to reproducibly generate a large number of hESCs with high purity and consistency while maintaining their pluripotency. Self-renewal of hESCs is commonly achieved by culturing hESCs on a feeder layer of mouse embryonic fibroblast (MEFs) or human fibroblast feeder cells (hFFs), or in conditioned media (CM) derived from MEFs[21,99-102]. The feeder layer provides a suitable substrate for hESC attachment and releases nutrients and signaling factors, conditioning the media for maintenance of hESC pluripotency. Since MEFs or hFFs are viable for only a few days, the hESCs must be transferred regularly onto new feeder layers for continued renewal, which is a costly and labor-intensive procedure[103]. Importantly, viruses or other undesired macromolecules from feeder cells may be transmitted to the hESC population and ultimately to the recipient of stem cell-based therapy[101,103]. In the absence of the appropriate proliferative environment, hESCs differentiate spontaneously, with accompanying changes in morphology, the loss of embryonic stem cell markers including OCT4, and the loss of pluripotency[104]. Compared with the cell-based feeder systems, artificial ECMs offer several advantages, including reduced risk of pathogen transmission and ease of scale-up[104].

The ECM is believed to play a major role in stem cell renewal, in which ECM components either function as signaling molecules through integrin receptors or increase the sensitivity of cytokine receptors on stem cells[101,102]. The use of ECM proteins as coating materials on substrates for stem cell renewal has been actively pursued in recent studies[97]. However, the matrices coated with proteins face the challenge of continued support for long-term cell function, as these coating materials can be depleted quickly over time. Furthermore, protein-based materials need to overcome the challenges of source-dependent variation, potential immune rejection, and infection by human and nonhuman pathogens[100,101,105]. While synthetic polymer coatings including Synthemax (mTeSR®) and PMEDSAH (StemPro®) are able to maintain hESC pluripotency when paired with specific serum-free defined media, these 2D films do not fully recapitulate the full range of microenvironmental cues found in the native 3D hESC niche. No current synthetic polymers, with or without ECM and growth factors, have been able to maintain the pluripotency and undifferentiated state of hESCs in a xeno-free culture medium for an extended time[97].

The appropriate microenvironment is critical to the successful renewal of hESCs. It is likely that in addition to the direct effects of the ECM, hESCs are exposed to a wide range of signaling environments via the formation of hESC colonies, which possess the additional properties of size and distribution[106], which in turn create local signaling and nutrient diffusion gradients within the scaffold itself. *In vivo*, hESCs are found in niches with defined tissue architecture[106]. During embryonic development, hESCs reside in a 3D environmental milieu that regulates cell replication and differentiation via complementary mechanisms including the presentation of immobilized signaling molecules in a defined manner, the modulation of matrix stiffness, and the creation of cytokine gradients[102,107]. A stem cell niche is defined by production of local signal(s) and spatial organization of cells receptive to those signals to generate location-dependent control over contrasting cell fate decisions such as self-renewal and differentiation[106]. For example, hESCs preferentially form tight contacts with undifferentiated neighbors while excluding contacts with differentiated cells, ultimately forming colonies of undifferentiated cells[106]. Effectively, hESCs self-regulate local cell density. Thus, the hESCs continually redefine the culture microenvironment via proliferation and migration. In traditional feeder cell-based culture, the supporting feeder cells provide mechanical contact, direct cell–cell contacts to hESC superficial to the colonies, and secrete relevant signaling factors throughout the cell culture media. The complexity of the hESC proliferation niche is extremely complex and challenging to reproduce.

4.3 3D SCAFFOLDS AS A SCAFFOLD FOR HESC RENEWAL

Although researchers have not come to a consensus on the exact governing mechanisms of stem cell self-renewal, studies have shown that the interaction between the ECM and the integrins on hESC membranes plays a critical role[101,102,108]. We hypothesize that hESCs in a properly constructed 3D matrix may sustain self-renewal in the absence of feeder cells. The chitosan-alginate (CA) complex scaffold has many advantages compared to 3D synthetic polymers and protein scaffolds. Recent studies have also demonstrated that GAGs play an important role in regulating hESC adhesion and self-renewal[109,110], which is mimicked by chitosan. Furthermore, the spatial control possible with the CA scaffold may allow us to address key requirements for ECM stiffness and topology that are necessary to recreate in the hESC niche. Interestingly, low

oxygen tension may decrease the rate of stem cell differentiation and increase proliferative potential[102], which a 3D scaffold may create, compared to 2D culture. Although it probably will not be necessary to mimic all aspects of the niche to greatly increase stem cell self-renewal, it almost certainly will be necessary to simultaneously mimic multiple components of the niche[102]. In this study, a highly porous scaffold made from chitosan and alginate complex is used to exploit the role of the ECM in stem cell renewal.

Chapter 5: 2D Microenvironments for Myogenic Differentiation

5.1 Muscle Tissue Engineering

Regenerating a large population of muscle cells is important for muscle injury repair and the study of metabolic biological functions[71,111]. Though autologous graft surgery remains the ubiquitous approach for muscle injury repair, this treatment is severely limited by donor tissue availability, compelling the investigation of alternative methods. Muscle satellite cells have been expanded *in vitro*[112]; however, the limited cell numbers are inadequate for therapeutic success[113]. Additionally, only limited progress has been made toward the myogenic differentiation of adult mesenchymal stem cells (MSCs)[48,114,115].

Skeletal muscle is primarily composed of post-mitotic, multi-nucleated muscle fibers required for locomotion, and in addition, regulating metabolism through glycogen storage, insulin uptake, and amino acid catabolism[112]. Therefore, skeletal muscle health is essential to overall health and well-being. Damaged skeletal muscle fibers are repaired by satellite cells, a population of muscle tissue-specific stem cells[112]. In response to fiber damage, healthy muscle satellite cells begin proliferation and differentiation into mature myoblasts, which migrate rapidly to the injury site to fuse with each other or with damaged myoblasts at the wound site to restore tissue function[116]. In a recent study, autologous transplantation of muscle-derived stem cells via injection to the wound site improved angiogenesis and muscular strength and decreased fibrosis compared to results in control groups[117]. Unfortunately, pathologies including congenital myopathy, denervation, and atrophy from disuse may also decrease the number and proliferative potential of the native satellite cells[112]. Therefore, we need a therapeutic approach to generate muscle stem cell populations form alternative sources for myogenic tissue engineering.

A bioactive cell culture environment combined with relevant cell types, growth factors, and topological properties is needed to facilitate the proliferation and differentiation of myoblasts. While muscle satellite cells have been expanded *in vitro*, the limited cell population is inadequate for successful therapy[112]. Mesenchymal stem cells (MSCs) may provide sufficient

myoblast supply via directed myogenic differentiation; however, only limited progress has been made along this path[115]. For instance, the application of Wnt3a, a signaling protein involved in mesodermal lineage commitment, is reported to induce myogenic differentiation of MSCs after 10 days of culture; however, only 3.76% of the induced MSCs showed myosin-heavy-chain (MHC) expression, suggesting that Wnt3a alone cannot induce the differentiation of large myogenic populations[32,85], limiting the use of MSCs as a cell source.

5.2 hESCs as a Source of Myogenic Cells

Alternatively, pluripotent embryonic stem cells (ESCs) have considerable advantages over adult stem cells as a cell source due to their capacity for unlimited proliferation in an undifferentiated state and their ability to differentiate into various lineages of cells[118,119]. In recent studies mouse and human ESCs (hESCs) have been transfected to induce the expression of Pax3, a transcript factor responsible for activation of myogenic regulatory factors.[120,121] Nevertheless, only 16–21% of the Pax3-expressing hESCs exhibited the terminal myogenic differentiation marker MHC. Also, cells modified by gene transfection are not ideal for therapeutic use as gene expression is difficult to control[122]. Myogenic cells have also been obtained from mESCs induced by using retinoic acid[123] or by sorting cells with an antibody specific for myogenic cells from mouse iPSCs[124]. Inspiringly, one study demonstrated success in myogenic differentiation of hESCs by using a stroma-free induction system[83]. However, this technique has a very low conversion rate and is time-consuming, and has not led to a major advance[125]. Though using feeder layers can increase differentiation efficiency, the process is costly and labor intensive, and yet bears the risk of transmitting virus and other unwanted macromolecules from feeder cells. Therefore, for muscle tissue engineering, the need is urgent for an hESC culture system with well-defined cell-culture conditions without using feeder layers for enhanced myogenic differentiation.

While hESCs hold promise as a treatment for muscle injury, their efficient expansion and differentiation in traditional culture conditions of hanging drops and feeder layers remain a challenge as these environments are less likely to represent the *in vivo* state and produce large

populations of muscle cells[24,126]. Therefore, it is of interest to develop a cell culture system that can enhance myogenic differentiation of hESCs. The ideal *in vitro* model of the myogenic microenvironment should mimic the anisotropic arrangement, mechanical properties, and surface chemistry found in the extracellular matrix (ECM) of muscle tissue. The effects of the ECM and accompanying microenvironment are key regulators of the myogenic commitment and differentiation of stem cells and myogenic precursors into mature myoblasts[40,41,48,115,127,128]. Nanofibrous scaffolds have been evaluated extensively in tissue engineering applications to mimic ECM microenvironment conditions[129].

5.3 2D Aligned Nanofibers as a Scaffold for Myogenic Differentiation

The generation of myogenic precursors from hESCs using a rationally designed cell culture system on a nanofibrous tissue engineering scaffold is a promising approach to producing sufficient myogenic cell populations for regeneration muscle therapies and studying embryo myogenesis from multipotent progenitor cells[31,130,131] and adult myogenic precursor cells[38,40]. A highly aligned C-PCL nanofibrous scaffold developed in our lab supported skeletal muscle cell attachment and proliferation, promoting skeletal muscle morphogenesis and aligned myotube formation coinciding with the nanofiber orientation[40]. This combination of natural and synthetic polymers possesses unique physiochemical properties. Environmental cues from the nanofibrous ECM combined with the signaling function of soluble growth factors may produce a significantly more effective system to induce the myogenic differentiation of hESCs.

Chapter 6: 2D Microenvironments for Tenogenic Differentiation

6.1 Tendon Tissue Engineering

Injuries to tendons are common clinical problems and account for 7% of all physician visits for injuries in the United States[132,133]. Tissue regeneration after injury remains a formidable challenge due to poor and slow healing capacity of the native tendon[134,135]. Autologous graft surgery is the current gold standard for tendon injury repair, but this treatment is severely limited by donor tissue availability. Allografts and xenografts alleviate the demand for donor tissue, but can cause complications such as non-specific inflammatory reactions, reduced strength, joint-stiffness, repair-rupture, and donor-site morbility[136,137]. Tissue-engineered tendons with mechanical and functional characteristics similar to the native tissue may prevent these complications and provide an alternative treatment modality. Tissue engineering strategies to improve tendon repair healing include the use of scaffolds, growth factors, cell seeding, and combination of these approaches[138]. The biological scaffolds derived from animal proteins, in particular collagen, are increasingly being used in clinical practice[136,139]. However, the use of these biological scaffolds is hindered by their low mechanical strength, non-specific cellular induction, and occasional inflammatory responses, which contribute to implant failure[140]. A variety of synthetic polymers, such as polyurethane, ePTFE, and polyester, have been investigated for tendon repair.[136] While these synthetic polymer scaffolds have superior mechanical properties over biologically derived scaffolds[136]. their use can cause a series of problems including a high rate of postoperative infection, chronic immune response post implantation, and poor cellularity[136,140]. The progress toward clinical use of tendon tissue engineering is hindered by the difficulty in obtaining tendon regenerating cells and suitable scaffolds[134,141].

6.2 BMSCs as a Tendon Tissue Engineering Cell Source

Several cell types including tenocytes, adipose mesenchymal stem cells, and bone mesenchymal stem cells have been investigated for tendon tissue engineering. Tenocytes, mature tendon generating cells, have limited numbers and proliferative ability in the adult[142,143]. Furthermore, tendon cell recovery requires the destruction of healthy tendon tissue, further hindering patient recovery. Adipose mesenchymal stem cells express relevant tenocyte differentiation markers in differentiating culture conditions, but no expression of Collagen I[144], which makes up the bulk of tendons and ligaments (60% w/w)[145]. Bone mesenchymal stem cells (BMSCs) are multipotent stromal cells that can differentiate into various cell types[146-150]. Via recombinant expression of the tenogenic differentiation gene scleraxis, BMSCs exhibited terminal differentiation marker protein Collagen I[151]. However, cells modified by gene transfection are not ideal candidates for transplant therapy as stable endogenous growth factor expression is difficult to implement[122]. Alternatively, numerous combinations of ECM materials and soluble growth factors have recently been explored for the tenogenic differentiation of BMSCs[146,152-155]. Though this approach showed great promise in tenogenesis of BMSCs, its tenogenic differentiation efficiency by existing materials in combination with growth factors is very low[146,156,157]. Furthermore, cell differentiation on these materials required a long time of 2 to 12 weeks which is not desirable for therapeutic applications, and yet BMSC confluence was not always achieved even with extended culture periods[152,153,155,15819-21]. Thus, an appropriate combination of scaffolds and growth factors has yet to be developed for tenogenic differentiation of BMSCs.

6.3 2D Aligned Nanofibers as a Scaffold for Tenogenic Differentiation

The generation of tenogenic precursors from BMSCs using a rationally designed cell culture system on a nanofibrous tissue engineering scaffold is a potential approach for the fabrication of a tissue-engineered tendon construct. The ideal tenogenic scaffold should thus have anisotropic properties as native ECM, possess sufficient mechanical strength to support the healing tissue, and provide a favorable substrate for cell attachment, proliferation, and matrix deposition[137,145,146,155,159]. A rationally designed tendon engineering scaffold must provide these ECM properties. Environmental cues from the nanofibrous ECM combined with the signaling function of soluble growth factors may produce a significantly more effective system to induce the tenogenic differentiation of BMSCs.

Chapter 7: Feeder-free Self-renewal of Human Embryonic Stem Cells in 3D Porous Natural Polymer Scaffolds

7.1 INTRODUCTION

Human embryonic stem cells (hESCs) are routinely cultured on fibroblast feeder layers or in fibroblast-conditioned medium, which requires continued supply of feeder cells and poses the risks of xenogenic contamination and other complications such as feeder-dependent outcome. Here, we demonstrate a strategy that supports sustained self-renewal of hESCs in a three-dimensional porous natural polymer scaffold, comprised of chitosan and alginate, without the support of feeder cells or conditioned medium.

We first investigated the proliferation, functionality, and pluripotency of hESCs cultured in CA scaffolds *in vitro*. We assessed the pluripotency of the renewed hESCs both *in vitro* by evaluation of cellular proliferation, functionality, and gene activities for 21 days. The self-renewed stem cells can be easily recovered for subculture by decomposing the scaffold under a mild condition. We developed an effective method to harvest the renewed hESCs from CA scaffolds for subculture by decomposing CA scaffolds in a mild condition and then subcultured recovered hESCs for 14 days and verified their pluripotency. Pluripotency of hESCs *in vivo* was evaluated by directly implanting hESC-populated CA scaffolds into the abdominal cavities of SCID nude mice to induce cell differentiation and teratoma formation.

In addition to providing a clean environment for stem cell renewal, this strategy, with the demonstrated biocompatibility and biodegradability of chitosan and alginate, may potentially allow for the direct implantation of stem cell-populated scaffolds for a broad spectrum of applications in tissue engineering and regenerative medicine.

7.2 METHODS

7.2.1 Chitosan-alginate scaffold synthesis

Chitosan and alginate solutions were prepared separately by dissolving 4.8 g of chitosan in 80 mL 1 N acetic acid and 4.8 g sodium alginate in 120 mL 1N NaOH, respectively. The two solutions were then mixed in a blender and stirred for 1 hr to obtain a 4.8% w/v (2.4% chitosan, 2.4% alginate) solution. The resultant solution was heated and maintained at 70°C for 1 hr. The pH of the solution was adjusted to 7–7.4 by addition of 2N acetic acid. The solution was then placed into a 24-well plate, maintained at –20°C for 24 hrs, and lyophilized to form scaffolds. The scaffolds were then cross-linked by immersion in 1% w/v CaCl2 solution for 10 min, and washed with deionized water.

7.2.2 Compressive and tensile strength

Compressive mechanical modulus of CA scaffolds were tested using an Instron 4505 mechanical tester with 10 kN load cells following the guidelines in ASTM D5024-95a. The specimens were cylinders of 13-mm diameter and 12-mm thickness. The crosshead speed of the Instron tester was set at 0.4 mm per minute, and load was applied until the specimens were compressed to approximately 30% of their original thickness. Compressive modulus was calculated as the slope of the initial linear portion of the stress–strain curve.

Tensile modulus was evaluated using a custom-made micro-tensile testing machine. The load cell has a loading range of ±30 grams with an incremental accuracy of 0.001 grams. Scaffolds were cut in rectangular shape with a cross-section of 6 mm × 10 mm. The tensile modulus was calculated from the stress–strain curve.

7.2.3 Pore size and porosity

The porosity and pore size distribution of the scaffold were measured by an Auto Pore IV mercury porosimeter (Micrometritis Instrument Co., Nacross, GA). The Washburn equation was used to calculate the pore diameter. Porosity (%), total pore volume (ml/g), total pore area

(m2/g), and the pore size distribution of the scaffold were determined by measuring the volume of the mercury infused. For each measurement, cylindrical scaffolds of 3-mm diameter and 3-mm length were placed in a 10-mL penetrometer, subjected to a vacuum of 50 mm Hg, and infused with mercury. Samples weights were measured before and after the mercury infusion.

7.2.4 Cell culture and seeding

Human embryonic stem cells (hESCs), BG01V, were maintained on irradiated human fibroblast feeder layers (ATCC USA) in ES-Dulbecco's modified Eagle's medium (DMEM) as defined by ATCC. ES-DMEM was prepared from a 1:1 mixture of DMEM and Ham's F-12 medium containing 1.2 g/L sodium bicarbonate, 2.5 mM L-glutamine, 15 mM HEPES, and 0.5 mM sodium pyruvate supplemented with: 2.0 mM L-alanyl-L-glutamine, 0.1 mM non-essential amino acids, 0.1 mM 2-mercaptoethanol, 10 ng/ml bFGF (R&D Systems), 5% (V/V) knockout serum replacement (Invitrogen), 15% (V/V) fetal bovine serum, and 100 units/ml penicillin/streptomycin. The cultures were incubated at 37ºC in the atmosphere supplemented with 5% CO2, with the cell culture media changed daily. A solution of 200 units/ml collagenase IV in DMEM/F12 media was used to detach hESCs from the feeder layer.

CA scaffolds were sterilized with ethylene oxide gas, and cut into discs of 2-mm thickness and 13-mm diameter (Fig. 1) and fit into 24-well tissue culture plates (Corning Life Sciences). The scaffolds were incubated for 24 hrs in hESC culture media prior to cell seeding. hESCs suspended in hESC media were then seeded directly onto the scaffolds and maintained following the cell culture protocol described above. hESCs on hFF layers as a control were subcultured every 6 days.

7.2.5 hESC proliferation assessment

Cell proliferation was assessed using the oxidation–reduction indicator alamarBlue (Alamar BioSciences, Sacramento, CA). The numbers of hESCs grown in CA scaffolds and on hFF layers, with initial cell seeding of 50,000, for 21 days, were measured in quadruplicate at specified time intervals. Every 6 days, hESCs cultured on hFF layers were passaged and 50,000

hESCs transferred to a fresh hFF layer. For each cell number measurement, the culture was washed with PBS, and incubated in 1 mL of ES-DMEM with 10% alamarBlue substrate for 50 min or 25 min with cell numbers up to 500,000 and 3,000,000, respectively, or with 2 mL of ES-DMEM with 10% alamarBlue substrate for 30 min or 20 min with cell numbers up to 10,000,000 and 20,000,000, respectively, at 37°C and 5% CO2. Absorbance of the solution was measured spectrophotometrically with a microplate reader (Versamax, Molecular Devices) at 570 and 600 nm. Calibration curves for each range of cell population generated with known numbers of hESC counted by cell counter on both CA scaffolds and hFF layers were used to quantify the number of cells in each culture.

7.2.6 Alkaline phosphatase activity assay

The StemTAG™ alkaline phosphatase activity assay kit (Cell Biolabs) was used to quantitatively measure the alkaline phosphatase (ALP) activities of hESCs on both hFF and scaffold constructs in triplicate at specified time intervals over 21 days. The cell constructs were rinsed with cold PBS, and hESCs were detached with collagenase IV, and lysed with Cell Lysis Buffer (Sigma). After incubation at 4^{o}C for 10 min, the cell suspension was centrifuged at 12,000 G for 10 min to remove cell debris, retaining the supernatant. We mixed 50 µl cell lysate with 50 µl StemTAG™ ALP activity assay substrate (Sigma) in a 96-well plate. The reaction mixture was incubated for 30 min at 37^{o}C in 5% CO2, until the reaction was stopped by the addition of 50 µl stop solution (Sigma). The absorbance of the product was measured at 405 nm, compared to the absorbance of 50 µl of Cell Lysis Buffer.

7.2.7 Quantitative RT-PCR

Cell-scaffold constructs were homogenized by vortexing and passing through QIAshredder columns. Total RNAs were isolated from hESCs in CA or on hFF in triplicate using RNeasy, and 30 ng of total RNA for each sample was converted to cDNA using the QuantiTect Reverse Transcription Kit following the manufacturer's instructions (Qiagen).

SYBR Green PCR Master mix (Qiagen) was used for template amplification with a primer for each of the transcripts examined. Thermocycling for all targets were carried out in a solution of 30 µl containing 0.3 µM primers (Integrated DNA Technologies) and 4 pg cDNA from the reverse transcription reaction under following conditions: 15 seconds at 94°C, 30 s at 55°C, and 30 s at 72°C. The reaction was monitored in real time using a MiniOpticon (BioRad). Primers are listed in Table 1.

Table 1: Pluripotency PCR primers

Gene symbol	Forward Primer	Reverse Primer
Undifferentiation markers		
OCT4	5'-CTT GCT GCA GAA GTG GGT GGA GGA A	5'-CTG CAG TGT GGG TTT CGG GCA
NANOG	5'-CCT GAA CCT CAG CTA CAA AC	5'-TGC CAC CTC TTA GAT TTC AT
TERT	5'-CGG AAG AGT GTC TGG AGC AA	5'-GGA TGA AGC GGA GTC TGG A
TDGF1	5'-CAG GAA TTT GCT CGT CCA TCT CGG	5'-TAG TAC GTG CAG ACG GTG GTA GTT
REX1	5'-TGA AAG CCC ACA TCC TAA CG	5'-CAA GCT ATC CTC CTG CTT TGG
Endoderm markers		
FOXA2	5'-TGT TGC AGG GAA GTC TTA CT	5'-ATG GTT TTA CAC CGA GTC AC
AFP	5'-AAG CCA CAA ATA ACA GAG GA	5'-GTC TTC TCT TCC CCT GAA GT
GLUC	5'-GGA TCT GGC AGC GCC GCG AAG ACG AGC GG	5'-TTT TCC CAT CCA TTG TGG GAC
Mesoderm markers		
FLK-1	5'-ACC ACA GTC CAT GCC ATC AC	5'-TTC ACC ACC CTG TTG CTG TA
ACTA2	5'-TGT GGC ATC CAC GAA ACT AC	5'-GGA GCA ATG ATC TTG ATC TTC A
TNNT2	5'-AGG CGC TGA TTG AGG CTC AC	5'-ATA GAT GCT CTG CCA CAG C
Ectoderm markers		
NCAM	5'-CAA AAA GGT GGA TAA GAA CG	5'-CAG GTA AGA GTG ACC TGC TC
SOX1	5'-ATG CAC CGC TAC GAC GTG A	5'-CTT TTG CAC CCC TCC CAT TT
Cell motility, normalization		
ACTB	5'-TTA GTT GCG TTA CAC CCT TT	5'-AAT GTG CAA TCA AAG TCC TC

7.2.8 SEM

Cell-scaffold constructs for SEM were fixed overnight in Karnovsky's fixative containing 2% paraformaldehyde and 2% glutaraldehyde, and dehydrated with sequential washes with 50%, 75%, 95%, and 100% ethanol. The samples were then air-dried and sputter-coated with Au/PD for observation with a JEOL 7000 SEM.

7.2.9 Immunocytochemistry

Cell-cultured constructs were fixed in 4% paraformaldehyde and washed in 0.2% Tween® 20 in PBS (PBST) for 30 min. The construct was then incubated in a 1:400 dilution of mouse monoclonal antibody to SSEA4 (Abcam) in PBST for 1 hr at room temperature. Following the incubation, the construct was washed in PBS for 30 min prior to incubation in a 1:500 dilution of

rabbit polyclonal anti-mouse antibody conjugated to FITC (Abcam) in PBS for 1 hr. Finally, the construct was counterstained with a 1:500 solution of DAPI in PBS for 10 min. The construct was then rinsed with and maintained in PBS. Microscopy analysis was performed using a Zeiss 510 Zeta Microscope (Carl Zeiss).

7.2.10 Flow cytometry

We cultured 5×10^4 hESCs on each of CA scaffolds for 21 days and hFF layers for 6 days. The cells were detached from the hFF and CA and processed for FACS analysis to detect SSEA4-positive cells. Mouse anti-human SSEA4 antibody (Abcam) and FITC-labeled rabbit anti-mouse secondary antibody (Abcam) were used at 10 μg/mL in a 3% suspension of BSA (Sigma) in DPBS (Gibco). Cells were analyzed with a BD FACSCanto flow cytometer (Becton Dickinson Biosciences).

7.2.11 hESC recovery and subculture

To recover hESCs cultured on CA scaffolds, the cell-scaffold constructs were chemically decomposed and mechanically separated from hESCs. First, the constructs were rinsed gently in hESC media to remove non-adherent cells. The constructs were then decomposed in 10 mL of 100 mM EDTA and 100 mM K_2HPO_4 solution at room temperature for 5 min, with gentle homogenization using a syringe plunger. The resultant suspension was then forced through a 100-μm pore ceramic frit (GE Healthcare) to remove scaffold debris. Finally, cells were collected by centrifugation at 200 G for 5 min, and resuspended in cell culture media. Cell viability and recovery efficiency were determined by the Trypan Blue exclusion assay (Gibco) and hemocytomer. To evaluate the proliferation of hES cells recovered from CA scaffolds, cells were serially cultured on CA scaffolds, recovered, and subcultured again on CA scaffolds. We seeded 50,000 hES cells in quadruplicate onto 13-mm diameter × 2-mm height CA scaffolds and cultured for 14 days as described in the Cell Culture and Seeding section. Proliferation was evaluated by alamarBlue (Alamar BioSciences, Sacramento, CA) as described above. After 14 days, cells were recovered and recovery efficiency determined. These recovered cells were then

subcultured onto new CA scaffolds for an additional 14 days with proliferation and recovery assessed again.

7.2.12 Animal surgery, histology, and immunohistology

Ten healthy SCID nude mice (Jackson Laboratories), weighing between 25–30 grams, were hosted by the UW Department of Comparative Medicine in the sixth floor animal facility. The animal protocol was approved by UW IACUC. Anesthesia was induced by ketamine/xylazine, and a 3 × 5 × 5-mm piece of the hESC-scaffold construct cultured for 21 days was inserted into the peritoneal cavity. The inserted construct was harvested one month later after euthanasia with CO2 gas.

The explants were preserved in 4% paraformaldehyde, fixed in paraffin wax, sectioned at 5 μm, and affixed onto glass slides. One set of tissue sections was stained with either Von Kossa, Picrosirius, or silver per standard procedures for histological analysis. Another set of tissue sections was dewaxed by three xylene washes, followed by xylene removal with methanol, and rinsed with cold water. Antigen retrieval was performed by boiling the dewaxed sections in 20 mM sodium citrate buffer, pH 6.0, for 15 min. The sections were then rinsed in cold water for 10 min to allow the antigen sites to reform. The sections were permeabilized with 0.025% Triton X-100 in PBS at room temperature for 10 min, and blocked with a solution of 10% rabbit serum and 1% BSA in PBS for 2 hrs at room temperature to prevent cross-reaction of the secondary antibody with endogenous immunoglobins in the tissue. The sections were then incubated with various mouse monoclonal primary antibodies in TBS with 1% BSA at 4^{o}C for 18 hrs. We used the primary antibodies (Abcam) against neural cell adhesion molecule (NCAM; 1:50): cardiac Troponin T (cTnT; 1:1), forkhead box 2 (FOXA2; 1:2000), alpha smooth muscle actin (α-SMA; 1:50), and glucagon (1:50).

Following incubation with the primary antibodies, the sections were rinsed twice with 0.025% Triton X-100 in PBS for 5 min, and incubated for 2 hrs at room temperature in rabbit anti-mouse IgG secondary antibody conjugated to either FITC or rhodamine fluorophores (Abcam) at 1:500

dilution in PBS. The sections were rinsed gently twice in PBS solution and counterstained in a 1:500 solution of DAPI in 0.025% Triton X-100 in PBS (Abcam) for 30 min. The sections were then rinsed with and maintained in PBS until analyzed using a Zeiss 510 Zeta Microscope (Carl Zeiss).

7.3 RESULTS

7.3.1 Synthesis and characterization of chitosan–alginate scaffolds

The porous structure of CA scaffolds was created through a process of thermally induced phase separation and subsequent solvent sublimation[35]. The as-synthesized cylindrical scaffolds were cut into sections of 13-mm diameter and 2-mm thickness for subsequent *in vitro* studies (
Figure 7-1). The CA scaffolds have a highly porous structure with interconnected pores, a porosity of ~95%, an average pore size of ~65 µm, and a narrow size distribution. The compressive and tensile modules of the scaffolds are much higher than those of pure chitosan scaffolds due to strong ionic interaction of amine groups in chitosan with carboxyl groups in alginate[35], providing a sustainable cell culture environment for hESC renewal in culture media.

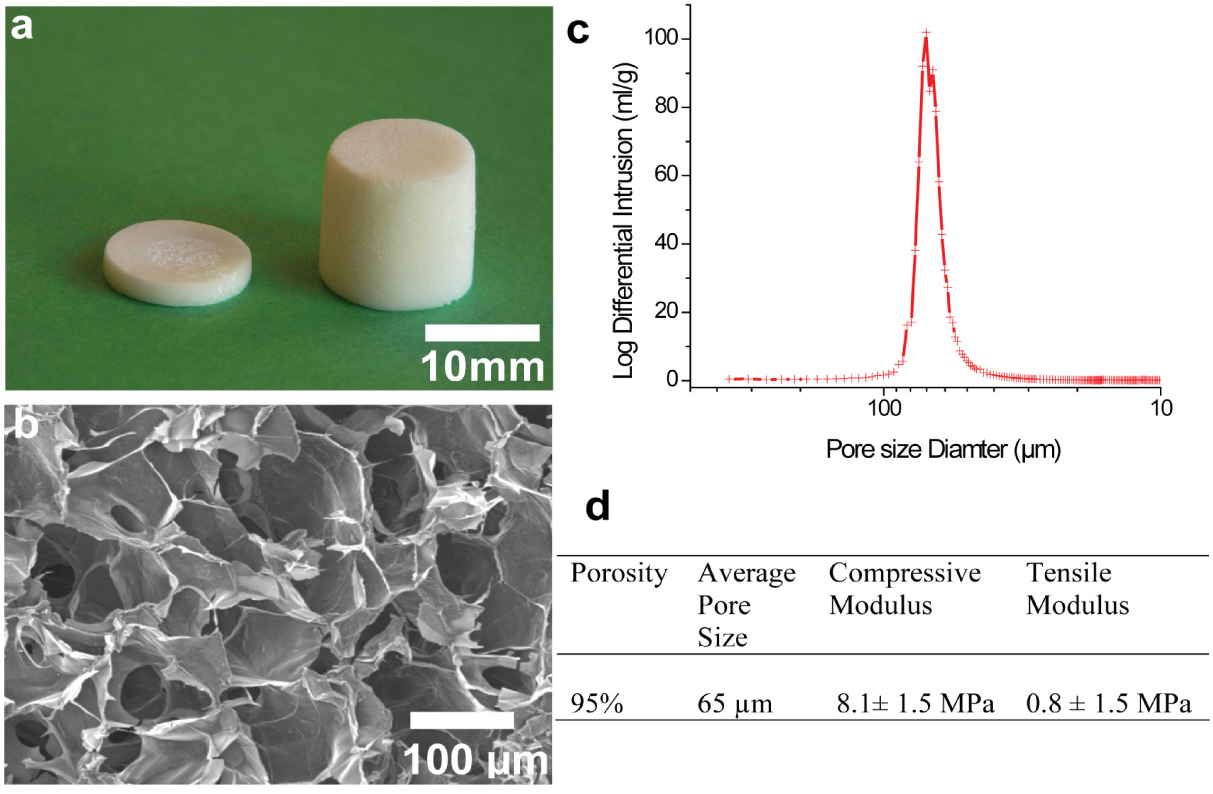

d

Porosity	Average Pore Size	Compressive Modulus	Tensile Modulus
95%	65 µm	8.1± 1.5 MPa	0.8 ± 1.5 MPa

Figure 7-1: Physical properties of CA scaffolds. (a) As-synthesized chitosan–alginate scaffolds and a scaffold section used in stem cell renewal. (b) SEM image showing the highly porous structure of the scaffold. (c) Pore size distribution of the scaffold assessed by mercury porosimetry. (d) Summary of physical and mechanical properties of the scaffold.

7.3.2 Cell proliferation and ALP activity

The self-renewal of hESC was started by directly seeding stem cells on CA scaffolds that were maintained in normal cell culture media. hESC proliferation in CA scaffolds was assessed by the alamarBlue assay and compared with hESCs cultured on hFF layers as a reference. Cell proliferation rates in both systems were comparable in the first 6 days. Thereafter, hESCs grown on hFF layers detached from the degrading hFF layers, and needed to be transferred to new culture plates with fresh hFF layers every 6 days, while hESC in CA scaffolds continued to proliferate without any need of subculturing for the entire culture period of 21 days (Figure 7-2**a**). hESC proliferation in CA scaffolds was exponential in the first 12 days, but essentially linear thereafter. We believe that this was due to the initial rapid migration and expansion of the cells as they continually occupied the inner walls of the porous structure of the scaffold, after which further expansion of the cell population was confined to within the scaffold pores. In principle, the duration of the sustained proliferation is limited only by the dimensions of the scaffold and the diffusion parameters of nutrition and metabolic exchange between the culture medium and the interconnected scaffold pores.

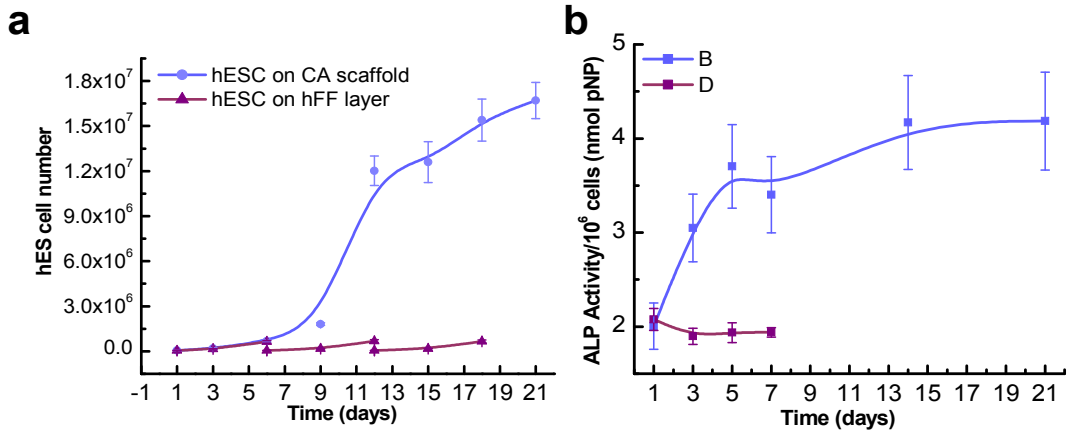

Figure 7-2: *In vitro* assessment of hESC proliferation and pluripotency in CA scaffolds. (**a**) Cell proliferation as a function of time by alamarBlue assay. The hESCs proliferated in the CA scaffold without subculturing for 21 days, while hESC on hFF layers were subcultured every 6 days. (**b**) ALP activity as a function of cell culture time.

We confirmed the undifferentiated state of the hESCs by alkaline phosphatase activity (ALP), gene activity, cell morphology, and expression of surface marker stage-specific embryonic antigen-4 (SSEA4).

Alkaline phosphatase (ALP) is a characteristic biochemical marker of undifferentiated hESCs[101,160,161]. The ALP activity (normalized to the cell number) of hESCs grown on CA scaffolds was measured over 21 days and compared with hESCs grown on hFF layers (Figure 7-2**b**). The ALP activity of hESCs in CA scaffolds increased for the first week and reached a plateau after day 15 while the ALP activity of hESCs on hFF layers demonstrated a slight initial decrease and reached a plateau at day 3. The alkaline phosphatase activity of hESCs on chitosan-alginate scaffolds cultured for 7 days without feeder cells was three times higher than that of the hESCs co-cultured with feeder cells on tissue culture plates.

7.3.3 In vitro assessment of hESC pluripotency

The gene expression patterns of hESCs cultured in CA scaffolds and on hFF layers were quantified by real-time PCR (RT-PCR). These genes have been suggested as markers of undifferentiated hESCs or their differentiated derivatives[86,162]. Among the thirteen genes evaluated, OCT 4, NANOG, TERT, TDGF 1, and REX1 are known to be associated with the pluripotent state of hESCs[163-165]. Alternatively, the lineage marker genes, including FOXA2, AFP, and Gluc for endoderm[166-168], Flk-1, ACTA2 (alpha smooth muscle actin), and TNNT2 (cardiac troponin) for mesoderm[169-171], and NCAM and SOX1 for ectoderm germ layer cells[172,173], are commonly known to be associated with differentiation of hESCs. Total RNA was harvested from hESCs grown in CA scaffolds every 7 days over 21 days and from hESCs grown on hFF feeder layers for 7 days. The transcription levels of the 13 representative genes were measured and their values are presented relative to the expressions by hESCs cultured on hFF, normalized against β-Actin expression. hESCs grown in CA scaffolds for 21 days expressed the five pluripotent marker genes (Oct4, NANOG, TERT, TDGF1, and REX1) at the levels comparable to those expressed by hESCs grown on hFF layers for 7 days (Figure 7-3). The continued expression of these marker genes suggests the persistence of pluripotent state of hESCs in CA scaffolds. The levels of lineage marker genes (FOXA2, AFP, Gluc, Flk-1, ACTA2,

TNNT2, NCAM, and SOX1) expressed by hESCs grown in CA scaffolds were also similar to the levels expressed by those grown on hFF layers.

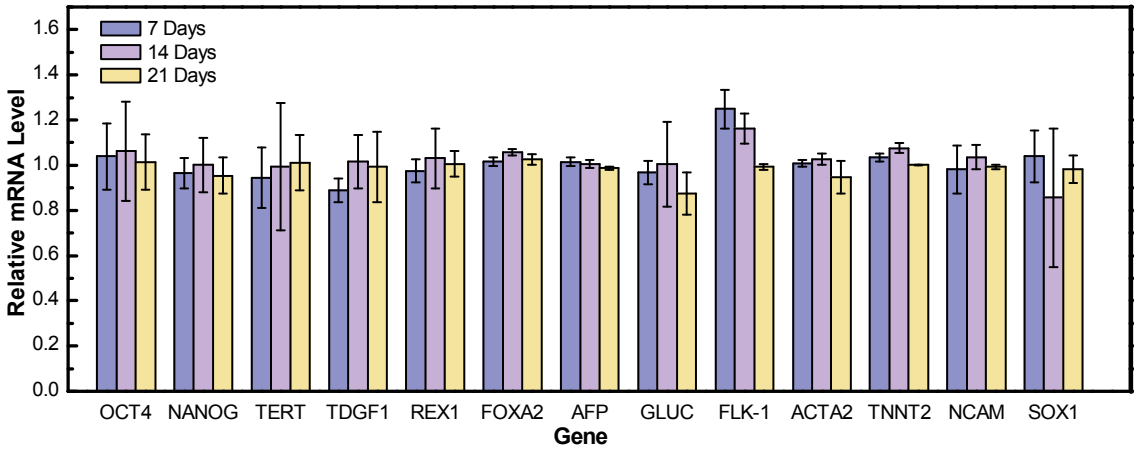

Figure 7-3: *In vitro* assessment of pluripotency of hESCs in CA scaffolds. Gene activity of hESCs cultured in CA scaffolds for 21 days, assessed by RT-PCR. The values are presented as relative to the expressions by hESCs cultured on hFF layers, and normalized against β-Actin expression. All the results are expressed as the mean ± standard deviation, n=3.

The undifferentiated state of hESCs was further assessed by immunological detection of the SSEA4, which is widely used as a surface marker of pluripotent stem cells[160], and by cell morphology examination with SEM. After 21 days of culture in CA scaffolds, hESCs were stained with DAPI (Figure 7-4**a**) and mouse anti-SSEA-4 antibody (Figure 7-4**b**). The overlaid image Figure 7-4**c**) shows that the hESCs maintained SSEA4 expression and formed dense clusters in CA scaffolds. The image at higher magnification (Figure 7-4**d**) shows no evidence of differentiated cells. Morphology of the hESCs in CA scaffolds was visualized using SEM. The cells formed dense clusters of embryoid bodies on the pore walls within the scaffold (Figure 7-4**e**), and the SEM image at higher magnification reveals a spherical shape that is the characteristic cell morphology of undifferentiated hESCs (Figure 7-4**f**). The SSEA4 level (94%) expressed by hESC cells harvested from CA scaffolds was essentially equal to that expressed by hESCs grown on hFF layers, as quantified by flow cytometry (Figure 7-4**g** and **4h**).

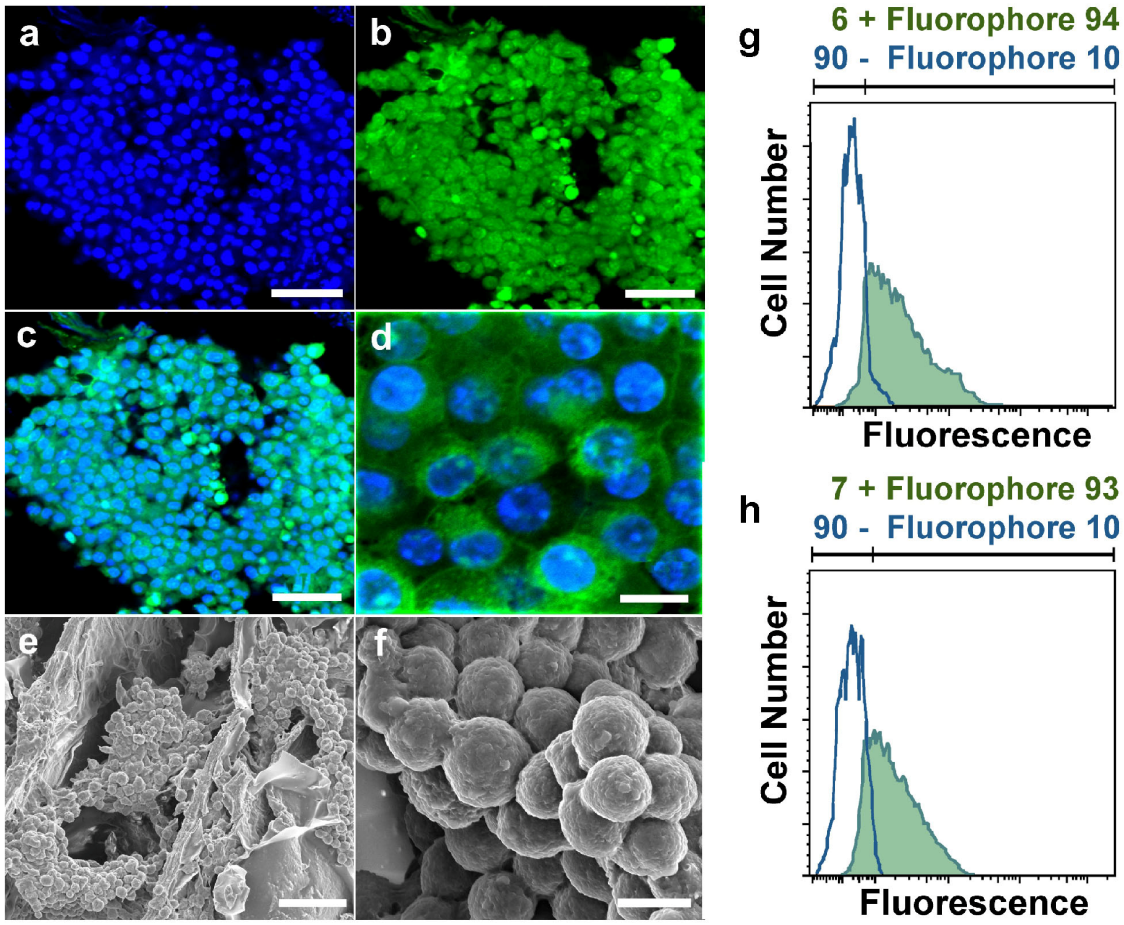

Figure 7-4: *In vitro* assessment of the undifferentiated state of hESCs, assessed by immunological detection of the SSEA 4 and cell morphology. (**a**) & (**b**) hESCs grown in CA scaffolds, stained with DAPI (blue) and SSEA 4 antibody (green), showing cell localization and SSEA4 expression. (**c**) The overlay of (a) and (b). (**d**) The overlay image at higher resolution, revealing the details of the co-localization of SSEA4 and cells. (**e**) SEM image of hESCs grown within the porous structure of CA scaffolds. (**f**) SEM image at higher magnification showing cell morphology and cluster structure. (**g**) & (**h**) The SSEA4 activity of hESCs harvested from CA scaffolds (21 days) and on hFF layers (7 days), respectively, quantified by flow cytometry. Scale bars are 40 μm for (a) to (c), 10 μm for (d) and (f), and 50 μm for (e).

7.3.4 In vivo assessment of hESC pluripotency

To assess the potential of hESCs grown in CA scaffolds to form derivatives of all three embryonic germ layers (endoderm, mesoderm, and ectoderm), cells were cultured in CA scaffolds for 21 days, and the cell-scaffold constructs of 3 mm × 5 mm × 5 mm were implanted into the abdominal cavities of SCID nude mice to induce cell differentiation and teratoma

formation. The mice were sacrificed one month following implantation. The harvested teratomas had an average diameter of 15 mm, much larger than the original implants. Although the tumor was adherent to the surrounding tissues, no invasion of adjacent organs, such as intestine, liver, or peritoneal membrane, was observed. The teratoma was grossly heterogeneous, and histological images revealed the formation of mesodermal and endodermal types of tissues including calcified regions, collagen, blood vessels, and muscle tissue (Figure 7-5). Tissues of ectodermal lineage were not obvious in histological examination of H&E and picrosirius red stained sections. Immunohistochemical fluorescent staining of teratoma sections was applied to confirm the formation of the three germ layers. Glucagon is a marker of the endoderm[168], and has been used to study hESCs differentiated into pancreatic cells[166]. Alpha smooth muscle actin, cardiac troponin (TNNT2), and FOXA2 are all mesoderm tissue markers[169-171]. NCAM was selected as a marker for detection of ectoderm formation[172]. The confocal images show various tissues labeled with antibodies (

Figure 7-6). The first column displays antibody-labeled epitopes in either red or green color, indicating the presence of specific cells/tissues. The second column shows cell localization by nuclear staining. The third column is the overlay of the first and second columns, providing the spatial relation between cell-specific epitopes and cell localization. The distinctive branched cellular network of cardiac tissue is visible with cardiac troponin-stained samples (

Figure 7-6, cardiac troponin). The images also show striated muscles (

Figure 7-6, smooth muscle) and distinct clusters of cells with strong FOXA2 expression (

Figure 7-6, FOXA2). These results confirm that the hESCs cultivated in CA scaffolds are capable of differentiation into mesodermal tissue. A distinct group of cells with glucagons expression indicates the presence of endodermal tissue (

Figure 7-6, glucagon). NCAM staining is localized within the cell-distributed area, positively showing the ectoderm formation (

Figure 7-6, NCAM).

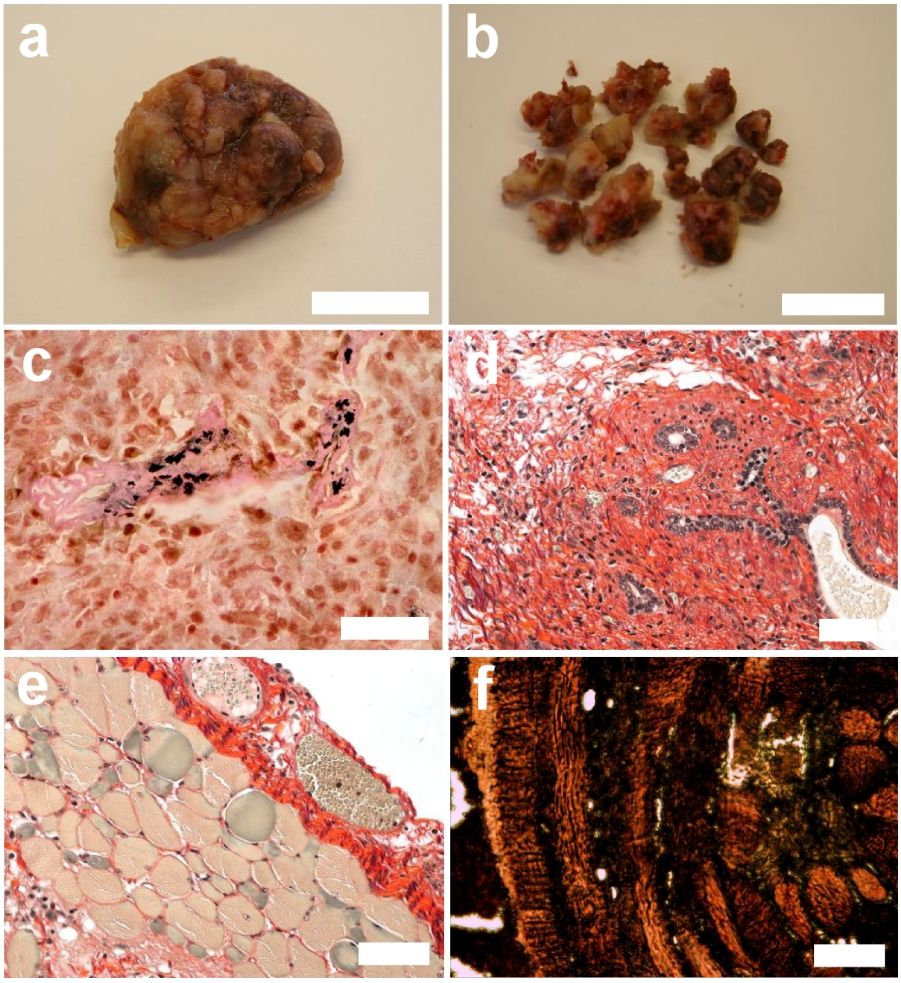

Figure 7-5: Histological analysis of teratomas retrieved after one month implantation of hESC-scaffold constructs in SCID mice. (a) An explanted teratoma (scale bar: 1 cm). (b) A dissected teratoma showing nodules of tissue (scale bar: 1 cm). (c) The explant stained with Von Kossa showing islands of calcification (black) in the center of the specimen, indicating initial bone formation (scale bar: 50 μm). The calcification suggests that mono-nucleated cells in the center may be osteogenic cell types. (d) The explant stained with picrosirius for collagen (red) and cells (dark grey) indicating the formation of dense collagen and cell-lined lumens that are similar to secretory linings (seen in other ductular tissue) (scale bar: 50 μm). (e) The explant stained with picrosirius red showing formation of blood vessels and clusters of large polygonal cells that resemble adipocytes and hepatocytes (scale bar: 100 μm). (f) The explant stained with silver showing formation of cross-striated muscle with characteristic pattern of striations (scale bar: 100 μm).

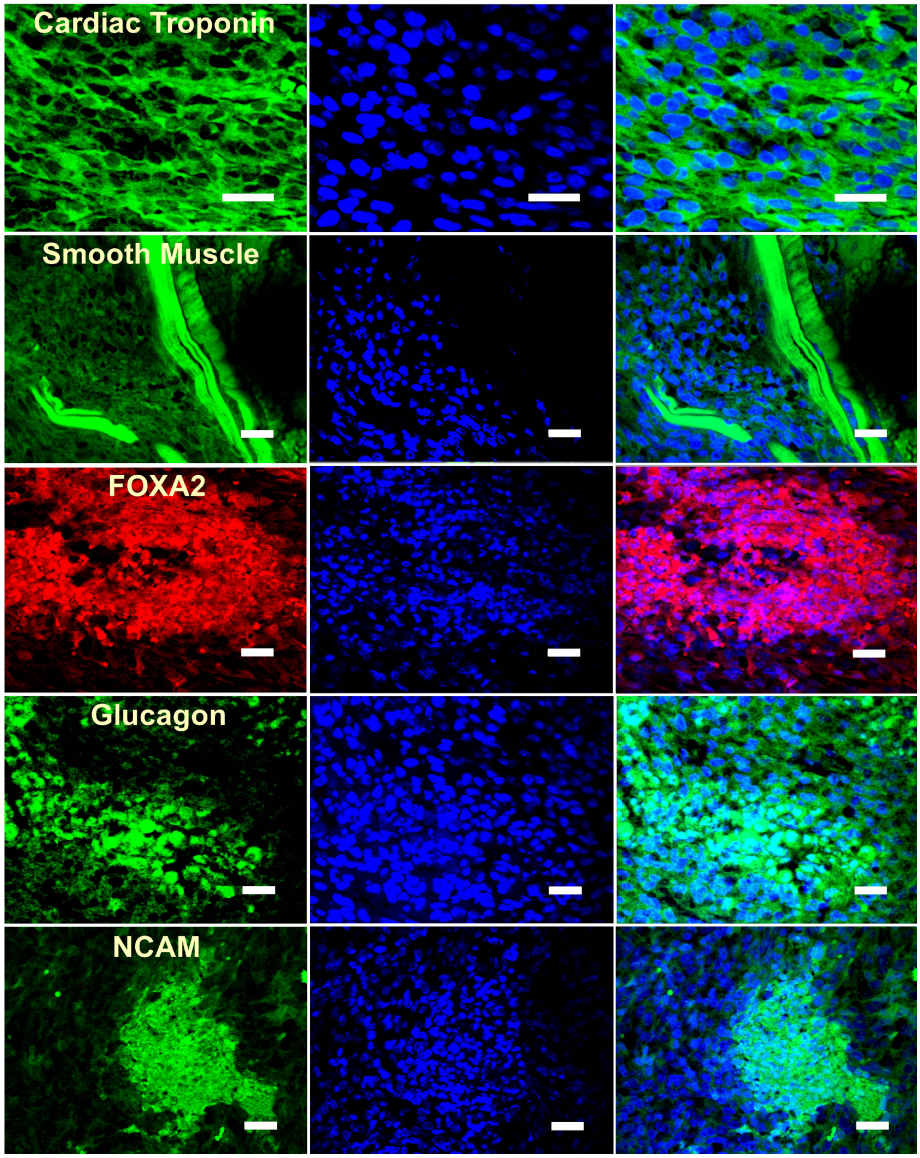

Figure 7-6: Assessment of the *in vivo* pluripotency of hESCs cultured in CA scaffolds for 3 weeks. The explants were harvested from SCID mice 1 month after implantation. Tissue sections were DAPI-stained (second column) for nuclei and immunocytochemically stained (first column) for cardiac troponin, smooth muscle actin, FOXA2, glucagon, and NCAM lineage markers. The third column is overlaid images from columns 1 and 2. Scale bars represent 20 μm.

7.3.5 hESC recovery and subculture

To further explore the capability of the present method in renewal of a large number of undifferentiated hESCs from CA scaffolds, the renewed cells were subjected to subculture and

the subcultured cells were assessed for pluripotency. Specifically, CA scaffolds seeded with an initial population of 50,000 hES cells were cultured for 14 days, and then dissolved in a solution of 100 mM EDTA and 100 mM K_2HPO_4 at room temperature. The harvested cells were then subcultured on new CA scaffolds for another 14 days. At the end of each 14-day period, hES cells were counted, cell viability was assessed by the Trypan Blue assay, SSEA4 expression was analyzed by flow cytometry analysis, and gene transcription analysis was examined by real-time PCR (RT-PCR). Cell proliferation profiles over two subsequent 14 days are shown in Figure 7-7**.** Proliferation behavior for the second 14 days (subculture) is consistent with the one in the first 14 days**.** Cell recovery yield, the number of cells harvested from the CA scaffold divided by the total number of cells in the CA, was determined by AlamaBlue. The cell recovery yields at 14 and 28 days are 85% ± 2.3 and 88% ± 2.9, respectively. Cell viability exceeded 95% after both recovery procedures. Additionally, SSEA 4 expression by hESCs culture in CA scaffolds measured by flow cytometry analysis at both intervals was found to be consistently greater than that observed on hFF (Figure 7-8). The gene expression profiles of hESC both subcultured in and released from CA scaffolds were in agreement with those in Figure 7-3 (data are not shown).

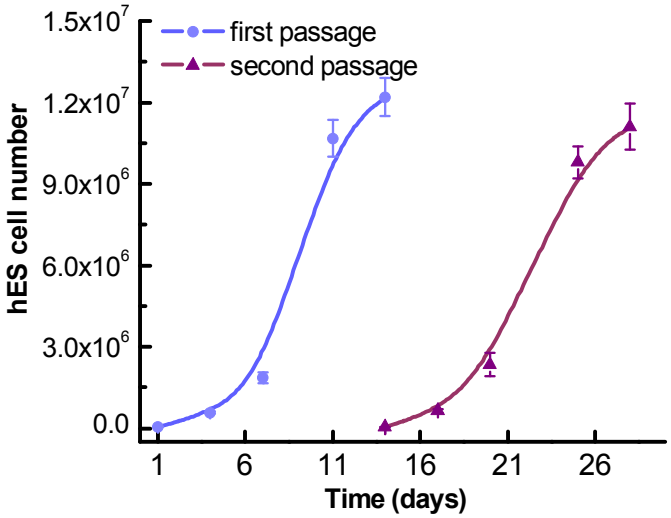

Figure 7-7: Assessment of proliferation by hESC subcultured from CA scaffolds over two passages by alamarBlue assay.

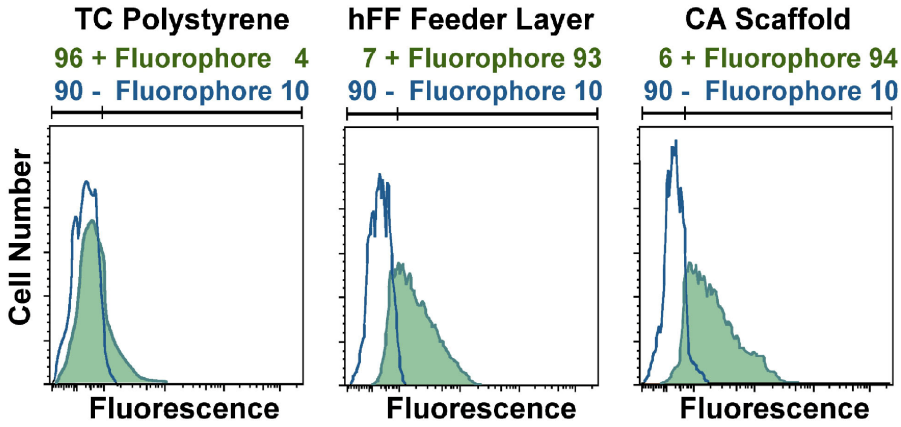

Figure 7-8: *In vitro* assessment of undifferentiated state of hESC by SSEA 4 expression. (**a**) SSEA 4 expression of hESCs harvested from hFF layers after 7 days of culture. (**b**) SSEA 4 expression of hESCs recovered from CA scaffolds after 14 days of culture. (**c**) SSEA 4 expression of hESCs recovered from CA scaffolds after 14 days of culture and subcultured for an additional 14 days.

7.4 Discussion

Via an alternative approach, we have demonstrated that CA scaffolds effectively support self-renewal of hESCs without the need of feeder cell layers or conditioned media, eliminating potential biological contamination. Our results suggest that the 3D CA porous scaffold, with the combined material properties and structural advantages, provides cues that promote adhesion and proliferation of stem cells without feeder layers in unconditioned culture media, potentially mimicking the 3D structure of native tissue. As the biocompatibility and biodegradability of CA scaffolds has been proven[35,36], CA scaffolds populated with hESCs can be directly implanted for additional *in vivo* structural support for tissue engineering. We further showed that the renewed stem cells can be easily harvested at a high yield for subculture. This method prevents problems associated with using trypsin or collagenase to release cells, by which: 1) cell function might be affected; 2) many cells cannot be detached from 3D scaffolds, resulting in a low cell yield; 3) hESCs embryoid bodies cannot be obtained.

Three-dimensional porous matrices produced from natural polymers such as chitosan and alginate have the potential to provide a reliable, low-cost solution for functional and structural restoration of damaged or dysfunctional tissues through stem cell therapy. Unlike most other

natural polymers, CA scaffold can be prepared from solutions of physiological pH, and thus growth factors can be uniformly incorporated into scaffolds during the synthetic process with less risk of denaturation[35]. Encapsulating growth factors in the scaffold matrix provides a sustained supply of the growth factors for stem cell expansion and differentiation both *in vitro* and *in vivo*, while the release rate of the growth factor can be controlled by the degradation rate of the scaffold, which is controllable by scaffold synthesis conditions.

7.5 SUMMARY

In this study, we presented a strategy that supports sustained self-renewal of hESCs by using a 3D porous natural polymer scaffold requiring no feeder cells or conditioned medium. This strategy has the potential to provide a reliable, low-cost solution for functional and structural restoration of damaged or dysfunctional tissues through stem cell therapy. Unlike most other natural polymers, CA scaffolds can be prepared from solutions of physiological pH, and thus growth factors can be uniformly incorporated into scaffolds during the synthetic process with less risk of denaturation. Encapsulating growth factors in the scaffold matrix provides a sustained supply of the growth factors for stem cell expansion and differentiation both *in vitro* and *in vivo*, while the release rate of the growth factor can be controlled by the degradation rate of the scaffold, which is controllable by scaffold synthesis conditions. This attribute can be beneficial for expanding a large number of stem cells in bioreactors, making the clinical use of stem cell therapy a reality. In addition to providing a clean environment for stem cell renewal, this strategy, with the demonstrated biocompatibility and biodegradability of chitosan and alginate, may potentially allow for the direct implantation of stem cell populated scaffolds for a broad spectrum of applications in tissue engineering and regenerative medicine.

Chapter 8: Wnt3a Induction of Human Embryonic Stem Cells on Aligned Nanofibrous Matrices for Myogenic Differentiation

8.1 INTRODUCTION

The myogenic cells in adult skeletal muscle are present in various stages of differentiation and commitment. Skeletal muscle comprises bundles of muscle fibers formed by multinucleated cells through the fusion of muscle cells into contractile myofibers[174]. Satellite cells are the predominant myoblast progenitor type, express the myogenic regulatory proteins PAX7 and MYOD, and are found interspersed among the myofibers[174]. During acute injury, the satellite cells proliferate, migrate to the wound site, and then fuse with the damaged myoblasts[111]. However, degenerative disorders, including Duchenne muscular dystrophy, which results from incorrect function of the patient's myogenic cells, cannot be treated by the native stem cell population. Instead, the transplant of healthy myogenic progenitors may be an approach to restoring muscle function via fusion with host myofibers and subsequent restoration of healthy cellular metabolism[174]. This approach requires the generation *in vitro* of large populations of myogenic progenitor cells.

Human embryonic stem cells, with their potential to proliferate indefinitely, are a promising avenue for treatment of degenerative diseases requiring systemic delivery of progenitor cells, such as muscular dystrophy. Recently, progress has been made toward the directed differentiation of hESCs into myogenic precursors via activation of the Wnt signaling pathway. However, the role of environmental cues of the extracellular matrix in hESC differentiation is largely unexplored. Here we show that by utilizing an aligned chitosan–polycaprolactone nanofiber ECM substitute we are able to enhance the myogenic differentiation of hESCs. These highly anisotropic nanofibrous matrices better replicate the *in vivo* myofibrillar microenvironment than do traditional two-dimensional culture substrates. The correlation between the expression of protein and mRNA markers of myogenic lineage and changes in both ECM and soluble factors was investigated *in vitro*. BG01v hESCs cultured in serum-free,

Wnt3a-containing media on aligned chitosan–polycaprolactone nanofibers displayed increased expression of MyoD, Myogenin, Myf5, Myf6, and MHC, markers associated with myogenic differentiation. Morphological changes including templating along nanofibers and elongation characteristics of myogenic differentiation were observed on cells cultured on aligned chitosan-PCL nanofibers. Our investigation indicates that the anisotropic properties of aligned nanofibrous substrates play a significant role in the myogenic differentiation of hESCs. The high differentiation efficiency for the myogenic lineage suggests that aligned nanofibers can potentially function as a model system for embryonic myogenesis.

In this study, we develop an *in vitro* cell culture system for the myogenic induction of hESCs that integrates soluble factors with aligned chitosan-PCL nanofibrous ECM. The myogenic behavior of BG01v hESCs were investigated in culture conditions with media that contains various soluble growth factors and with substrates of varying compositions and topologies. The use of soluble recombinant Pax3 to stimulate myogenic differentiation, likewise the combination of aligned nanofibers with soluble Wnt3a and RA, are novel approaches to induce myogenic specification in hESCs. The myogenic commitment of hESCs on aligned nanofibers was compared to those on randomly oriented nanofibers and film of the same composition serving as topographical controls, and on PCL fibers and collagen I films serving as material controls. The ability of culture conditions to regulate the myogenesis was evaluated by changes in protein and gene expression profiles, and cell morphology.

8.2 METHODS

8.2.1 Cell culture substrate fabrication

Collagen films were fabricated as previously described from freshly harvested rat tail collagen.[175] Aligned and randomly oriented chitosan-PCL nanofibers and films were fabricated as previously described using methods developed in our lab.[39] Briefly, a 5 wt% chitosan (85% deacetylated, medium molecular weight; Aldrich, St Louis, MO) solution in trifluoroacetic acid (TFA, Aldrich) was prepared by refluxing at 70°C for 3 hrs and a 10 wt% PCL solution was prepared by dissolving PCL (80,000 molecular weight, Aldrich) in 2,2,2,-trifluoroethanol (TFE, Aldrich). Chitosan and PCL solutions were then mixed at a ratio of 40:60 and vortexed to produce a working chitosan–PCL solution. The solution was electrospun at 22 kV on a rotating grounded drum (200 rpm) or a pair of grounded parallel electrodes (separation distance 4 cm), to collect randomly oriented and aligned nanofibers, respectively. Dilute solutions of chitosan (1 wt%) and PCL (1.7 wt%) were mixed at the same ratio and spin-cast to form two-dimensional films. The collected nanofiber samples were attached to 10-mm diameter coverslips using poly (L, lactide) (Boehringer Ingelheim, Germany) dissolved in hexafluoroisopropanol (Aldrich) at 3.5 wt%. To remove residual acids from chitosan–PCL, the samples were neutralized with 14% ammonium hydroxide for 5 min, followed by rinsing with a copious amount of DI water. Prior to cell culture studies, the samples were sterilized by incubating in 100% ethanol and rinsing with DI water.

8.2.2 Cell culture

BG01v hESCs (ATCC) were expanded as previously described[87] and seeded at 100,000 cells/cm^2 on either collagen I films, randomly oriented PCL nanofibers, chitosan-PCL films, randomly oriented chitosan-PCL nanofibers, or aligned chitosan-PCL nanofibers. hESCs were cultured for 24 hrs on these samples in standard proliferation culture media (ATCC) to facilitate attachment, and subsequent differentiation was induced with either proliferation media without serum (serum free media), proliferation media without serum and containing 20 nM Wnt3a

(Wnt3a$^+$, R&D Systems), 25 nM retinoic acid (RA$^+$, Sigma), or 20 nM Pax3 (Pax3$^+$, AbNova) for 48 hrs.

8.2.3 Immunostaining

For flow cytometry analysis, cells were detached from substrates with Versene (Gibco), while for immunocytochemistry studies the samples were fixed in 4% methanol-free formaldehyde in PBS for 15 min. The samples were then washed in ice-cold PBS, and the cellular membrane was permeabilized with 0.25 vol% Triton X-100 (Aldrich) in PBS for 10 min. Following permeabilization, the samples were incubated with 10% fetal calf serum (Sigma) in PBS for 30 min to block non-specific protein binding, and with primary antibodies (Abcam) at a 1:100 dilution in PBS with 0.25 vol% Triton X-100 for 1 hr at room temperature. The samples were then incubated in a 1:500 dilution of FITC-conjugated rabbit secondary antibody (Abcam) in PBS for 1 hr at room temperature. The samples were rinsed three times with PBS after each step. For flow cytometry, cells were analyzed on a FACSCanto (BD Biosciences). For confocal imaging, the samples were mounted to a coverslip with Prolong Gold Antifade reagent with DAPI (Invitrogen), cured overnight, and imaged with a confocal fluorescent microscope (Zeiss Meta 510 Confocal Microscope, Germany).

8.2.4 Real-time PCR

To extract RNA, the samples were rinsed briefly in PBS to remove serum, and processed with a Qiagen RNeasy Plus kit: the lysis buffer was pipetted firmly over the substrates to detach cells, and the Qiagen protocol was followed. The mRNA was concentrated in a 30-µl volume, and mRNA reverse transcription was performed with a Bio-Rad iScript cDNA Synthesis kit. DNA transcripts were then probed using Bio-Rad iQ SYBR Green Supermix. Thermocycling was performed with a BioRad CFX96 real-time detection system at the following conditions: 95°C for 15 min, 45 cycles of denaturation (15 s, 94°C), annealing (30 s, 55°C), and extension (30 s, 72°C). The relative expression of each gene (Table 2) was normalized by the GAPDH gene expression.

Table 2: Myogenesis PCR primers

Gene symbol	Forward Primer	Reverse Primer
OCT4	5'-CTTGCTGCAGAAGTGGGTGGAGGAA	5'-CTGCAGTG GGGTTTCGGGCA
Wnt1	5'-TCTCTGTCGTGGAGCCATTGAACA	5'-AACTCGTGGCTCTGTATCCACGTT
Wnt3a	5'-GCATCAAGATTGGCATCCAGGAGT	5'-TGCACATGAGCGTGTCACTGCAAA
Wnt7a	5'-GGGCGCAAGCATCATCTGTAACAA	5'-GCCATTGCGGAACTGAAACTGACA
Pax3	5'-TGTTCAGCTGGGAAATCCGAGACA	5'-GTCGATGCTGTGTTTGGCCTTCTT
Pax7-1	5'-TGAAGTCCAGCCAGATGGAACAGT	5'-TGTTGGAGCCATAGTACGGAAGCA
Myf5	5'-TGCCCTTGTTAATTACCGGAGCGA	5'-TATGCAGGAGCCGTCGTAGAAGTA
Myf6	5'-AGAAGTGGCAGAAGGCTCTCCTTT	5'-TCTTGCAAGCCCAGATCAGACACT
MyoD1	5'-TGTAGCAGGTGTAACCGTAACCCA	5'-ATTCCCTGTAGCACCACACACCAT
MYOG	5'-GCCTTGATGTGCAGCAACAGCTTA	5'-AACTGCTGGGTGCCATTTAAACCC
MHC (MHY1)	5'-AAGAGATGGCGGGTCTGGATGAAA	5'-TGGTCAGGGTGTTGACTTTGTCCT

8.2.5 Scanning electron microscopy

Samples were removed from media after 3 days of culture, rinsed with PBS, and fixed with Karnovsky's fixative overnight. After fixing, samples were briefly rinsed with DI water and dehydrated with sequential rinses with 50, 75, and 100% ethanol for 15 min each. Samples were sputter-coated with Au/Pd for 30 s at 18 mA and imaged with SEM.

8.2.6 Statistical Methods

Statistical analyses were performed using one-way analysis of variance (ANOVA). We considered p values less than 0.05 statistically significant, and differences between samples within a group were evaluated using a Student's t-test ($p < 0.05$).

8.3 RESULTS

8.3.1 Identification of myogenic conditions

To identify prospective combinations of an ECM-like substrate and soluble growth factors for the myogenic differentiation of hESCs, we examined the expression of the myogenic marker protein MyoD[176]. MyoD is a myogenic transcription regulatory factor that plays an early role in myogenic differentiation and is commonly used to identify myogenic progenitors[84,177-179]. Flow cytometry was used to evaluate the percentage of cells expressing MyoD 48 hrs after induction in 25 microenvironments with each consisting of a substrate (random PCL fibers, Collagen I film, random chitosan-PCL (C-PCL) fibers, C-PCL film, or aligned C-PCL fibers) and a growth media treatment (Wnt3a, RA, Pax3, serum-free media, or standard cell culture media) (Figure 8-1**)**. The growth factor set was chosen as they are involved in the myogenic activation and muscle development. Soluble Wnt3a addition is known to activate the Wnt pathway and induce activation of the myogenic differentiation genes[32], including MyoD, myogenin, Pax7, and Myo5. Pax3 is a transcription factor that contributes to muscle development[180,181] and has successfully induced differentiation of hESCs into the myogenic fate[120]. Retinoic acid upregulates Pax3 and MyoD expression, initiating myogenesis[182]. As shown in Figure 8-1**a**, C-PCL materials supported more cells with MyoD expression than those on the PCL and collagen controls, with a maximum of ~22% on aligned C-PCL nanofibers in $Wnt3a^+$ media. $Wnt3a^+$ media consistently induced a higher degree of MyoD expression of cells than did the other media (RA, Pax3, no serum, standard media) for all the substrate materials tested. Among the substrates tested in the serum-free medium containing $Wnt3a^+$, the C-PCL material substrates induced greater MyoD expression than did random PCL fibers or collagen substrates I (Figure 8-1**b**). For hESCs cultured on aligned C-PCL nanofibers, RA^+, $Pax3^+$, and standard media treatments induced lower levels of MyoD expression than did the serum-free condition, which in turn was less effective than the $Wnt3a^+$ treatment (Figure 8-1**c**). The combination of $Wnt3a^+$ media and C-PCL materials were identified as the most effective environments for the induction of MyoD expression in BG01v hESCs and were further investigated.

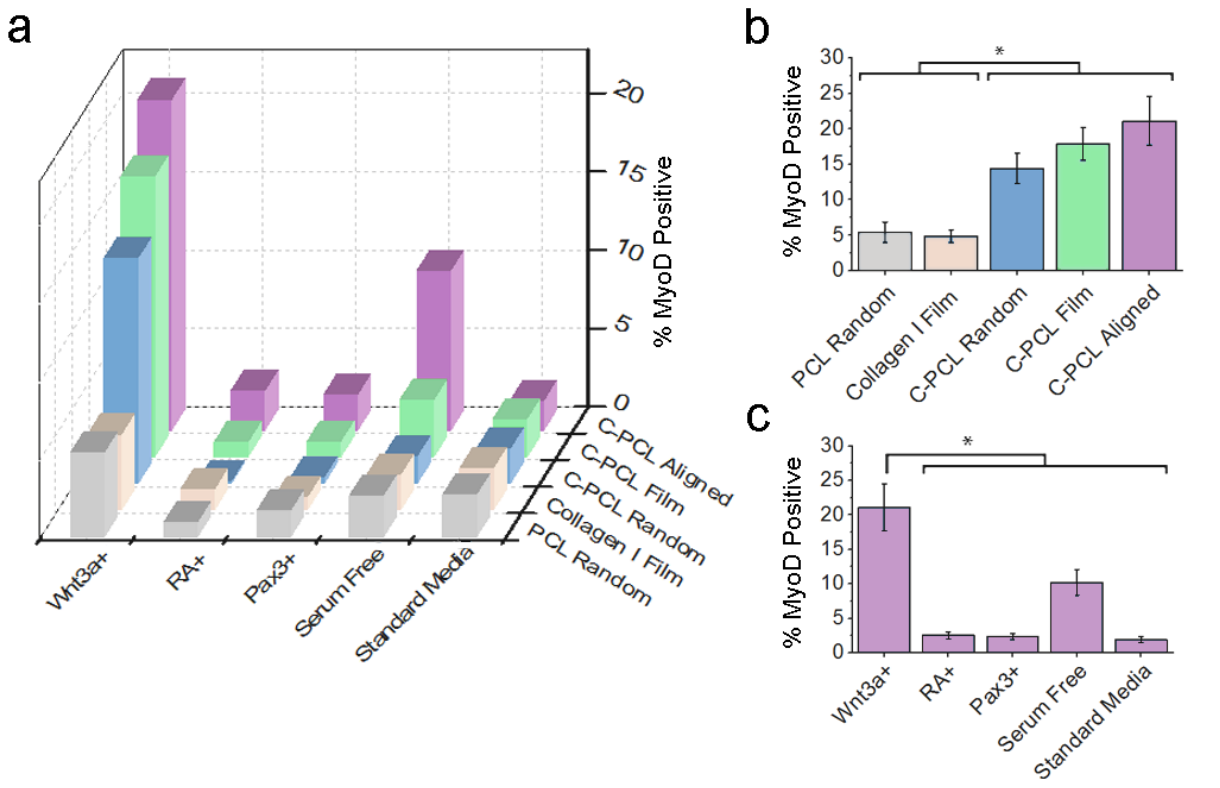

Figure 8-1: Flow cytometry analysis of the combinatorial effect of cell culture conditions including random PCL fiber, Collagen I film, random C-PCL fibers, C-PCL film, or aligned C-PCL fibers, and one media type, either Wnt3a+, RA+, Pax3+, serum-free media, or standard cell culture media (medium and substrate types) on MyoD expression of human embryonic stem cells. (a) Populations of BG01v hESCs that express MyoD 48 hrs after culture in various media formulations and substrate materials. Population values along (b) Wnt3a and (c) aligned C-PCL nanofiber conditions. Results are mean ± SD, and * indicates that at each of the means in that group is statistically different from all means in the other group, $p < 0.05$, n = 3.

8.3.2 Morphological Analysis

SEM images were acquired to examine hESC morphology in controlled micro-environments (Figure 8-2a). After 48 hrs of culture in standard media, hESCs retained a spherical morphology on all substrates (Collagen I, C-PCL film, and C-PCL aligned). Specifically, hESCs displayed stacked cell colonies on collagen I and C-PCL aligned (Figure 8-2**a**), but loosely dispersed as single cells on C-PCL films, indicating reduced initial adhesion and limited colony formation on the film (Figure 8-2**a**). hESCs cultured on all substrates in Wnt3a$^+$ medium displayed

significantly different morphologies (Figure 8-2**b**) than in standard media. On collagen I, cells displayed spherical and spindle morphologies. On C-PCL films, hESCs exhibited a more spread and flattened morphology. Notably on C-PCL aligned nanofibers, hESCs displayed an elongated morphology along the orientation of the aligned nanofibers, with a few spherical cells adhered to the surface of the aligned cells.

To further illustrate the ability of ECM topology to direct hESC alignment, cellular alignment was quantified by SEM image analysis. The direction of each hESC was defined as an angle value relative to the orientation of the aligned nanofibers. Quantitative morphometric analysis confirmed that ECM topology can direct hESC alignment (Figure 8-2c). Long-range alignment of hESCs was observed on C-PCL aligned. In contrast, no long-range order was observed in hESCs cultured on collagen I or C-PCL film.

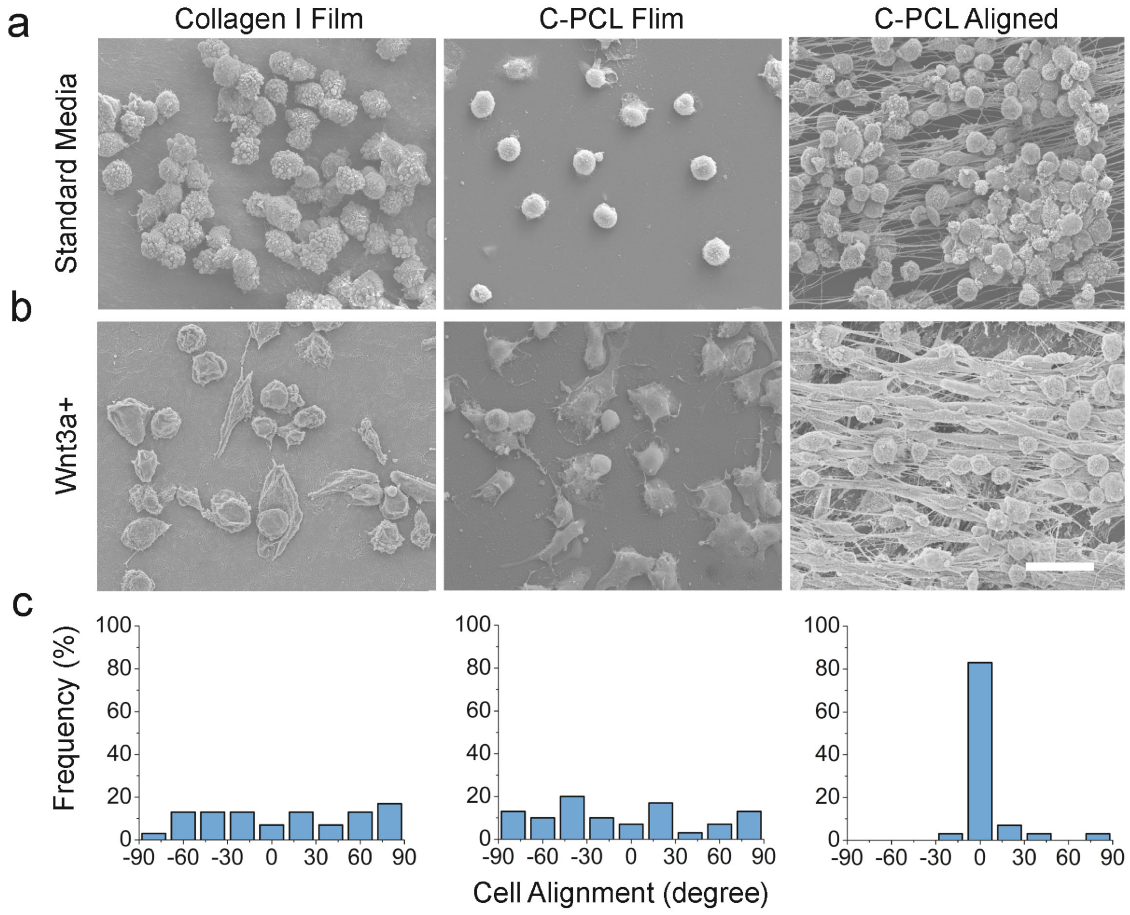

Figure 8-2: SEM images showing the morphology of hESCs cultured in different controlled conditions. hESCs were cultured on either collagen I (left column), C-PCL films (middle column), or C-PCL aligned (right column) for 48 hrs (a) in standard medium or (b) in $Wnt3a^{+}$ medium. The scale bar represents 25 µm. (c) Normalized histograms of hESCs orientation after 48 hrs of culture in $Wnt3a^{+}$ medium.

8.3.3 Gene expression analysis

The change in myogenic gene transcription is indicative of myogenic differentiation. Real-time PCR was performed to examine the myogenic gene expressions of hESCs cultured in controlled micro-environments (Figure 8-3). Seven marker genes (Pax3, Pax7, My5, My6, MyoD, myogenin, and MHC) associated with myogenic differentiation were examined. Pax 7, a paired box transcription factor, is essential for satellite cell formation and particularly important for satellite cell function[124]. Myf5 is the earliest marker of myogenic activity, followed by Myf6 and

MyoD[183]. MyoD signaling upregulates myogenin activity, while activities of both MyoD and myogenin genes are upregulated by Myf5 and Myf6 activities[183]. Myogenin activity is a later regulator of the myogenic program and is necessary for the expression of muscle structural protein MHC[183]. When hESCs were cultured on collagen I in $Wnt3a^+$ medium, only three of the examined genes (Pax3, Pax7, and MyoD) were elevated as compared to those cultured in standard and serum-free media (Figure 8-3**a**). hESCs cultured on PCL randomly oriented nanofibers displayed myogenic gene expressions similar to those on collagen I (Figure 8-3**b**). On C-PCL films, hESCs showed significant up-regulation of all myogenic gene expressions except MHC (Figure 8-3**c**). hESCs on C-PCL randomly oriented nanofibers display increased myogenic gene expressions except for Myf6 as compared to standard and serum-free media when cultured in $Wnt3a^+$ medium (Figure 8-3**d**). Notably, on C-PCL aligned nanofibers, hESCs showed significant increases in the expressions in all myogenic genes in both serum-free and $Wnt3a^+$ media as compared to hESCs cultured in standard (Figure 8-3**e**).

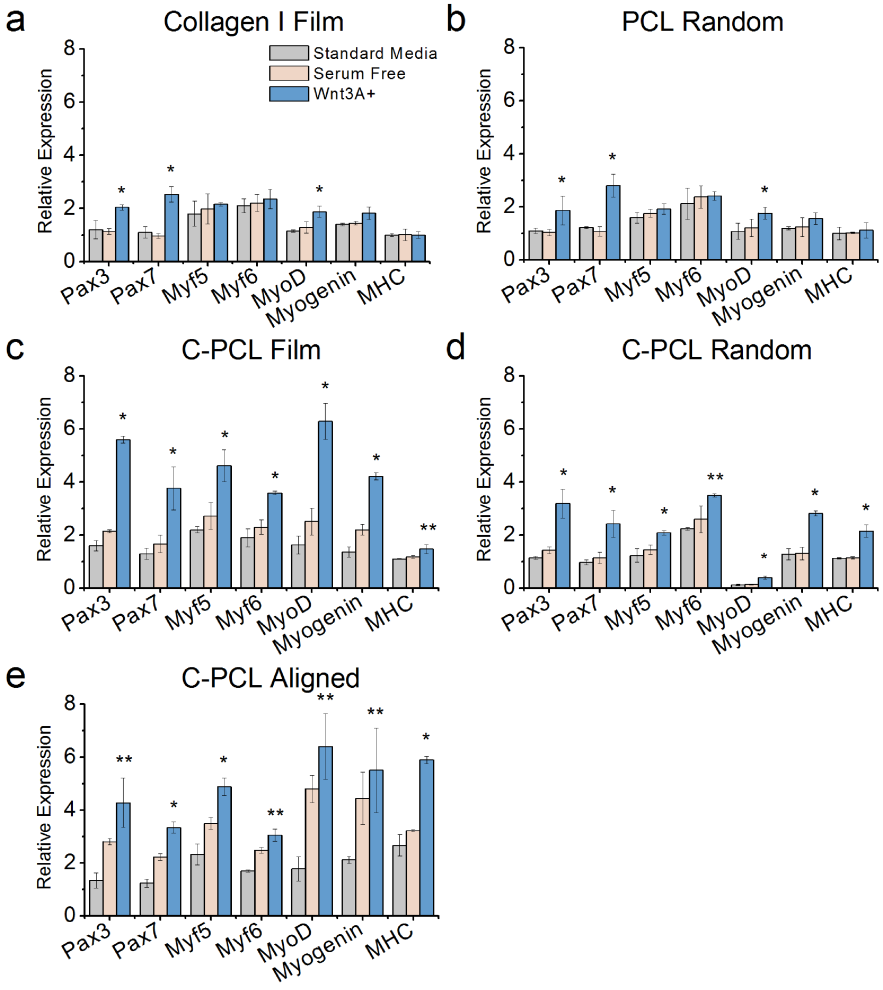

Figure 8-3: Myogenic gene expressions of hESCs cultured for 48 hrs on (a) collagen I, (b) PCL randomly oriented fibers, (c) C-PCL films, (d) C-PCL randomly oriented fibers, and (e) C-PCL aligned fibers in standard medium, serum-free medium, and Wnt3a^{+} medium. The values are presented as relative to the expression of GAPDH. All the results are expressed as the mean ± SD; * indicates the value is statistically different from the other in the same group; ** indicates the value is statistically different from the standard media value in that group, $p < 0.05$, n = 3.

The mRNA expression of genes associated with pluripotency and Wnt signaling pathway of hESCs was also evaluated by real-time PCR (Figure 8-4). OCT4 is a hallmark gene of hESC pluripotency, and the decreased OCT4 expression indicates differentiation[184,185]. Wnt1, Wnt3a, and Wnt7a are known as gatekeepers of the myogenic program, and their elevated expression indicates myogenic differentiation[32,33,178]. When cultured in Wnt3a^{+} medium, hESCs on all

substrates showed a small, but not statistically significant, decrease in OCT4 expression compared to hESCs cultured in standard and serum-free media. For hESCs cultured on collagen I (Figure 8-4**a**) or PCL randomly oriented nanofibers (Figure 8-4**b**) in the Wnt3a^{+} medium, an elevated expression of Wnt3a was observed compared to cells cultured in standard or serum-free media. When cultured on C-PCL films in Wnt3a^{+} media ((Figure 8-4**c**), hESCs showed increased expressions of both Wnt3a and Wnt7a compared to those cultured in both standard and serum-free, indicating the occurrence of myogenesis[33]. hESCs on C-PCL random induced statistically significant increases in expressions of Wnt1, Wnt3a and Wnt7a genes when cultured in Wnt3a^{+} medium (Figure 8-4**d**), which is expected at the onset of myogenic differentiation[30,32,33,186]. C-PCL aligned were uniquely able to induce increased expressions of Wnt related genes of hESCs when they are cultured in both serum-free and Wnt3a^{+} media compared to those cultured in standard media (Figure 8-4**e**).

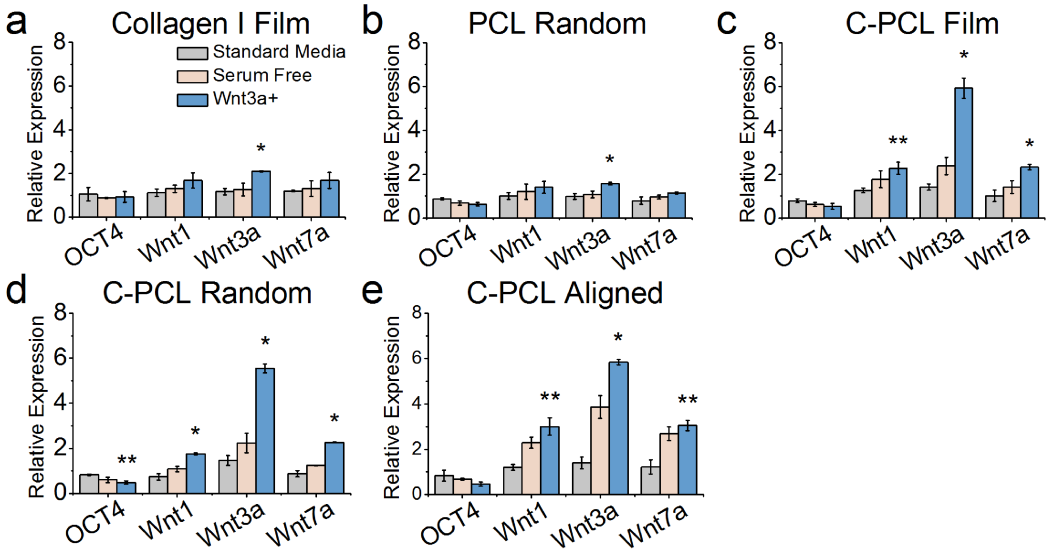

Figure 8-4: Pluripotency and Wnt signaling pathway assessment of hESCs cultured for 48 hrs on (a) collagen I, (b) PCL randomly oriented fibers, (c) C-PCL films, (d) C-PCL randomly oriented fibers, and (e) C-PCL aligned fibers in either standard medium, serum-free medium, or Wnt3a^{+} medium. The values are presented relative to the expressions of GAPDH. All the results are expressed as mean ± SD; * indicated the value is statistically different from the other in the same group; ** indicates the value is statistically different from the standard media value in that group, $p < 0.05$, n = 3.

8.3.4 Protein expression analysis

After gene transcription into mRNA, depending on downstream processing, the mRNA may translate into functional proteins. To examine the distribution of myogenic marker proteins in different culture micro-environments, hESCs were immunofluorescently stained for Myf5, Myf6, MyoD, myogenin, and MHC (FITC, green), and counterstained for cell nuclei (DAPI, blue). As expected, fluorescence images of hESCs cultured on both collagen I (

Figure 8-5**a**) and C-PCL aligned (

Figure 8-5**b**) for 48 hrs showed weak protein expressions of myogenic marker genes. These results suggest that nanofibers alone could not enhance myogenic differentiation.

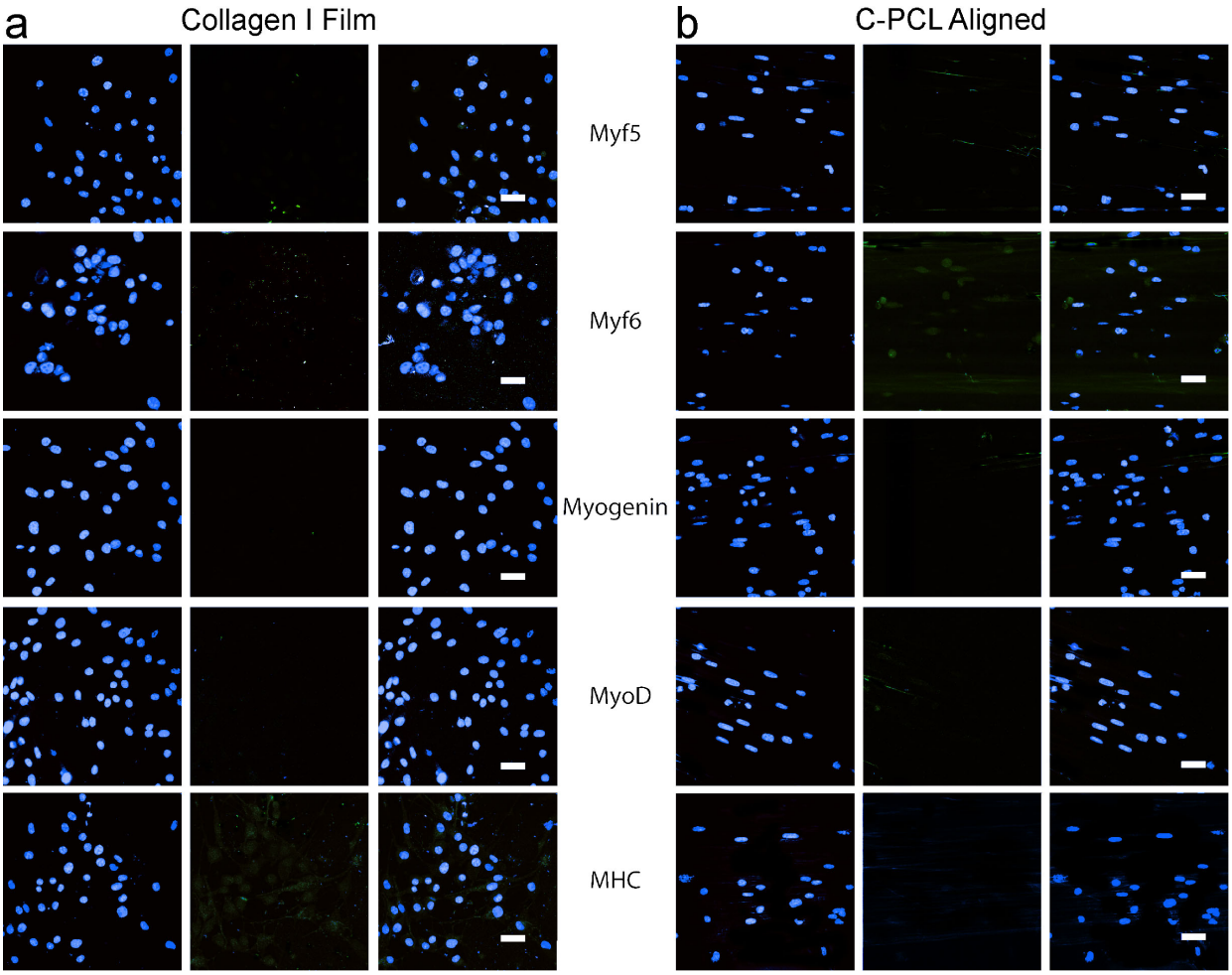

Figure 8-5: Immunochemical analysis of hESCs cultured for 48 hrs in standard conditions. hESCs were cultured on collagen I (left) or aligned C-PCL nanofibers (right). Cells were stained with DAPI to identify nuclei (blue), and specific antibodies to the proteins of interest (green). DAPI images (column 1) and specific antibody images (column 2) were merged (column 3) to illustrate co-localization of protein targets to cellular nuclei. Scale bars represent 20 μm.

When cultured in Wnt3a^{+} medium, the myogenic marker proteins of hESCs highly expressed on both collagen I (

Figure 8-6**a**) and C-PCL aligned (

Figure 8-6**b**). In contrast, hESCs cultured on C-PCL films displayed no expression of myogenic proteins (absence of green color) in either standard medium or Wnt3a^{+} medium (

Figure 8-7). In addition, MHC expression was only faintly visible in hESCs cultured on collagen I (

Figure 8-6**a**), but was highly expressed in hESCs cultured on C-PCL aligned (

Figure 8-6**b**).

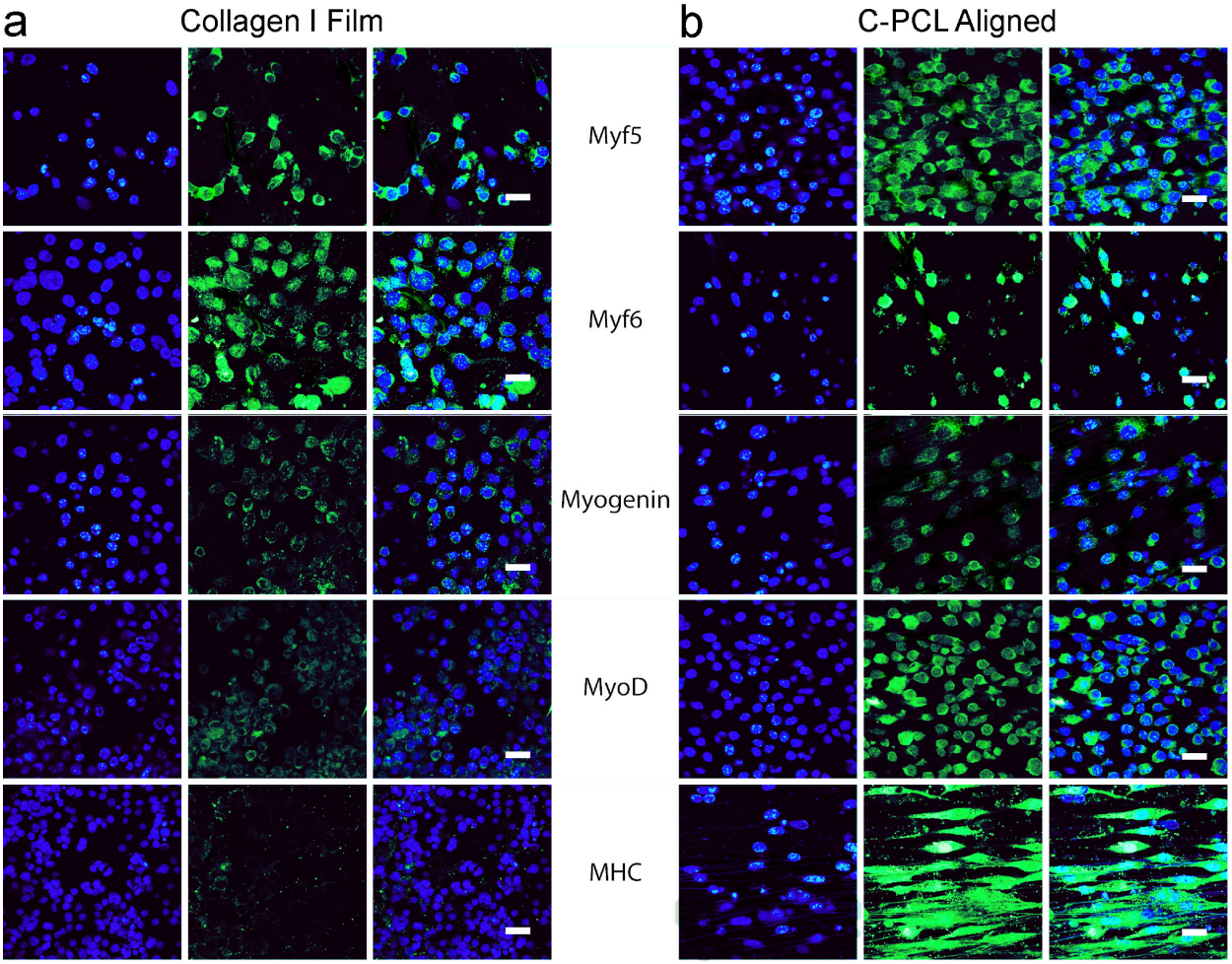

Figure 8-6: Immunochemical analysis of hESCs cultured for 48 hrs in differentiating conditions. BG01v cells were cultured on either collagen I (left) or aligned C-PCL nanofibers (right) in media containing Wnt3a. Cells were stained with DAPI to identify nuclei (blue), and specific antibodies to the proteins of interest (green). DAPI images (column 1) and specific antibody images (column 2) were merged in column 3 to illustrate co-localization of protein targets to cellular nuclei. Scale bars represent 20 μm.

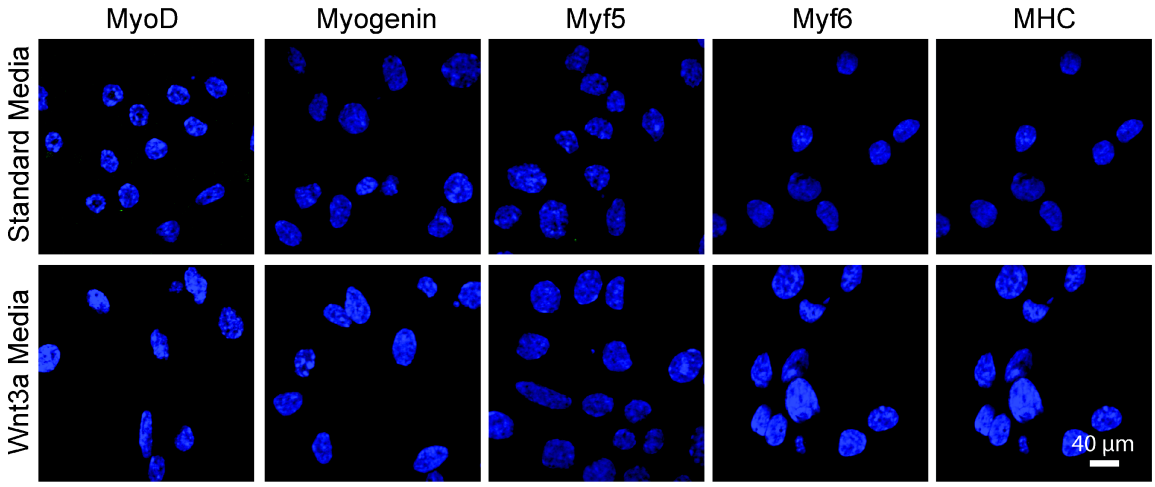

Figure 8-7: Immunochemical analysis of hESCs cultured for 24 hrs in standard media, and 48 hrs in Wnt3a^{+} differentiating conditions on C-PCL films. Cells were stained with DAPI to identify nuclei (blue), and specific antibodies to the proteins of interest (green).

Flow cytometry was then used to quantify the myogenic protein expression of hESCs (
Figure 8-8). Myf5 expression was detected in 83% of hESCs cultured on C-PCL aligned, while only in 18% of hESCs on collagen I. Myf6 expression was also observed in 91% of hESCs cultured on C-PCL aligned, compared to 21% on collagen I. Myogenin expression was detected in 81% of hESCs cultured on C-PCL aligned, compared to 24% on collagen I. Finally, MHC expression was detected in 63% of hESCs cultured on C-PCL aligned, compared to 4% on collagen I. Together, these results indicate that culture on aligned nanofibers in the presence of Wnt3a promotes the directed myogenic differentiation of hESCs.

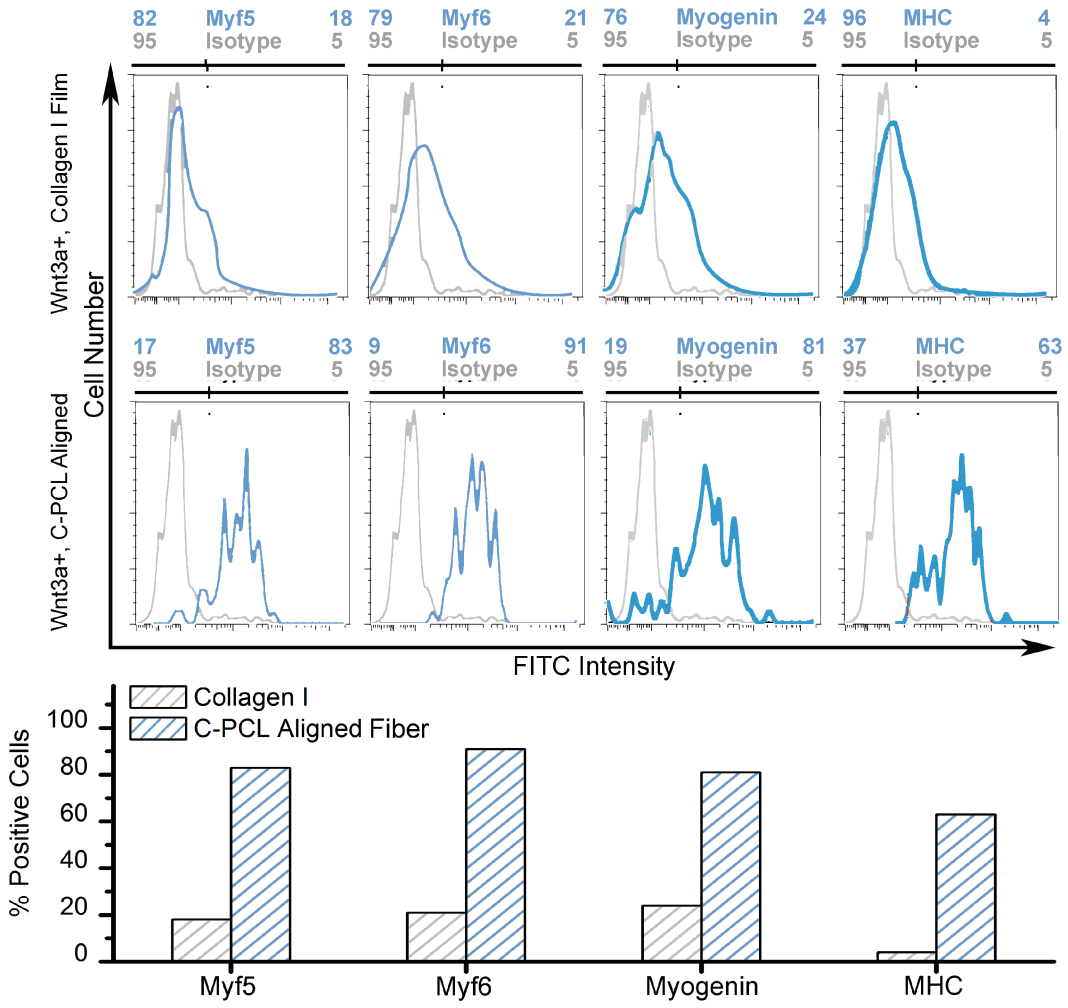

Figure 8-8: Myogenic protein expressions of hESCs cultured for 48 hrs in Wnt3a^{+} medium on collagen I films (top row) and C-PCL aligned nanofibers (middle row) as assessed by flow cytometry. hESCs were stained against Myf5, Myf6, myogenin, and MHC (red peaks), compared with hESCs stained with isotype-IgG as negative controls (black peaks). Population percentage of hESCs stained positive by specific proteins are presented graphically (bottom row).

8.4 Discussion

The study of myogenic differentiation of hESCs and the successful use of hESC-derived myoblasts for clinical applications will require highly efficient differentiation into the relevant cell types. In the work presented here, a novel myogenic differentiation system was developed using a combination of an aligned C-PCL nanofibrous scaffold and a soluble Wnt3a signaling factor. Here we have demonstrated a myogenic microenvironment capable of inducing greater

expression of MHC in hESCs than previously reported, while also avoiding the use of gene transfection or lengthy differentiation periods.

Our initial screening of candidate myogenic conditions was based on expression of the MyoD protein (Figure 8-1), an early marker for myogenic commitment[179]. Serum-free media resulted in notable increases in MyoD expression compared to proliferation media, specifically in hESCs cultured on C-PCL film and aligned C-PCL fibers, which is consistent with previous studies where serum-free media induced myogenic differentiation[83]. MyoD expression was not elevated in either $Pax3^{+}$ of RA^{+} treatments at the 48-hr time point, suggesting that these growth factors stimulate slower action of differentiation pathways. This finding is consistent with the observation that the addition of either Pax3[11-13] or RA[182] induce myogenic differentiation over the span of weeks. The addition of soluble Wnt3a elevated MyoD expression for all conditions after only 48 hrs of treatment, but not uniformly. In a separate study, less than 9% of the hESCs cells were MHC+ after 25 days induction in RA[187]. While Wnt3a has been repeatedly observed to play a key role in regulating myogenesis[28,30-32,179]. our findings further suggest that the degree of the myogenic response is highly dependent on the combination of both soluble signals and interaction with an ECM-like matrix. Increasingly, the cellular microenvironment has been found to affect cell behavior and fate[24,126]. The combination of C-PCL materials and Wnt3a induced greater increases in MyoD activity than any other combination tested, suggesting a synergistic interaction between the signaling pathways leading to myogenic commitment.

Visualization of cell morphology by SEM revealed significant differences between conditions before and after induction of differentiation (Figure 8-2). Collagen I films, C-PCL films, and aligned C-PCL fibers are particularly illustrative when compared to each other; these three materials represent, respectively, a common myogenic and tissue engineering substrate[37,38,127,188,189], a topologically featureless two-dimensional C-PCL surface, and an aligned C-PCL fiber matrix with both ECM-scale topology and long-range anisotropy. After 24 hrs in standard media, hESCs in all conditions continue to exhibit spherical morphology typical of undifferentiated BG01v[190]. However, hESC adhesion to C-PCL film was poor, with minimal cell spreading. Forty-eight hours after the induction of differentiation in $Wnt3a^{+}$ media, the topology-induced guidance of the hESC was more evident. While elongated and spread hESCs

were evident on both collagen I and C-PCL films, the orientation of the cell elongation is random. In contrast, hESCs on aligned C-PCL fibers were nearly entirely elongated and aligned parallel to the fiber direction. These images suggest that the majority of hESCs cultured on the aligned C-PCL fibers differentiated rapidly under the morphogenetic guidance of the fibers, as has been similarly observed in other studies of cell differentiation on fibers[38-40,71,191]. Thus, the topology of the C-PCL ECM replacement was a critical factor for the rapid myogenic differentiation of hESCs.

The expression of myogenic protein markers was significantly different between 24 hrs in proliferation media (

Figure 8-5) and 48 hrs in differentiation media (

Figure 8-6). As anticipated from the cell morphology results, expression of myogenic markers after culture in proliferation media was only minimally observed in either collagen I or aligned C-PCL fiber cultured cells. Quantitative assessment of myogenic protein expression (Figure 8-8) in differentiating conditions corroborated immunohistological observations (

Figure 8-6). Significantly, while MyoD, myogenin, Myf5, and Myf6 expression were observed in hESCs cultured on both collagen I and aligned C-PCL fibers, expression levels of these proteins were consistently elevated in the aligned C-PCL fiber condition. MHC expression was detected only in hESCs cultured on aligned C-PCL fibers, suggesting that terminal myogenic differentiation was achieved only in the aligned fiber extracellular environment.

Myogenic gene expression profiles of hESCs cultured in varying media conditions and substrates mimicking the ECM highlight the significant additive effects of appropriate microenvironmental signals toward myogenic differentiation. Comparing standard media, to serum-free media, and $Wnt3a^{+}$ media, increasing myogenic activity can be observed in the transition from 2D to randomly oriented nanofibers, and then to aligned nanofibers (Figure 8-3). Interestingly, in the highly myogenic aligned C-PCL fiber condition, both serum-free and $Wnt3a^{+}$ differentiating media induced similar magnitudes of myogenic protein expression, suggesting that in this case, the influence of the ECM dominated the role of soluble factors in regulating the myogenic program. When examining genes relating to pluripotency and embryogenesis, we observed

similar patterns in changes to gene expression from the combination of soluble and matrix factors (Figure 8-4). Expression of the pluripotency marker OCT4 declined slightly, but progressively in increasingly complex differentiating microenvironments. Wnt signaling via β-catenin likely acts as a molecular switch that regulates the transition from cell proliferation to myogenic differentiation[33], while concurrently, Wnt7a activation is implicated in the symmetric expansion of ES[186], which may allow for the greater density of cells in highly differentiated aligned C-PCL fiber cultures as observed in SEM.

Though the Wnt pathway is important for myogenic differentiation, the effect of soluble Wnt factors in media cultures systems have not been investigated. Importantly, in this study we demonstrated the first implementation of Wnt3a-soluble media condition and aligned ECM-like material to induce myogenic differentiation of upwards of 63% of hESCs. The efficient and fast commitment of hESCs to myogenic progenitors on the aligned C-PCL illustrates the promise of a tailored microenvironment with appropriate soluble growth factors for treatment for muscle injury.

8.5 SUMMARY

We have demonstrated a novel approach for the rapid, highly efficient differentiation of hESCs into myogenic precursors using a combination of soluble Wnt3a and aligned C-PCL nanofibers. The unique topology of the aligned nanofibers significantly increased expression of mRNA and protein markers of myogenic differentiation, resulting in hESCs terminally differentiated to the myogenic lineage based on gene expression analysis of MHC. This cell culture system would facilitate studies of myogenesis by shortening experimental times, and serving as a consistent model of embryonic myogenesis. In addition, the system can be used to quickly generate large populations of highly committed myogenic progenitors, which are necessary for any cell-based therapy. Taking into consideration the demonstrated biocompatibility of chitosan and PCL, this work may allow for the direct construction of myogenic progenitor constructs for a broad spectrum of applications in tissue engineering and regenerative medicine.

Chapter 9: Tenogenic Differentiation of Human Bone Marrow Stem Cells on Aligned Nanofibrous Matricies

9.1 INTRODUCTION

In this study, we investigate whether C-PCL nanofibers in combination with TGF-β3 growth factor can provide an adequate environment that can significantly improve and accelerate the tenogenic differentiation of BMSCs. TGF-β3, a member of the transforming growth factor beta protein family, is essential for tendon progenitor cell maintenance and tenocyte function regulation[156,157]. It was demonstrated that inhibition of TGF-β3 signaling with SB-431542 prevented the formation of tendon-like tissue from BMSCs[146]. TGF-β3 negative mice embryos do not develop tendons in the limbs, trunk, tail, or head[157]. In addition, many studies showed that TGF-β3 is an effective growth factor for inducing tenogenic differentiation of human BMSCs, and only a very low concentration is needed[146,156,157]. As discussed previously, BMSCs are a promising candidate cell source for tendon repair as they are readily available in the adult, and being autologous, are not limited by challenges with immunorejection.

For tendon tissue engineering, the scaffold candidate should desirably mimic the native tendon extracellular matrix (ECM) in structure and function. The scaffold should thus have anisotropic properties as native ECM, possess sufficient mechanical strength to support the healing tissue, and provide a favorable substrate for cell attachment, proliferation, and matrix deposition[137,145,146,155,159]. Our previous studies demonstrated that the highly aligned C-PCL nanofibers support the proliferation and differentiation of various anisotropically aligned cell types, including nerve and muscle cells[192,193]. Chitosan, a biodegradable natural polysaccharide derived by the partial deacetylation of chitin, shares structural similarities to glycosaminoglycans present in the native tendon ECM. PCL is a biocompatible polymer with excellent stability *in vivo*.[140] By combining chitosan with mechanically strong PCL, C-PCL nanofibers exhibit high stability, excellent mechanical properties, and good cellular compatibility[194]. More importantly, the aligned C-PCL nanofibers have an elastic modulus of 51.54 ± 9.54 MPa in the direction longitudinal to the fiber orientation[195]. which is comparable to the modulus of the flexor

digitorum profundus in the hand with typical modulus of 39.15 ± 9.98 MPa[196]. The C-PCL aligned nanofibers are a potential candidate material for tendon tissue engineering.

The tenogenic commitment of BMSCs on aligned C-PCL nanofibers was compared with those on tissue culture polystyrene (TCPS) as a material control, and with those on C-PCL film and randomly oriented C-PCL nanofibers of the same composition as topographical controls, in standard proliferation medium or differentiation medium containing TGF-B3. Tenogenic commitment was characterized via analysis of cell morphology, orientation, and gene and protein expressions over 10 days.

9.2 METHODS

9.2.1 Chitosan-poly-caprolactone material synthesis

Aligned and randomly oriented C-PCL nanofibers with 200-nm diameter and 2D films were fabricated using the methods developed previously in our lab[39]. Briefly, 5 wt% chitosan (85% deacetylated, medium molecular weight; Aldrich, St Louis, MO) solution in trifluoroacetic acid (TFA, Aldrich) was prepared by refluxing at 70°C for 3 hr, and a 10 wt% PCL solution was prepared by dissolving PCL (80,000 Da, Aldrich) in 2,2,2,-trifluoroethanol (TFE, Aldrich). Chitosan and PCL solutions were then mixed at a ratio of 40:60 by volume and vortexed to produce a working C-PCL solution. The solution was electrospun at 22 kV on a rotating grounded drum (200 rpm) or a pair of grounded parallel electrodes (4 cm, separation distance), to collect randomly oriented and aligned nanofibers, respectively. Dilute solutions of chitosan (1 wt%) and PCL (1.7 wt%) were mixed at the same ratio as that for producing C-PCL nanofibers, and the resultant solution was spin-casted to form 2D films. The collected nanofiber samples were attached to 10-mm diameter coverslips using poly (L, lactide) (Boehringer Ingelheim, Germany) dissolved in hexafluoroisopropanol (Aldrich) at 3.5 wt%. To remove residual acids from C-PCL, the samples were neutralized with 14% ammonium hydroxide for 5 min, followed

by rinsing with a copious amount of DI water. Prior to cell culture studies, the samples were sterilized by 70% ethanol.

9.2.2 Cell culture

Primary human BMSCs (Millipore) were expanded according to the manufacturer supplied protocols. BMSCs were seeded at 50,000 cells/cm^2 on each sample of tissue culture polystyrene (TCPS), C-PCL films, randomly oriented C-PCL nanofibers (C-PCL rand.), and aligned C-PCL nanofibers (C-PCL aligned). To induce tenogenic differentiation, mesenchymal stem cell expansion medium (standard medium) supplemented with 10 ng/ml TGF-β3 (R&D Systems) was prepared. BMSCs were cultured in either standard medium for proliferation (-TGF-β3 proliferation medium), or standard medium supplemented with 10 ng/ml TGF-β3 for differentiation induction (+TGF-β3 differentiation medium). The cell culture medium was refreshed every other day.

9.2.3 Morphological analysis

Cell–material samples were removed from medium, rinsed with PBS, and fixed in DMEM (Gibco) containing 2.5% glutaraldehyde (Sigma) overnight at 4^{o}C. After fixing, samples were rinsed three times with DI water and dehydrated with sequential incubation in 25%, 50%, 75%, 95%, and 100% ethanol for 10 min each. To assess the morphology, the samples were dried with a critical point dryer (Denton DCP-1, Cherry Hill, NJ), sputter-coated with Au/Pd for 80 s at 18 mA on an SPI sputter coater, and then imaged with a JEOL 7000F scanning electron microscope.

9.2.4 Orientation analysis

To determine BMSC orientation, images of aligned nanofiber samples were oriented horizontally. The angle of cell body relative to the horizontal axis was measured, with the value of 0º denoting parallel to the orientation of the aligned nanofibers, and 90º representing perpendicular to the nanofiber orientation.

9.2.5 Gene expression analysis

Cell-scaffold constructs were homogenized by vortexing and passing through QIAshredder columns (Qiagen). Total RNAs were isolated using RNeasy (Qiagen), and 30 ng of the total RNA for each sample was converted to cDNA using the iScript cDNA Synthesis Kit following the manufacturer's instruction (BioRad). iQ SYBR Green Supermix (BioRad) was used for template amplification with a primer for each of the transcripts examined. Thermocycling was performed at the following conditions: 95°C for 15 min, 45 cycles of denaturation (94°C, 15 s), annealing (55°C, 30 s), and extension (72°C, 30 s). The reaction was monitored in real time using a CFX96 (BioRad). The relative expression of each gene was normalized by β-actin (ACTA2) expression of each sample. The primers used are listed in Table 3.

Table 3: Tenogenesis PCR primers

Gene symbol	Forward Primer	Reverse Primer
β-actin (ACTA2)	5'- TCGCATCAAGGCCCAAGAAA	5'- CAGGATTCCCGTCTTAGTCCC
Scleraxis (SCXA)	5'- GAACACCCAGCCCAAACA	5'- CTGCGAATCGCTGTCTTTCT
Tenomodulin (TNMD)	5'- GATCCTGTGACCAGAACTGAAA	5'- CGAAGTAGATGCCAGTGTATCC
Collagen I (COL1A1)	5'- ACATGTTCAGCTTTGTGGACC	5'- CATGGTACCTGAGGCCGTTC
Collagen III (COL3A1)	5'- ATGTTGTGCAGTTTGCCCAC	5'- TCGTCCGGGTCTACCTGATT

9.2.6 Cell viability and protein expression imaging

To visualize viable BMSCs and Collagen I protein expression, samples were rinsed with PBS to remove culture medium. The samples were then incubated for 30 min in a solution of 10% FBS in PBS to block non-specific protein binding, and then conjugated with monoclonal mouse anti-Collagen I antibody (Abcam) at a 1:100 dilution in PBS with 1% bovine serum albumin (BSA, Sigma) for 1 hour at 37^{o}C. The samples were then incubated in a 1:500 dilution of Texas Red

conjugated rabbit anti-mouse secondary antibody (Abcam) in PBS for one hour at 37^{o}C. The samples were rinsed three times with PBS for after each step. Twenty minutes prior to imaging, fluorescein diacetae (FDA) was added to the PBS to a final concentration of 2 μg/ml. Samples were imaged on a Nikon upright fluorescent microscope with Texas Red and fluorescein filters. The percentage of Collagen I-positive cells/total viable cells was quantified from fluorescent images, with 50 nuclei counted per triplicate sample per condition.

9.2.7 Protein expression analysis

To quantify protein expression, BMSCs were detached from the material sample with Versene (Gibco) for 10 min at room temperature, counted with a hemocytometer, frozen at −80 °C, and lysed with RIPA buffer (Sigma). Cell lysate, which was equivalent to at least 100k cells, was resuspended in Laemmli buffer (BioRad), and spotted onto a PVDF membrane (BioRad). The membrane was probed with monoclonal mouse anti-Collagen I antibody (Abcam) at a 1:200 dilution in PBS, washed with PBS, labeled with alkaline phosphatase conjugated goat anti-mouse secondary antibody (BioRad) at 10 μg/ml in PBS, and visualized with Immun-Star alkaline phosphatase reagent (BioRad) on a ChemiDoc (BioRad). The relative intensity was measured with ImageJ to perform quantitative densitometric immunofluorescent analysis.

9.2.8 Statistical analysis

Acquired data are expressed as mean ± SD. Statistical significance was determined using one-way analysis of variance (ANOVA) and Student's *t*-test. Values of $p < 0.05$ were considered statistically significant.

9.3 RESULTS

9.3.1 Morphological analysis

Human primary BMSCs were seeded at the density of 50,000 cells/cm^2 on tissue culture polystyrene (TCPS), C-PCL films, randomly oriented C-PCL nanofibers (C-PCL Rand.), or aligned orientated C-PCL nanofibers (C-PCL Align.). BMSCs were cultured in either standard medium for proliferation (–TGF-β3 proliferation medium), or standard medium supplemented with 10 ng/ml TGF-β3for differentiation (+TGF-β3 differentiation medium).

The morphology of BMSCs cultured on various substrates scaffolds under different cell culture conditions was examined with SEM imaging. Significant differences in BMSC morphology were observed 24 hrs after cell seeding in different cell culture conditions (Figure 9-1). While cell density and degree of initial spreading were similar among all eight culture conditions tested, distinct responses to substrate topology were observed. On TCPS, C-PCL film, and C-PCL random materials, BMSCs oriented in random directions. Stellate morphology was observed on TCPS and C-PCL films in both -TGF-β3 proliferation medium and +TGF-β3 differentiation media. On both random and aligned nanofibers, fibroblast morphology was observed.

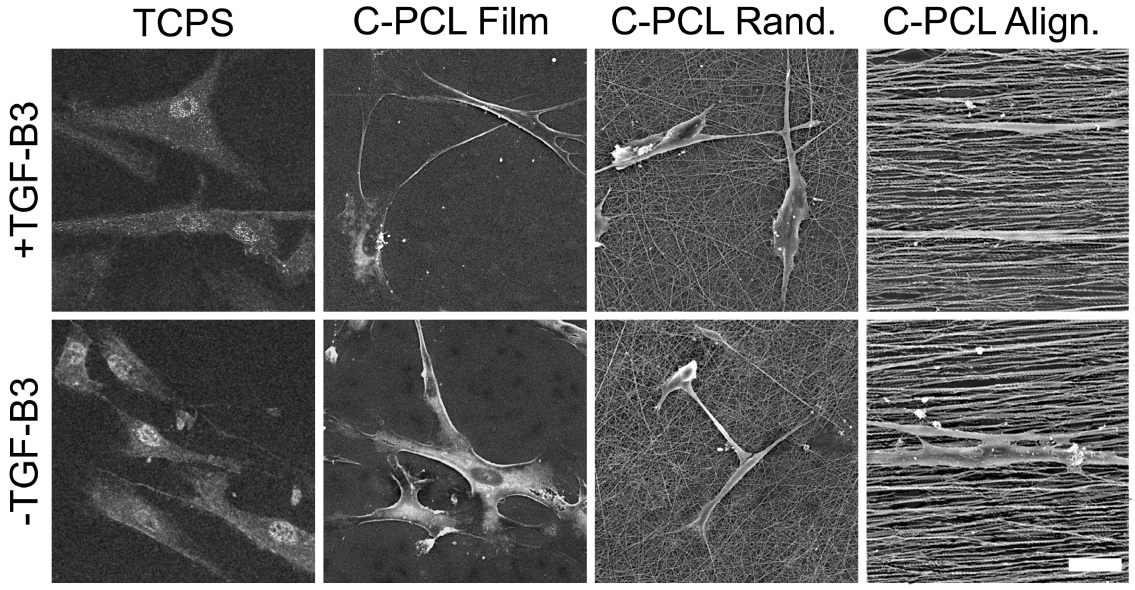

Figure 9-1: SEM images of BMSCs cultured for 24 hrs on TCPS, C-PCL films, C-PCL randomly oriented nanofibers (C-PCL Rand.) and C-PCL aligned nanofibers (C-PCL align.) in standard culture medium (bottom row) and +TGF-β3 differentiation medium (top row). Aligned C-PCL nanofibers (C-PCL Align.) are oriented horizontally in the images. Scale bar represent 25 μm.

The BMSCs had uniform adhesion and coverage on all the samples in all media tested after 5 days of cell culture (Figure 9-2). The number and size of BMSCs in all culture conditions increased over time during this period. Generally, for the same material substrate, the cell density was higher in -TGF-β3 proliferation medium than in +TGF-β3 differentiation medium. Specifically, when cultured on TCPS in either medium, BMSCs were observed to form a monolayer where BMSCs were parallel to each other, but with an overall random orientation across the entire surface. On C-PCL films, BMSCs were observed to form layers superimposed on top of each other, with local regional alignment similar to those observed on TCPS. On C-PCL random, BMSCs were observed to form multi-layered aggregates with no apparent cellular alignment. On C-PCL aligned, BMSCs formed a dense monolayer, with cells aligned parallel to the direction of the nanofiber orientation. After 10 days in culture, further increased cell density and cellular spreading were observed on TCPS, C-PCL film, and C-PCL random (Figure 9-3), as compared to cells cultured for 5 days. Comparing the cells on the same materials but in different culture media, the BMSC density was again greater in -TGF-β3 proliferation medium than in +TGF-β3 differentiation medium.

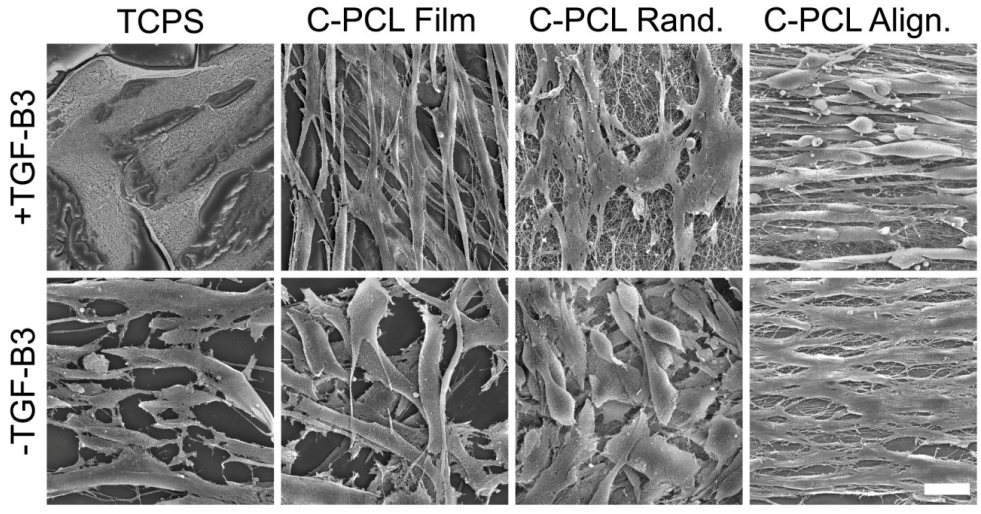

Figure 9-2: SEM images of BMSCs cultured for 5 days on TCPS, C-PCL films, C-PCL randomly oriented nanofibers (C-PCL Rand.) and C-PCL aligned nanofibers (C-PCL Align.) in standard culture medium (bottom row) and +TGF-β3 differentiation medium (top row). Aligned C-PCL nanofibers (C-PCL Align.) are oriented horizontally in the images. Scale bar represent 25 μm.

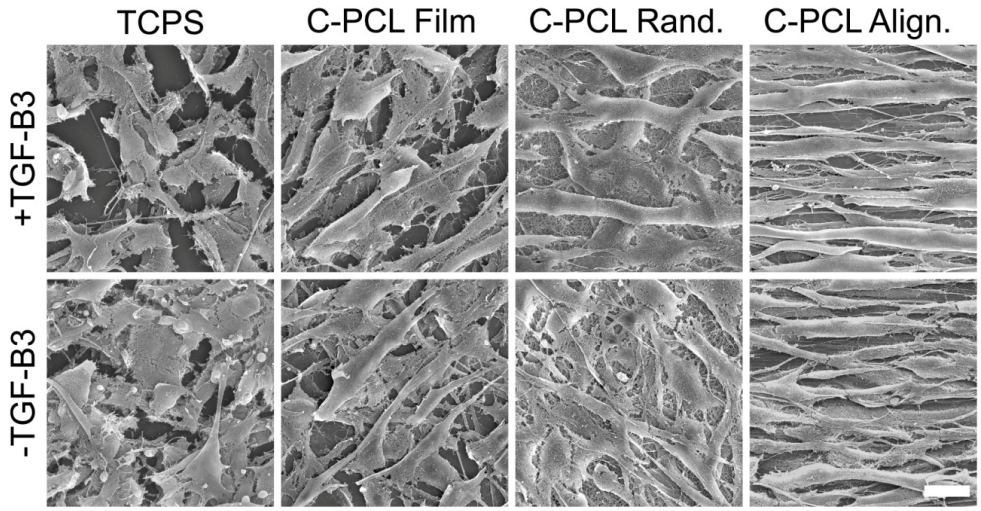

Figure 9-3: SEM images of BMSCs cultured for 10 days on TCPS, C-PCL films, C-PCL randomly-oriented nanofibers (C-PCL Rand.) and C-PCL aligned nanofibers (C-PCL Align.) in standard medium (bottom row) and +TGF-β3 differentiation medium (top row). Aligned C-PCL nanofibers (C-PCL Align.) are oriented horizontally in the images. Scale bar represent 25 μm.

9.3.2 Orientation analysis

To further determine if BMSCs can be directed by ECM topology as an environmental cue, cellular orientation was quantified through the analysis of SEM images. As BMSCs established a consistent cell shape and size after 5 days of culture in +TGF-β3 differentiation medium, imaging data from 5 and 10-day time points were analyzed (Figure 9-4). The orientation of each BMSC was assigned an angle value relative to the direction of aligned nanofibers. Quantitative morphometric analysis confirmed that the environmental role of nanofiber topology in directing BMSC orientation when cultured in +TGF-β3 differentiation medium (Figure 9-4). Long-range orientation of BMSCs along the aligned nanofibers was observed on C-PCL aligned after 5 days of culture (Figure 9-4, upper row), which was maintained at day 10 (Figure 9-4, lower row). In

contrast, no long-range order was observed for BMSCs cultured on TCPS, C-PCL film, or C-PCL random materials.

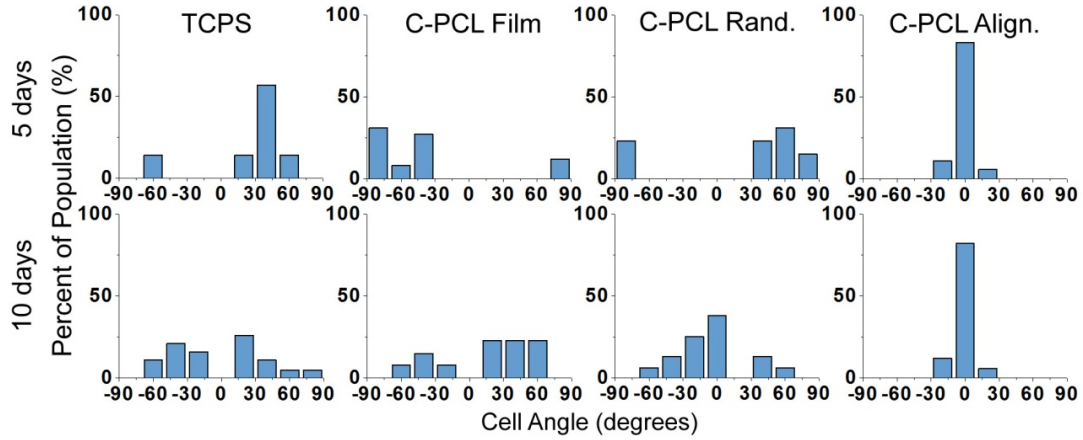

Figure 9-4: Quantitative morphometric analysis of BMSC orientation relative to samples after cultured in +TGF-β3 differentiation medium for 5 days (top row) and 10 days (bottom row) on TCPS, C-PCL films, C-PCL randomly oriented nanofibers, and C-PCL aligned nanofibers. Cells aligned horizontally were assigned a value of 0 degrees.

9.3.3 Gene expression analysis

To determine whether the tenogenic marker expressions were altered by the culture conditions, the mRNA expression of the cultured BMSCs were evaluated with real-time quantitative PCR after 5 and 10 days of cell culture. Tenogenic differentiation is regulated by the activity of scleraxis (SCXA)[151] and tenomodulin (TNMD),[197] while the COL1A1 gene for proteins Collagen I (a structural protein in mature tendon) and the COL3A gene for synthesis of Collagen III are highly regulated in differentiated tenocytes.[147,148,150] Scleraxis, a marker of tenogenic commitment,[198] is a regulatory protein induced during embryogenesis and the early formation of tendon tissues, and positively upregulates tenomodulin expression.[151] Tenomodulin is a marker for tendon proliferation and maturation,[197] and it is expressed in series after scleraxis *in vivo* in developing tendon tissues.[14,28] Collagens are the primary ECM proteins that comprise the tendon, with Collagen I composing the majority of total tendon mass, and approximately 95% of total protein mass.[145] Over-expression of both Collagens I and III are hallmarks of the early stages of tendon repair.[152]

The combination of environmental and biological cues had profound effects on BMSC gene expression profiles (Figure 9-5). Scleraxis was highly upregulated in both C-PCL random and C-PCL aligned regardless of TGF-β3 addition (Figure 9-5). Interestingly, tenomodulin, a downstream marker of tenogenic differentiation and maturation relative to scleraxis,[20, 3515,31] was strongly upregulated only on C-PCL random and C-PCL aligned in combination of TGF-β3 (Figure 9-5). Similarly, the expression of Collagen III, a structural protein in mature tendon, was increased after 10 days of cell culture only in the presence of both C-PCL aligned nanofibers and TGF-β3, compared to BMSCs on either TCPS or C-PCL films in any culture conditions. Therefore, while environmental cues alone can initiate tenogenic differentiation, the addition of growth factor TGF-β3 as biological cue may be necessary for tenocyte maturation. While increased Collagen III expression is associated with the wound healing response,[199,200] Collagen I constitutes 60% of the dry weight of native tendons, and is the essential protein for tendon function. After 10 days of cell culture, BMSCs cultured on C-PCL aligned in +TGF-β3 differentiation medium were observed to have greatest Collagen I transcription compared with all other culture conditions (Figure 9-5).

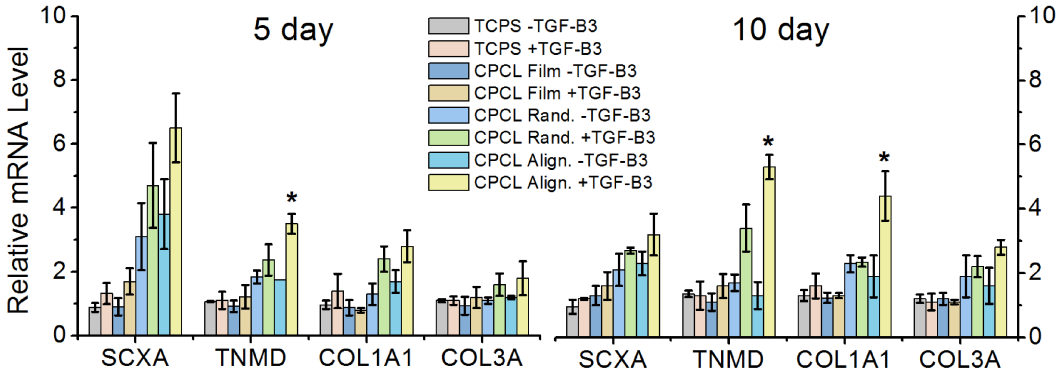

Figure 9-5: Gene expression of tenogenic markers assessed by real-time PCR after cells were cultured for 5 days (left) and 10 days (right) on various substrates in either standard culture medium (-TGF-β3) or +TGF-β3 differentiation medium (+TGF-β3). The values are presented as relative to the expression of BMSCs cultured for 1 day in standard proliferation conditions. Statistically significant values from others in the same group (*), are $p < 0.05$.

9.3.4 Protein expression analysis

To further verify tenogenic differentiation in tenogenic conditions, the protein expression profiles of cultured BMSCs were assessed by immunofluorescence staining. BMSCs were immunofluorescent-labeled for Collagen I and counter-stained for cell viability by fluorescein diacetae (FDA), which is metabolized into fluorescent green fluorescin by living cells only, and thus only viable cells are labeled green.[201] Cells were viable and well spread 24 hours after seeding, but the expression of Collagen I (yellow) was very limited for all culture conditions (Figure 9-6). The collagen I expression was well localized to viable BMSCs for all the culture conditions after cells were cultured for 5 days (Figure 9-7) and 10 days (Figure 9-8). Cell counting for Collagen I expressing cells as a percentage of total viable cells confirmed that the percentage of Collagen I expressing BMSCs increased most rapidly in +TGF-β3 differentiation medium on C-PCL aligned, with the greatest percentages of Collagen I expressing cells at both 5 days and 10 days versus all other culture conditions (Figure 9-9).

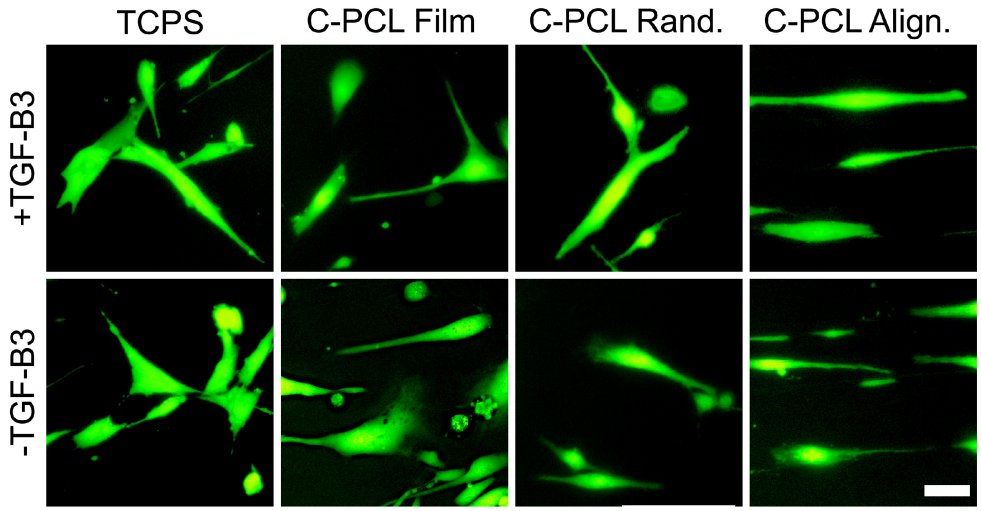

Figure 9-6: Fluorescence images of viable BMSCs cultured on various substrates in either standard culture medium (-TGF-β3) or +TGF-β3 differentiation medium (+TGF-β3) for 24 hrs, assessed by FDA staining (green) along with Collagen I expression determined by immunofluorescent staining (yellow). Aligned C-PCL nanofibers (C-PCL Align.) are oriented horizontally. The scale bar represents 25 μm.

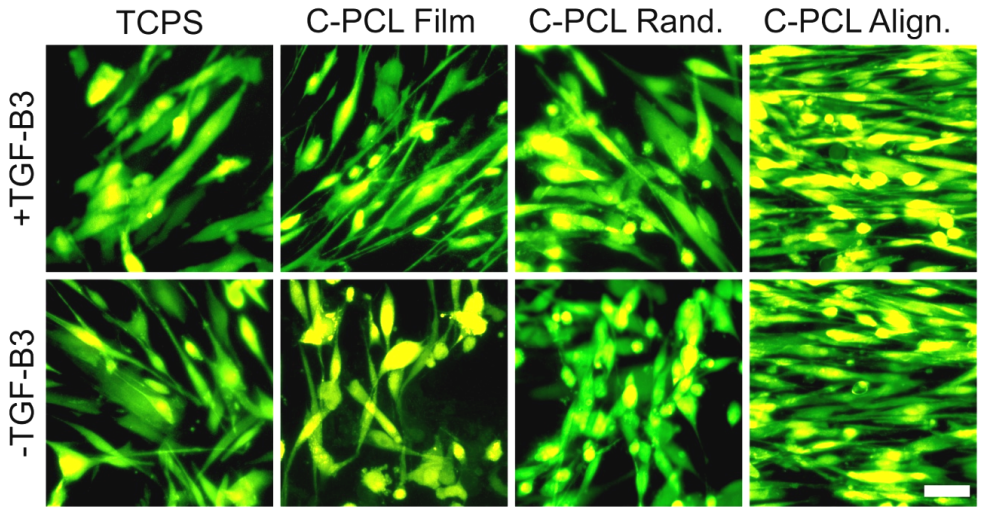

Figure 9-7: Fluorescence images of viable BMSCs cultured on various substrates in either standard culture medium (-TGF-β3) or +TGF-β3 differentiation medium (+TGF-β3) for 5 days, assessed by FDA staining (green) along with Collagen I expression determined by immunofluorescent staining (yellow). Aligned C-PCL nanofibers (C-PCL Align.) are oriented horizontally. The scale bar represents 25 μm.

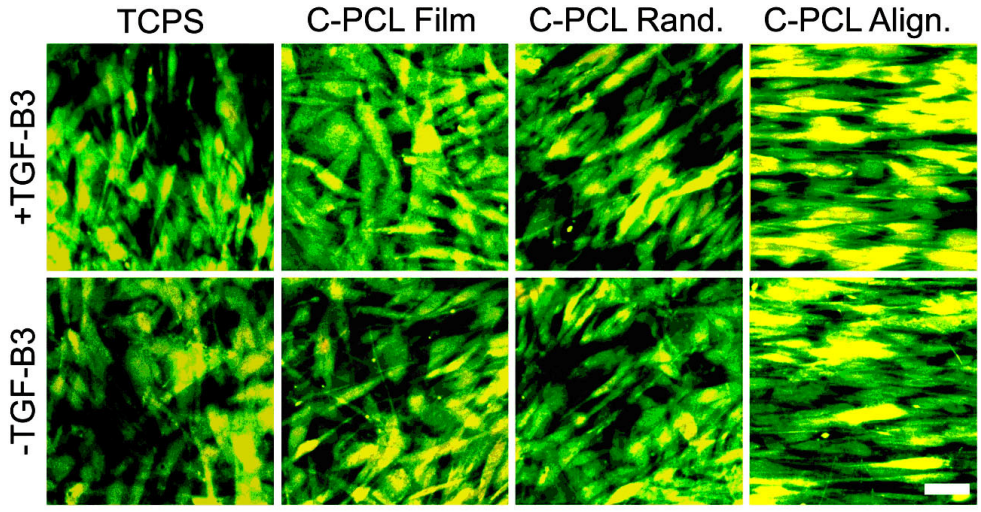

Figure 9-8: Fluorescence images of viable BMSCs cultured on various substrates in either standard culture medium (-TGF-β3) or +TGF-β3 differentiation medium (+TGF-β3) for 10 days, assessed by FDA staining (green) along with Collagen I expression determined by immnofluorescent staining (yellow). Aligned C-PCL nanofibers (C-PCL align.) are oriented horizontally. The scale bar represents 25 μm.

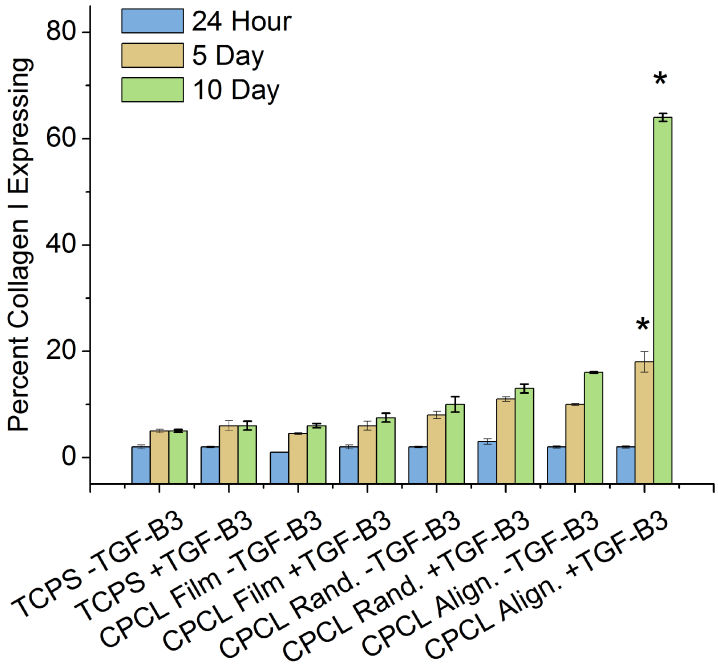

Figure 9-9: Collagen I positive cells as a percentage of total viable cells. BMSCs were cultured for either 24 hrs, 5 days, or 10 days on various substrates in either standard culture medium (-TGF-β3) or +TGF-β3 differentiation medium (+TGF-β3). Statistically significant values from others at the same timepoint (*) are $p < 0.05$.

Furthermore, dot blot analyses were performed to quantify the production of Collagen I. The result indicated that the combination of +TGF-β3 differentiation medium with either C-PCL random or C-PCL aligned induced significantly increased Collagen I production after 5 days of culture (Figure 9-10). After 10 days of cell culture, the amount of Collagen I produced was greatest in the combination of C-PCL aligned and +TGF-β3 differentiation medium among all the culture conditions tested, with a 4-fold increase compared to those in proliferation conditions.

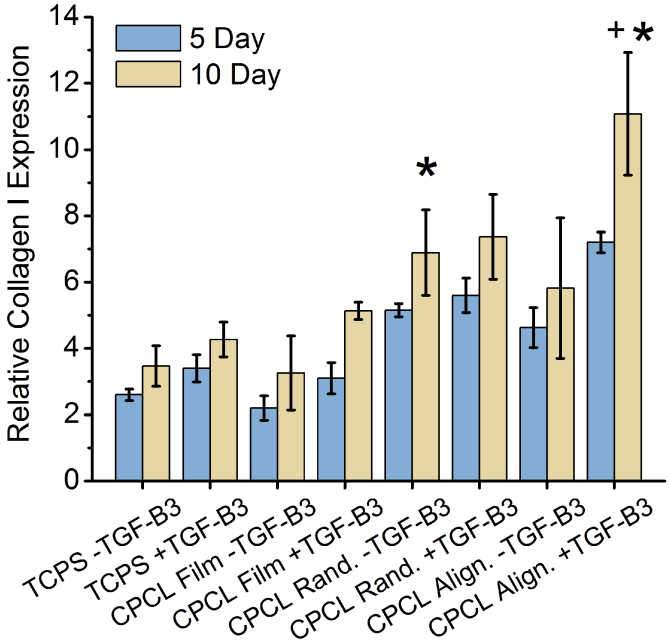

Figure 9-10: Collagen I expression determined by dot blot analysis after 5 and 10 days of cell culture. BMSCs were cultured on various substrates in either standard culture medium (-TGF-β3) or +TGF-β3 differentiation medium (+TGF-β3). The values are presented relative to the expression of BMSCs cultured for 1 day in standard proliferation conditions. Statistically significant values from others in the same group (*), or from all other values (+) are $p < 0.05$.

9.3.5 Discussion

Overall, significant differences in cell morphology were found between tested samples. For the same sample material, there was no significant difference in cell morphology between cells cultured in -TGF-β3 proliferation medium and +TGF-β3 differentiation medium. Significantly, when cultured on TCPS and C-PCL film in either medium, the BMSCs maintained a monolayer structure. On C-PCL random, the BMSCs exhibited increased spreading, with no local alignment similar to those observed on C-PCL films. On C-PCL aligned, the BMSCs morphology was similar to the cells cultured for 5 days, both maintaining a high level, uniform alignment along the nanofiber orientation. Notably, the *in vivo* tendon tissue is composed of tenocytes arranged in longitudinal rows along each collagen fascicle.[139] The C-PCL aligned material has induced an anatomically relevant cell morphology that the C-PCL 2D films and random nanofibers were not able to achieve after 5 days, highlighting the importance of the ECM nanotopology. When BMSCs were cultured on C-PCL aligned, cell–nanofiber interaction continued to be favored over

cell–cell attachment after 10 days of culture, and all BMSCs on C-PCL aligned spread out into a monolayer aligned parallel to the orientation of nanofibers. In contrast, BMSCs cultured on TCP, C-PCL films and C-PCL random formed overlapping cells layers without long-range organization. The C-PCL film and C-PCL random as material controls for the C-PCL aligned demonstrate the importance of nanotopology in addition to material properties. This result verified the importance of ECM topology in directing cell morphology.

The tenogenic differentiation efficiency of the cells on C-PCL aligned in +TGF-β3 differentiation medium is much higher than that reported in the literature.[22, 23, 25] For example, the mRNA expression of Collagen I of BMSCs cultured on CPCL aligned in bFGF differentiation medium increased five-fold at day 1 while BMSCs cells on Collagen I silk sponges with dynamic mechanical stimulation did not yield increased Collagen I mRNA expression until 14 days of culture, and increased scleraxis was observed at day 7 but decreased at day 14.[155] BMSCs on knitted PLGA silk fibers resulted in up-regulation of Collagen I mRNA at day 14 after induction of differentiation with bFGF by a factor of only 1.3 compared to day zero.[153] Additionally, the up-regulation of tenogenic markers including scleraxis were not observed,[153] indicating the lack of terminal tenogenic differentiation. BMSCs on braided poly(l-lactic acid) nanofibers in the presence of tenogenc growth factors and stimulated with cyclic tensile strain had 4.5-fold increase in scleraxis and no increase in Collagen I after 17 days of cell culture.[202] Therefore, while previous studies have demonstrated the expression of tenogenic markers, the combination of C-PCL nanofibers as an inductive ECM, with the soluble growth factor TGF-β3, induced high levels of expression of both key tenogenic markers, Collagen I and scleraxis.

The Collagen I protein translation confirms that the changes in mRNA expression induced by the culture conditions had translated directly into varying protein expression. A previous study that combined aligned fibers with soluble FGF-β for the tenogenic differentiation of BMSCs did not observe an increase in Collagen I production until 21 days of differentiation[153]. Comparatively, prior studies in tenogenic differentiation of BMSCs have demonstrated an increase in Collagen I mRNA expression after differentiation with exogenous TGF-β3 on 3D fibrin scaffolds at 7 days, but not an increase in Collagen I protein expression.[146] Taken together, gene and protein

expression results indicate that the aligned C-PCL nanofiber and TGF-β3 cell culture system can effectively differentiate BMSCs into tenocytes.

9.4 SUMMARY

We have established a bioengineering strategy to significantly enhance and accelerate the tenogenic differentiation of primary human BMSCs *in vitro* by using tissue-engineered tendon scaffolds composed of aligned C-PCL nanofibers in combination of exogenous TGF-β3. Morphological and orientation analysis of BMSCs revealed that the topology of ECM micro-environment is essential for determining the BMSC morphology and orientation. mRNA analysis of tenogenic differentiation markers indicated that C-PCL aligned nanofibers combined with TGF-β3 induced tenogenic differentiation into tenogenic lineage after 5 days of cell culture. Protein expression showed that when cultured on aligned C-PCL nanofiber with TGF-β3, BMSCs expressed significantly elevated Collagen I after 10 days of cell culture, compared to BMSCs cultured on TCP, C-PCL films, and random C-PCL nanofibers in either standard or differentiation medium. The speed of tenogenic differentiation from BMSCs is much greater than those achievable with existing scaffolds stimulated with growth factors or dynamic forces, which usually take weeks for tenogenic differentiation to occur. This study indicates that the combinative environmental and biological cues from aligned chitosan-poly-caprolactone nanofibers and TGF-β3 would provide synergistic effect to induce the tenogenic differentiation of BMSCs. The unique structural and biological properties of this culture system may provide an alternative approach to tendon repair.

Chapter 10: Conclusions

Three- and two-dimensional chitosan-based scaffolds and fiber matrices have been identified as generating cellular microenvironments capable of directing cell fate and function. We have demonstrated the use of 3D chitosan–alginate scaffolds for the maintenance of hESC pluripotency. Further, we have demonstrated that 2D chitosan–polycaprolactone nanofibers with unidirectional alignment provide a distinct set of ECM signaling cues that direct myogenic differentiation by hESCs, and tenogenic differentiation by BMSCs. Rational design strategies were applied to successfully generate cell culture microenvironments that elicited specific cellular responses. We have demonstrated potential tissue engineering applications of our 3D chitosan–alginate scaffolds and 2D chitosan–polycaprolactone nanofibers.

By culturing BG01v hESCs on 3D CA scaffolds in the presence of specific soluble factors, we maintained the pluripotency of the hESCs without the use of feeder cells or conditioned media. Both feeder cell contamination and the presence of undefined conditioned media are significant barriers to systematic studies of hESC behavior *in vitro* and would prevent the safe implantation of hESC *in vivo* and clinically. The elimination of both challenges with the culture method we developed represents a significant step forward in hESC culture technology. Additionally, the 3D microenvironment offered by the CA scaffold is fully biocompatible *in vivo*, and may be developed as a future device for hESC tissue engineering.

The myogenic differentiation of hESCs on 2D aligned C-PCL nanofibers was accomplished via the development of a novel differentiation media containing a defined combination of growth factors. To date, only limited success has been reported on the myogenic differentiation of hESCs, which may be a viable therapy for muscular degenerative diseases where the patient's native myogenic progenitor population is inadequate. Myogenic differentiation was accomplished with a higher efficiency and rate than previously reported from hESC, the result of combining both physical cues from the nanofibrous ECM, and soluble signaling factors. Future *in vivo* study of this muscle tissue construct in a skeletal muscle disease model is the necessary next step.

Adult BMSCs were differentiated into tenogenic cells on 2D aligned C-PCL nanofibers by developing a unique combination of nanotextured ECM and soluble signaling factors. This application addresses the specific lack of tendon grafts that combine high tenocyte cellularity with a scaffold material that recapitulates both the topology and mechanical properties of the native tendon tissue available in the clinical setting. The tissue engineered tendon graft expressed high levels of tendon specific markers including functional proteins, along with high cellularity and viability. Again, the significance of combinatorial signaling from the nanotopology of the ECM with specific soluble factors in directing differentiation was verified. The successful use of adult BMSCs in the generation of the tendon suggests the potential for tendon repair therapy using the patent's autologous progenitor cells. This tissue engineered tendon merits further *in vivo* study as a therapeutic method.

Each of the three applications developed here have significant potential for research and clinical treatment. The feeder-free maintenance of hESC with CA scaffolds may allow for the end of exogenous feeder cell contamination, along with providing a biocompatible 3D microenvironment suitable for differentiation into therapeutic progenitor cells and direct implantation into the patient. The rapid myogenic differentiation of hESC on 2D chitosan–polycaprolactone nanofibers paves the way for future scale-up into a muscle repair graft. Similarly, the tenogenic differentiation of BMSCs presents a highly promising alternative to current acellular tendon repair methodologies, by offering a personalized cellularized tendon graft for the patient. Overall, we have made significant discoveries into the combinatorial interactions of ECM topology with soluble growth factors in determining cell fate by determining that both factors are necessary for rapid and efficient cell differentiation.

References

1 Naderi, H., Matin, M. M. & Bahrami, A. R. Review Article: Critical issues in tissue engineering: biomaterials, cell sources, angiogenesis, and drug delivery systems. *Journal of Biomaterials Applications*, doi:10.1177/0885328211408946 (2011).

2 Cancedda, R., Giannoni, P. & Mastrogiacomo, M. A tissue engineering approach to bone repair in large animal models and in clinical practice. *biomaterials* **28**, 4240-4250, doi:10.1016/j.biomaterials.2007.06.023 (2007).

3 Kneser, U., Schaefer, D. J., Polykandriotis, E. & Horch, R. E. Tissue engineering of bone: the reconstructive surgeon's point of view. *Journal of Cellular and Molecular Medicine* **10**, 7-19, doi:10.1111/j.1582-4934.2006.tb00287.x (2006).

4 Ison, M. G. *et al.* Donor-Derived Disease Transmission Events in the United States: Data Reviewed by the OPTN/UNOS Disease Transmission Advisory Committee. *American Journal of Transplantation* **9**, 1929-1935, doi:10.1111/j.1600-6143.2009.02700.x (2009).

5 Israeli, M., Yussim, A., Mor, E., Sredni, B. & Klein, T. Preceeding the rejection: In search for a comprehensive post-transplant immune monitoring platform. *Transplant Immunology* **18**, 7-12, doi:10.1016/j.trim.2007.03.005 (2007).

6 Lutolf, M. P. & Hubbell, J. A. Synthetic biomaterials as instructive extracellular microenvironments for morphogenesis in tissue engineering. *Nat Biotech* **23**, 47-55 (2005).

7 Kim, I.-Y. *et al.* Chitosan and its derivatives for tissue engineering applications. *Biotechnology Advances* **26**, 1-21, doi:http://dx.doi.org/10.1016/j.biotechadv.2007.07.009 (2008).

8 Ripamonti, U., Roden, L., Ferretti, C. & Klar, R. Biomimetic matrices self-initiating the induction of bone formation. *J Craniofac Surg.* **22**, 1859-1870. (2011).

9 Seo, S. & Na, K. Mesenchymal stem cell-based tissue engineering for chondrogenesis. *J Biomed Biotechnol* **2011**, 806891. Epub 802011 Oct 806899. (2011).

10 Gott, M. *et al.* Tendon phenotype should dictate tissue engineering modality in tendon repair: a review. *Discov Med.* **12**, 75-84. (2011).

11 van der Veen, V. C., Boekema, B. K. H. L., Ulrich, M. M. W. & Middelkoop, E. New dermal substitutes. *Wound Repair and Regeneration* **19**, s59-s65, doi:10.1111/j.1524-475X.2011.00713.x (2011).

12 Takehara, N. & Matsubara, H. Cardiac regeneration therapy: connections to cardiac physiology. *Am J Physiol Heart Circ Physiol.* **301**, H2169-2180. Epub 2011 Sep 2130. (2011).

13 Critser, P. J., Voytik-Harbin, S. L. & Yoder, M. C. Isolating and defining cells to engineer human blood vessels. *Cell Proliferation* **44**, 15-21, doi:10.1111/j.1365-2184.2010.00719.x (2011).

14 Ghasemi-Mobarakeh, L. *et al.* Application of conductive polymers, scaffolds and electrical stimulation for nerve tissue engineering. *Journal of Tissue Engineering and Regenerative Medicine* **5**, e17-e35, doi:10.1002/term.383 (2011).

15 Williams, M. L., Kostrominova, T. Y., Arruda, E. M. & Larkin, L. M. Effect of implantation on engineered skeletal muscle constructs. *Journal of Tissue Engineering and Regenerative Medicine*, n/a-n/a, doi:10.1002/term.537 (2012).
16 Fukumitsu, K., Yagi, H. & Soto-Gutierrez, A. Bioengineering in Organ Transplantation: Targeting the Liver. *Transplantation proceedings* **43**, 2137-2138 (2011).
17 Smalley, K., Lioni, M. & Herlyn, M. Life isn't Flat: Taking Cancer Biology to the Next Dimension. *In Vitro Cell. Dev. BioL - Animal* **42**, 242-247 (2006).
18 Xu, F. & Burg, K. Three-dimensional polymeric systems for cancer cell studies. *Cytotechnology* **54**, 135-143 (2007).
19 Wu, L., Tang, Z.-Y. & Li, Y. Experimental models of hepatocellular carcinoma: developments and evolution. *Journal of Cancer Research and Clinical Oncology* **135**, 969-981 (2009).
20 Hirschhaeuser, F. *et al.* Multicellular tumor spheroids: An underestimated tool is catching up again. *Journal of Biotechnology* **In Press, Corrected Proof** (2010).
21 Godier, A. F. G. *et al.* Engineered microenvironments for human stem cells. *Birth Defects Research Part C: Embryo Today: Reviews* **84**, 335-347 (2008).
22 Huang, N. & Li, S. Regulation of the Matrix Microenvironment for Stem Cell Engineering and Regenerative Medicine. *Annals of Biomedical Engineering* **39**, 1201-1214, doi:10.1007/s10439-011-0297-2 (2011).
23 Kievit, F. M. *et al.* Chitosan-alginate 3D scaffolds as a mimic of the glioma tumor microenvironment. *Biomaterials* **31**, 5903-5910 (2010).
24 Leung, M. *et al.* Chitosan-alginate scaffold culture system for hepatocellular carcinoma increases malignancy and drug resistance. *Pharm Res* **27**, 1939-1948, doi:10.1007/s11095-010-0198-3 (2010).
25 Lund, A. W., Yener, B. l., Stegemann, J. P. & Plopper, G. E. The Natural and Engineered 3D Microenvironment as a Regulatory Cue During Stem Cell Fate Determination. *Tissue Engineering Part B: Reviews* **15**, 371-380, doi:doi:10.1089/ten.teb.2009.0270 (2009).
26 Tredan, O., Galmarini, C. M., Patel, K. & Tannock, I. F. Drug Resistance and the Solid Tumor Microenvironment. *J Natl Cancer Inst Monogr* **99**, 1441-1454, doi:10.1093/jnci/djm135 (2007).
27 Li, Z., Leung, M., Hopper, R., Ellenbogen, R. & Zhang, M. Feeder-free self-renewal of human embryonic stem cells in 3D porous natural polymer scaffolds. *Biomaterials* **31**, 404-412, doi:S0142-9612(09)01022-9 [pii] 10.1016/j.biomaterials.2009.09.070 (2010).
28 Higano, K., Takada, R., Ito, F., Takeichi, M. & Takada, S. Cytoskeletal reorganization by soluble Wnt-3a protein signalling. *Genes to Cells* **3**, 659-670 (1998).
29 Presta, M. *et al.* Fibroblast growth factor/fibroblast growth factor receptor system in angiogenesis. *Cytokine Growth Factor Rev* **16**, 159-178 (2005).
30 Brack, A. S., Conboy, I. M., Conboy, M. J., Shen, J. & Rando, T. A. A Temporal Switch from Notch to Wnt Signaling in Muscle Stem Cells Is Necessary for Normal Adult Myogenesis. *Cell Stem Cell* **2**, 50-59 (2008).
31 Portilho, D. M., Martins, E. R., Costa, M. L. & Mermelstein, C. S. A soluble and active form of Wnt-3a protein is involved in myogenic differentiation after cholesterol depletion. *FEBS Letters* **581**, 5787-5795 (2007).

32 Shang, Y.-c. *et al.* Wnt3a signaling promotes proliferation, myogenic differentiation, and migration of rat bone marrow mesenchymal stem cells. *Acta Pharmacol Sin* **28**, 1761-1774 (2007).

33 Tanaka, S., Terada, K. & Nohno, T. Canonical Wnt signaling is involved in switching from cell proliferation to myogenic differentiation of mouse myoblast cells. *J Mol Signal* **5**, 6-12 (2011).

34 Su, F.-C. Review: Roles of Microenvironment and Mechanical Forces in Cell and Tissue Remodeling. *Journal of Medical and Biological Engineering* **31**, 233, doi:10.5405/jmbe.944 (2011).

35 Li, Z., Ramay, H. R., Hauch, K. D., Xiao, D. & Zhang, M. Chitosan-alginate hybrid scaffolds for bone tissue engineering. *biomaterials* **26**, 3919-3928 (2005).

36 Li, Z. & Zhang, M. Chitosan-alginate as scaffolding material for cartilage tissue engineering. *J Biomed Mater Res A* **75**, 485-493 (2005).

37 Beier, J. *et al.* Collagen matrices from sponge to nano: new perspectives for tissue engineering of skeletal muscle. *BMC Biotechnology* **9**, 34 (2009).

38 Choi, J. S., Lee, S. J., Christ, G. J., Atala, A. & Yoo, J. J. The influence of electrospun aligned poly([var epsilon]-caprolactone)/collagen nanofiber meshes on the formation of self-aligned skeletal muscle myotubes. *Biomaterials* **29**, 2899-2906 (2008).

39 Cooper, A., Bhattarai, N. & Zhang, M. Fabrication and cellular compatibility of aligned chitosan-PCL fibers for nerve tissue regeneration. *Carbohydrate Polymers* **85**, 149-156, doi:DOI: 10.1016/j.carbpol.2011.02.008 (2011).

40 Cooper, A., Jana, S., Bhattarai, N. & Zhang, M. Aligned chitosan-based nanofibers for enhanced myogenesis. *Journal of Materials Chemistry* **20**, 8904-8911 (2010).

41 Lanfer, B. *et al.* The growth and differentiation of mesenchymal stem and progenitor cells cultured on aligned collagen matrices. *Biomaterials* **30**, 5950-5958 (2009).

42 Rosenthal, A., Macdonald, A. & Voldman, J. Cell patterning chip for controlling the stem cell microenvironment. *biomaterials* **28**, 3208-3216, doi:10.1016/j.biomaterials.2007.03.023 (2007).

43 Fischbach, C., Chen, R., Matsumoto, T. & al., e. Engineering Tumors with 3D Scaffolds. *Nat Med* **4**, 855-860 (2007).

44 Horning, J. L. *et al.* 3-D Tumor Model for In Vitro Evaluation of Anticancer Drugs. *Mol Pharm* **5**, 849-862, doi:10.1021/mp800047v (2008).

45 Griffith, L. G. & Swartz, M. A. Capturing complex 3D tissue physiology in vitro. *Nat Rev Mol Cell Biol* **7**, 211-224, doi:http://www.nature.com/nrm/journal/v7/n3/suppinfo/nrm1858_S1.html (2006).

46 Karande, T. S., Ong, J. L. & Agrawal, C. M. Diffusion in Musculoskeletal Tissue Engineering Scaffolds: Design Issues Related to Porosity, Permeability, Architecture, and Nutrient Mixing. *Annals of Biomedical Engineering* **32**, 1728-1743, doi:10.1007/s10439-004-7825-2 (2004).

47 Feng, B. *et al.* The effect of pore size on tissue ingrowth and neovascularization in porous bioceramics of controlled architecture in vivo. *Biomedical Materials* **6**, 015007 (2011).

48 Engler, A. J., Sen, S., Sweeney, H. L. & Discher, D. E. Matrix Elasticity Directs Stem Cell Lineage Specification. *Cell* **126**, 677-689 (2006).

49 Chen, S. S., Fitzgerald, W., Zimmerberg, J., Kleinman, H. K. & Margolis, L. Cell-Cell and Cell-Extracellular Matrix Interactions Regulate Embryonic Stem Cell Differentiation. *Stem Cells* **25**, 553-561, doi:10.1634/stemcells.2006-0419 (2007).

50 Baldrick, P. The safety of chitosan as a pharmaceutical excipient. *Regulatory Toxicology and Pharmacology* **56**, 290-299, doi:http://dx.doi.org/10.1016/j.yrtph.2009.09.015 (2010).

51 Yang, T.-L. Chitin-based Materials in Tissue Engineering: Applications in Soft Tissue and Epithelial Organ. *International Journal of Molecular Sciences* **12**, 1936-1963 (2011).

52 Hynes, R. O. The Extracellular Matrix: Not Just Pretty Fibrils. *Science* **326**, 1216-1219, doi:10.1126/science.1176009 (2009).

53 Muzzarelli, R. Human enzymatic activities related to the therapeutic administration of chitin derivatives. *Cell Mol Life Sci.* **53**, 131-140. (1997).

54 Azab, A. K. *et al.* Biocompatibility evaluation of crosslinked chitosan hydrogels after subcutaneous and intraperitoneal implantation in the rat. *Journal of Biomedical Materials Research - Part A* **83**, 414-422 (2007).

55 Tomihata, K. & Ikada, Y. In vitro and in vivo degradation of films of chitin and its deacetylated derivatives. *biomaterials* **18**, 567-575 (1997).

56 Onishi, H. & Machida, Y. Biodegradation and distribution of water-soluble chitosan in mice. *biomaterials* **20**, 175-182 (1999).

57 Gades, M. D. & Stern, J. S. Chitosan Supplementation and Fecal Fat Excretion in Men. *Obesity Research* **11**, 683-688, doi:10.1038/oby.2003.97 (2003).

58 Tapola, N. S., Lyyra, M. L., Kolehmainen, R. M., Sarkkinen, E. S. & Schauss, A. G. Safety Aspects and Cholesterol-Lowering Efficacy of Chitosan Tablets. *Journal of the American College of Nutrition* **27**, 22-30, doi:10.1080/07315724.2008.10719671 (2008).

59 Anderson, J. W., Nicolosi, R. J. & Borzelleca, J. F. Glucosamine effects in humans: A review of effects on glucose metabolism, side effects, safety considerations and efficacy. *Food and Chemical Toxicology* **43**, 187-201 (2005).

60 Zhang, J. *et al.* Chitosan Modification and Pharmaceutical/Biomedical Applications. *Marine Drugs* **8**, 1962-1987 (2010).

61 Sarmento, B. & das Neves, J. *Chitosan-Based Systems for Biopharmaceuticals: Delivery, Targeting and Polymer Therapeutics*. (Wiley, 2012).

62 Chan, B. P. & Leong, K. W. Scaffolding in tissue engineering: general approaches and tissue-specific considerations. *Eur Spine J* **17**, 467-479, doi:10.1007/s00586-008-0745-3 (2008).

63 Badylak, S. F. Xenogeneic extracellular matrix as a scaffold for tissue reconstruction. *Transplant Immunology* **12**, 367-377, doi:http://dx.doi.org/10.1016/j.trim.2003.12.016 (2004).

64 Hollister, S. J. Porous scaffold design for tissue engineering. *Nat Mater* **4**, 518-524 (2005).

65 Hu, J. *et al.* Visible light crosslinkable chitosan hydrogels for tissue engineering. *Acta Biomaterialia*, doi:10.1016/j.actbio.2012.01.029 (2012).

66 Lawrie, G. *et al.* Interactions between Alginate and Chitosan Biopolymers Characterized Using FTIR and XPS. *Biomacromolecules* **8**, 2533-2541, doi:10.1021/bm070014y (2007).

67 Berger, J., Reist, M., Mayer, J. M., Felt, O. & Gurny, R. Structure and interactions in chitosan hydrogels formed by complexation or aggregation for biomedical applications. *European Journal of Pharmaceutics and Biopharmaceutics* **57**, 35-52, doi:http://dx.doi.org/10.1016/S0939-6411(03)00160-7 (2004).

68 Peniche, C. & Argüelles-Monal, W. Chitosan based polyelectrolyte complexes. *Macromolecular Symposia* **168**, 103-116, doi:10.1002/1521-3900(200103)168:1<103::aid-masy103>3.0.co;2-k (2001).

69 Shin, S.-H., Purevdorj, O., Castano, O., Planell, J. A. & Kim, H.-W. A short review: Recent advances in electrospinning for bone tissue regeneration. *Journal of Tissue Engineering* **3**, doi:10.1177/2041731412443530 (2012).

70 Bhattarai, S. R. *et al.* Novel biodegradable electrospun membrane: scaffold for tissue engineering. *biomaterials* **25**, 2595-2602, doi:http://dx.doi.org/10.1016/j.biomaterials.2003.09.043 (2004).

71 Nisbet, D. R., Forsythe, J. S., Shen, W., Finkelstein, D. I. & Horne, M. K. Review Paper: A Review of the Cellular Response on Electrospun Nanofibers for Tissue Engineering. *Journal of Biomaterials Applications* **24**, 7-29, doi:10.1177/0885328208099086 (2009).

72 Vasita, R. & Katti, D. S. Nanofibers and their applications in tissue engineering. *Int J Nanomedicine* **1**, 15-30 (2006).

73 Pham, Q. P., Sharma, U. & Mikos, A. G. Electrospinning of polymeric nanofibers for tissue engineering applications: a. *Tissue Eng* **12**, 1197-1211 (2006).

74 Dahlin, R. F., Kasper, F. K. & Mikos, A. G. Polymeric nanofibers in tissue engineering. *Tissue Eng Part B Rev* **17**, 349-364 LID - 310.1089/ten.TEB.2011.0238 [doi] (2011).

75 Serrano, M. C. *et al.* In vitro biocompatibility assessment of poly(ε-caprolactone) films using L929 mouse fibroblasts. *biomaterials* **25**, 5603-5611, doi:10.1016/j.biomaterials.2004.01.037 (2004).

76 Choi, J. S., Lee, S. J., Christ, G. J., Atala, A. & Yoo, J. J. The influence of electrospun aligned poly(ε-caprolactone)/collagen nanofiber meshes on the formation of self-aligned skeletal muscle myotubes. *biomaterials* **29**, 2899-2906, doi:http://dx.doi.org/10.1016/j.biomaterials.2008.03.031 (2008).

77 Kim, M. S. *et al.* The Development of Genipin-Crosslinked Poly(caprolactone) (PCL)/Gelatin Nanofibers for Tissue Engineering Applications. *Macromolecular Bioscience* **10**, 91-100, doi:10.1002/mabi.200900168 (2010).

78 Bhattarai, N. *et al.* Natural-Synthetic Polyblend Nanofibers for Biomedical Applications. *Advanced materials* **21**, 2792-2797, doi:10.1002/adma.200802513 (2009).

79 Huang, Z.-M., Zhang, Y. Z., Kotaki, M. & Ramakrishna, S. A review on polymer nanofibers by electrospinning and their applications in nanocomposites. *Composites Science and Technology* **63**, 2223-2253, doi:http://dx.doi.org/10.1016/S0266-3538(03)00178-7 (2003).

80 Taylor, G. Electrically Driven Jets. *Proceedings of the Royal Society of London. A. Mathematical and Physical Sciences* **313**, 453-475, doi:10.1098/rspa.1969.0205 (1969).

81 Pham, Q. P., Sharma, U. & ikos, A. G. Electrospinning of polymeric nanofibers for tissue engineering applications: a. *Tissue Eng* **12**, 1197-1211 (2006).

82 Deitzel, J. M., Kleinmeyer, J. D., Hirvonen, J. K. & Beck Tan, N. C. Controlled deposition of electrospun poly(ethylene oxide) fibers. *Polymer* **42**, 8163-8170, doi:http://dx.doi.org/10.1016/S0032-3861(01)00336-6 (2001).

83 Barberi, T. *et al.* Derivation of engraftable skeletal myoblasts from human embryonic stem cells. *Nat Med* **13**, 642-648 (2007).

84 Barberi, T., Willis, L. M., Socci, N. D. & Studer, L. Derivation of multipotent mesenchymal precursors from human embryonic stem cells. *PLoS Med* **2**, e161 (2005).

85 Darabi, R. *et al.* Engraftment of embryonic stem cell-derived myogenic progenitors in a dominant model of muscular dystrophy. *Experimental Neurology* **220**, 212-216 (2009).
86 Zeng, X. *et al.* BG01V: a variant human embryonic stem cell line which exhibits rapid growth after passaging and reliable dopaminergic differentiation. *Restor Neurol Neurosci* **22**, 421-428 (2004).
87 Zeng, X. *et al.* Properties of Pluripotent Human Embryonic Stem Cells BG01 and BG02. *STEM CELLS* **22**, 292-312, doi:10.1634/stemcells.22-3-292 (2004).
88 Vazin, T. & Freed, W. J. Human embryonic stem cells: Derivation, culture, and differentiation: A review. *Restorative Neurology and Neuroscience* **28**, 589-603, doi:10.3233/rnn-2010-0543 (2010).
89 Thomson, J. A. *et al.* Embryonic Stem Cell Lines Derived from Human Blastocysts. *Science* **282**, 1145-1147, doi:10.1126/science.282.5391.1145 (1998).
90 Gruen, L. & Grabel, L. Concise Review: Scientific and Ethical Roadblocks to Human Embryonic Stem Cell Therapy. *Stem Cells* **24**, 2162-2169, doi:10.1634/stemcells.2006-0105 (2006).
91 Mountford, J. C. Human embryonic stem cells: origins, characteristics and potential for regenerative therapy. *Transfusion Medicine* **18**, 1-12, doi:10.1111/j.1365-3148.2007.00807.x (2008).
92 Klimanskaya, I., Chung, Y., Becker, S., Lu, S.-J. & Lanza, R. Human embryonic stem cell lines derived from single blastomeres. *Nature* **444**, 481-485, doi:http://www.nature.com/nature/journal/v444/n7118/suppinfo/nature05142_S1.html (2006).
93 Hardy, K., Martin, K. L., Leese, H. J., Winston, R. M. L. & Handyside, A. H. Human preimplantation development in vitro is not adversely affected by biopsy at the 8-cell stage. *Human Reproduction* **5**, 708-714 (1990).
94 Takahashi, K. *et al.* Induction of Pluripotent Stem Cells from Adult Human Fibroblasts by Defined Factors. *Cell* **131**, 861-872, doi:http://dx.doi.org/10.1016/j.cell.2007.11.019 (2007).
95 Pera, M. F. Stem cells: A new year and a new era. *Nature* **451**, 135-136 (2008).
96 Avery, S., Inniss, K. & Moore, H. The regulation of self-renewal in human embryonic stem cells. *Stem Cells and Development* **15**, 729-740, doi:10.1089/scd.2006.15.729 (2006).
97 Higuchi, A., Ling, Q.-D., Ko, Y.-A., Chang, Y. & Umezawa, A. Biomaterials for the Feeder-Free Culture of Human Embryonic Stem Cells and Induced Pluripotent Stem Cells. *Chemical Reviews* **111**, 3021-3035, doi:10.1021/cr1003612 (2011).
98 Mimeault, M., Hauke, R. & Batra, S. K. Stem Cells: A Revolution in Therapeutics[mdash]Recent Advances in Stem Cell Biology and Their Therapeutic Applications in Regenerative Medicine and Cancer Therapies. *Clin Pharmacol Ther* **82**, 252-264 (2007).
99 Ludwig, T. E. *et al.* Feeder-independent culture of human embryonic stem cells. *Nat Meth* **3**, 637-646 (2006).
100 Ludwig, T. E. *et al.* Derivation of human embryonic stem cells in defined conditions. *Nature biotechnology* **24**, 185-187 (2006).
101 Hoffman, L. M. & Carpenter, M. K. Characterization and culture of human embryonic stem cells. *Nature biotechnology* **23**, 699-708 (2005).

102 Dellatore, S. M., Garcia, A. S. & Miller, W. M. Mimicking stem cell niches to increase stem cell expansion. *Current Opinion in Biotechnology* **19**, 534-540 (2008).

103 Stacey, G. N. *et al.* The development of 'feeder' cells for the preparation of clinical grade hES cell lines: challenges and solutions. *J Biotechnol* **125**, 583-588 (2006).

104 Li, Y. J., Chung, E. H., Rodriguez, R. T., Firpo, M. T. & Healy, K. E. Hydrogels as artificial matrices for human embryonic stem cell self-renewal. *Journal of Biomedical Materials Research Part A* **79A**, 1-5, doi:10.1002/jbm.a.30732 (2006).

105 Bhattarai, N., Li, Z. S., Edmondson, D. & Zhang, M. Q. Alginate-based nanofibrous scaffolds: Structural, mechanical, and biological properties. *Advanced materials* **18**, 1463-+ (2006).

106 Peerani, R. *et al.* Niche-mediated control of human embryonic stem cell self-renewal and differentiation. *EMBO J* **26**, 4744-4755, doi:http://www.nature.com/emboj/journal/v26/n22/suppinfo/7601896a_S1.html (2007).

107 Lu, H. F. *et al.* A 3D microfibrous scaffold for long-term human pluripotent stem cell self-renewal under chemically defined conditions. *biomaterials* **33**, 2419-2430, doi:http://dx.doi.org/10.1016/j.biomaterials.2011.11.077 (2012).

108 Guilak, F. *et al.* Control of stem cell fate by physical interactions with the extracellular matrix. *Cell Stem Cell* **5**, 17-26, doi:S1934-5909(09)00293-8 [pii] 10.1016/j.stem.2009.06.016 (2009).

109 Klim, J. R., Li, L., Wrighton, P. J., Piekarczyk, M. S. & Kiessling, L. L. A defined glycosaminoglycan-binding substratum for human pluripotent stem cells. *Nature Methods* **7**, 989-994 (2010).

110 Gerecht, S. *et al.* Hyaluronic acid hydrogel for controlled self-renewal and differentiation of human embryonic stem cells. *Proceedings of the National Academy of Sciences of the United States of America* **104**, 11298-11303 (2007).

111 Ciciliot, S. & Schiaffino, S. Regeneration of Mammalian Skeletal Muscle. Basic Mechanisms and Clinical Implications. *Curr Pharm Des* **24**, 24 (2009).

112 Shadrach, J. L. & Wagers, A. J. Stem cells for skeletal muscle repair. *Philosophical Transactions of the Royal Society B: Biological Sciences* **366**, 2297-2306, doi:10.1098/rstb.2011.0027 (2011).

113 Chen, J. & Goldhamer, D. Skeletal muscle stem cells. *Reproductive Biology and Endocrinology* **1**, 101 (2003).

114 Burdzińska, A., Gala, K. & Pączek, L. Myogenic stem cells. *Folia Histochemica et Cytobiologica* **46**, 401-412 (2008).

115 Dang, J. M. & Leong, K. W. Myogenic Induction of Aligned Mesenchymal Stem Cell Sheets by Culture on Thermally Responsive Electrospun Nanofibers. *Adv Mater Deerfield* **19**, 2775-2779 (2007).

116 Hawke, T. J. & Garry, D. J. Myogenic satellite cells: physiology to molecular biology. *Journal of Applied Physiology* **91**, 534-551 (2001).

117 Ota, S. *et al.* Intramuscular Transplantation of Muscle-Derived Stem Cells Accelerates Skeletal Muscle Healing After Contusion Injury via Enhancement of Angiogenesis. *The American Journal of Sports Medicine* **39**, 1912-1922, doi:10.1177/0363546511415239 (2011).

118 Trounson, A. The production and directed differentiation of human embronic stem cells. *Endocrinology Review* **27**, 208-219 (2006).

119 Mizuno, Y. *et al.* Generation of skeletal muscle stem/progenitor cells from murine induced pluripotent stem cells. *FASEB J* **24**, 2245-2253, doi:fj.09-137174 [pii] 10.1096/fj.09-137174 (2010).
120 Darabi, R. *et al.* Functional skeletal muscle regeneration from differentiating embryonic stem cells. *Nat Med* **14**, 134-143 (2008).
121 Lagha, M. *et al.* Regulation of Skeletal Muscle Stem Cell Behavior by Pax3 and Pax7. *Cold Spring Harbor Symposia on Quantitative Biology* **73**, 307-315, doi:10.1101/sqb.2008.73.006 (2008).
122 Cutroneo, K. R. Comparison and evaluation of gene therapy and epigenetic approaches for wound healing. *Wound Repair and Regeneration* **8**, 494-502, doi:10.1046/j.1524-475x.2000.00494.x (2000).
123 Kennedy, K. A. *et al.* Retinoic acid enhances skeletal muscle progenitor formation and bypasses inhibition by bone morphogenetic protein 4 but not dominant negative beta-catenin. *BMC Biol* **7**, 67, doi:1741-7007-7-67 [pii]
10.1186/1741-7007-7-67 (2009).
124 Chang, H. *et al.* Generation of transplantable, functional satellite-like cells from mouse embryonic stem cells. *FASEB J* **23**, 1907-1919, doi:fj.08-123661 [pii]
10.1096/fj.08-123661 (2009).
125 Goudenege, S. *et al.* Myoblasts derived from normal hESCs and dystrophic hiPSCs efficiently fuse with existing muscle fibers following transplantation. *Mol Ther* **20**, 2153-2167, doi:mt2012188 [pii]
10.1038/mt.2012.188 (2012).
126 Kievit, F. M. *et al.* Chitosan-alginate 3D scaffolds as a mimic of the glioma tumor microenvironment. *Biomaterials* **31**, 5903-5910, doi:S0142-9612(10)00446-1 [pii]
10.1016/j.biomaterials.2010.03.062 (2010).
127 Chaudhuri, T., Rehfeldt, F., Sweeney, H. L. & Discher, D. E. in *Protocols for Adult Stem Cells* 185-202 (2010).
128 Zheng, J. K. *et al.* Skeletal myogenesis by human embryonic stem cells. *Cell Res* **16**, 713-722 (2006).
129 Lim, S., Mao, H. . Electrospun scaffolds for stem cell engineering. *Advanced Drug Delivery Reviews* **61**, 1084-1094 (2009).
130 Stern, M. M. *et al.* The influence of extracellular matrix derived from skeletal muscle tissue on the proliferation and differentiation of myogenic progenitor cells ex vivo. *Biomaterials* **30**, 2393-2399 (2009).
131 Riboldi, S. A. *et al.* Skeletal myogenesis on highly orientated microfibrous polyesterurethane scaffolds. *Journal of Biomedical Materials Research Part A* **84A**, 1094-1101 (2008).
132 Woodwell, D. A. & Cherry, D. K. National Ambulatory Medical Care Survey: 2002 summary. *Adv Data*, 1-44 (2004).
133 Wilson, J. J. & Best, T. M. Common overuse tendon problems: A review and recommendations for treatment. *Am Fam Physician* **72**, 811-818 (2005).
134 Chen, J. L. *et al.* Efficacy of hESC-MSCs in knitted silk-collagen scaffold for tendon tissue engineering and their roles. *biomaterials* **31**, 9438-9451, doi:S0142-9612(10)01017-3 [pii]
10.1016/j.biomaterials.2010.08.011 (2010).

135 Bi, Y. *et al.* Identification of tendon stem/progenitor cells and the role of the extracellular matrix in their niche. *Nat Med* **13**, 1219-1227, doi:nm1630 [pii] 10.1038/nm1630 (2007).
136 Longo, U. G., Lamberti, A., Maffulli, N. & Denaro, V. Tendon augmentation grafts: a systematic review. *British Medical Bulletin* **94**, 165-188, doi:10.1093/bmb/ldp051 (2010).
137 Sahoo, S., Toh, S. L. & Goh, J. C. A bFGF-releasing silk/PLGA-based biohybrid scaffold for ligament/tendon tissue engineering using mesenchymal progenitor cells. *biomaterials* **31**, 2990-2998, doi:S0142-9612(10)00005-0 [pii] 10.1016/j.biomaterials.2010.01.004 (2010).
138 Longo, U. G., Lamberti, A., Petrillo, S., Maffulli, N. & Denaro, V. Scaffolds in tendon tissue engineering. *Stem Cells Int* **2012**, 517165, doi:10.1155/2012/517165 (2012).
139 Benjamin, M., Kaiser, E. & Milz, S. Structure-function relationships in tendons: a review. *Journal of Anatomy* **212**, 211-228, doi:10.1111/j.1469-7580.2008.00864.x (2008).
140 Chen, J., Xu, J., Wang, A. & Zheng, M. Scaffolds for tendon and ligament repair: review of the efficacy of commercial products. *Expert Rev Med Devices* **6**, 61-73 (2009).
141 Thaker, H. & Sharma, A. K. Engaging stem cells for customized tendon regeneration. *Stem Cells Int* **2012**, 309187, doi:10.1155/2012/309187 (2012).
142 Docheva, D., Hunziker, E. B., Fässler, R. & Brandau, O. Tenomodulin Is Necessary for Tenocyte Proliferation and Tendon Maturation. *Molecular and Cellular Biology* **25**, 699-705, doi:10.1128/mcb.25.2.699-705.2005 (2005).
143 Bi, Y. *et al.* Identification of tendon stem/progenitor cells and the role of the extracellular matrix in their niche. *Nat Med* **13**, 1219-1227, doi:http://www.nature.com/nm/journal/v13/n10/suppinfo/nm1630_S1.html (2007).
144 Meligy, F. *et al.* The efficiency of in vitro isolation and myogenic differentiation of MSCs derived from adipose connective tissue, bone marrow, and skeletal muscle tissue. *In Vitro Cellular & Developmental Biology - Animal* **48**, 203-215, doi:10.1007/s11626-012-9488-x (2012).
145 Wang, J. H. C. Mechanobiology of tendon. *Journal of Biomechanics* **39**, 1563-1582, doi:http://dx.doi.org/10.1016/j.jbiomech.2005.05.011 (2006).
146 Kapacee, Z. *et al.* Synthesis of embryonic tendon-like tissue by human marrow stromal/mesenchymal stem cells requires a three-dimensional environment and transforming growth factor β3. *Matrix Biology* **29**, 668-677, doi:10.1016/j.matbio.2010.08.005 (2010).
147 Luo, Q. *et al.* Indirect co-culture with tenocytes promotes proliferation and mRNA expression of tendon/ligament related genes in rat bone marrow mesenchymal stem cells. *Cytotechnology* **61**, 1-10, doi:10.1007/s10616-009-9233-9 (2009).
148 Qiu, Y. *et al.* PEG-based hydrogels with tunable degradation characteristics to control delivery of marrow stromal cells for tendon overuse injuries. *Acta Biomaterialia* **7**, 959-966, doi:10.1016/j.actbio.2010.11.002 (2011).
149 Gulotta, L. V. *et al.* Application of Bone Marrow-Derived Mesenchymal Stem Cells in a Rotator Cuff Repair Model. *The American Journal of Sports Medicine* **37**, 2126-2133, doi:10.1177/0363546509339582 (2009).
150 Gurkan, U. A., Cheng, X., Kishore, V., Uquillas, J. A. & Akkus, O. Comparison of morphology, orientation, and migration of tendon derived fibroblasts and bone marrow

stromal cells on electrochemically aligned collagen constructs. *Journal of Biomedical Materials Research Part A* **9999A**, NA-NA, doi:10.1002/jbm.a.32783 (2010).

151 Shukunami, C., Takimoto, A., Oro, M. & Hiraki, Y. Scleraxis positively regulates the expression of tenomodulin, a differentiation marker of tenocytes. *Developmental Biology* **298**, 234-247, doi:10.1016/j.ydbio.2006.06.036 (2006).

152 Barber, J. G., Handorf, A. M., Allee, T. J. & Li, W.-J. Braided Nanofibrous Scaffold for Tendon and Ligament Tissue Engineering. *Tissue Engineering Part A*, 110906082646008, doi:10.1089/ten.tea.2010.0538 (2011).

153 Sahoo, S., Toh, S. L. & Goh, J. C. H. A bFGF-releasing silk/PLGA-based biohybrid scaffold for ligament/tendon tissue engineering using mesenchymal progenitor cells. *Biomaterials* **31**, 2990-2998, doi:10.1016/j.biomaterials.2010.01.004 (2010).

154 Caliari, S. R. & Harley, B. A. C. The effect of anisotropic collagen-GAG scaffolds and growth factor supplementation on tendon cell recruitment, alignment, and metabolic activity. *Biomaterials* **32**, 5330-5340, doi:10.1016/j.biomaterials.2011.04.021 (2011).

155 Chen, J. L. *et al.* Efficacy of hESC-MSCs in knitted silk-collagen scaffold for tendon tissue engineering and their roles. *Biomaterials* **31**, 9438-9451, doi:10.1016/j.biomaterials.2010.08.011 (2010).

156 Campbell, B. H., Agarwal, C. & Wang, J. H. C. TGF-ß1, TGF-ß3, and PGE; regulate contraction of human patellar tendon fibroblasts. *Biomechanics and Modeling in Mechanobiology* **2**, 239-245, doi:10.1007/s10237-004-0041-z (2004).

157 Pryce, B. A. *et al.* Recruitment and maintenance of tendon progenitors by TGF signaling are essential for tendon formation. *Development* **136**, 1351-1361, doi:10.1242/dev.027342 (2009).

158 Nerurkar, N. L., Sen, S., Baker, B. M., Elliott, D. M. & Mauck, R. L. Dynamic culture enhances stem cell infiltration and modulates extracellular matrix production on aligned electrospun nanofibrous scaffolds. *Acta Biomaterialia* **7**, 485-491, doi:10.1016/j.actbio.2010.08.011 (2011).

159 Yin, Z. *et al.* The regulation of tendon stem cell differentiation by the alignment of nanofibers. *Biomaterials* **31**, 2163-2175, doi:10.1016/j.biomaterials.2009.11.083 (2010).

160 Kerr, C. L., Hill, C. M., Blumenthal, P. D. & Gearhart, J. D. Expression of pluripotent stem cell markers in the human fetal ovary. *Hum. Reprod.* **23**, 589-599, doi:10.1093/humrep/dem411 (2008).

161 Dormeyer, W. *et al.* Plasma Membrane Proteomics of Human Embryonic Stem Cells and Human Embryonal Carcinoma Cells. *Journal of Proteome Research* **7**, 2936-2951 (2008).

162 Plaia, T. W. *et al.* Characterization of a new NIH-registered variant human embryonic stem cell Line, BG01V: A tool for human embryonic stem cell research. *Stem Cells* **24**, 531-546, doi:10.1634/stemcells.2005-0315 (2006).

163 Liu, N., Min Lu, Xuemei Tian & Zhongchao Han. Molecular mechanisms involved in self-renewal and pluripotency of embryonic stem cells. *Journal of Cellular Physiology* **211**, 279-286 (2007).

164 Rui Zhao & George Q. Daley. From fibroblasts to iPS cells: Induced pluripotency by defined factors. *Journal of Cellular Biochemistry* **105**, 949-955 (2008).

165 Ullmann, U. *et al.* Epithelial-mesenchymal transition process in human embryonic stem cells cultured in feeder-free conditions. *Mol Hum Reprod* **13**, 21-32 (2007).

166 Jiang, W. *et al.* In vitro derivation of functional insulin-producing cells from human embryonic stem cells. *Cell Res* **17**, 333-344 (2007).
167 Tamplin, O. *et al.* Microarray analysis of Foxa2 mutant mouse embryos reveals novel gene expression and inductive roles for the gastrula organizer and its derivatives. *BMC Genomics* **9**, 511 (2008).
168 Shiraki, N. *et al.* Differentiation of mouse and human embryonic stem cells into hepatic lineages. *Genes to Cells* **13**, 731-746 (2008).
169 Yang, M.-C. *et al.* The cardiomyogenic differentiation of rat mesenchymal stem cells on silk fibroin-polysaccharide cardiac patches in vitro. *biomaterials* **30**, 3757-3765 (2009).
170 Nelson, T. J. *et al.* CXCR4+/FLK-1+ Biomarkers Select a Cardiopoietic Lineage from Embryonic Stem Cells. *Stem Cells* **26**, 1464-1473 (2008).
171 Potta, S. P. *et al.* Functional Characterization and Transcriptome Analysis of Embryonic Stem Cell-Derived Contractile Smooth Muscle Cells. *Hypertension* **53**, 196-204, doi:10.1161/hypertensionaha.108.121863 (2009).
172 Freed, W. J. *et al.* Gene Expression Profile of Neuronal Progenitor Cells Derived from hESCs: Activation of Chromosome 11p15.5 and Comparison to Human Dopaminergic Neurons. *PLoS ONE* **3**, e1422 (2008).
173 Parmar, M. & Li, M. Early specification of dopaminergic phenotype during ES cell differentiation. *BMC Developmental Biology* **7**, 86 (2007).
174 Gharaibeh, B. *et al.* Biological approaches to improve skeletal muscle healing after injury and disease. *Birth Defects Research Part C: Embryo Today: Reviews* **96**, 82-94, doi:10.1002/bdrc.21005 (2012).
175 Rajan, N., Habermehl, J., Cote, M.-F., Doillon, C. J. & Mantovani, D. Preparation of ready-to-use, storable and reconstituted type I collagen from rat tail tendon for tissue engineering applications. *Nat. Protocols* **1**, 2753-2758 (2007).
176 Cerletti, M., Shadrach, J. L., Jurga, S., Sherwood, R. & Wagers, A. J. Regulation and Function of Skeletal Muscle Stem Cells. *Cold Spring Harbor Symposia on Quantitative Biology* **73**, 317-322, doi:10.1101/sqb.2008.73.054 (2008).
177 Ferri, P. *et al.* Expression and subcellular localization of myogenic regulatory factors during the differentiation of skeletal muscle C2C12 myoblasts. *Journal of Cellular Biochemistry* **108**, 1302-1317 (2009).
178 Ridgeway, A. G., Petropoulos, H., Wilton, S. & Skerjanc, I. S. Wnt Signaling Regulates the Function of MyoD and Myogenin. *Journal of Biological Chemistry* **275**, 32398-32405, doi:10.1074/jbc.M004349200 (2000).
179 Zhao, P. & Hoffman, E. P. Embryonic myogenesis pathways in muscle regeneration. *Developmental Dynamics* **229**, 380-392 (2004).
180 Buckingham, M. & Relaix, F. d. r. Vol. 23 645-673 (2007).
181 Ridgeway, A. G. & Skerjanc, I. S. Vol. 276 19033-19039 (2001).
182 Kennedy, K. *et al.* Retinoic acid enhances skeletal muscle progenitor formation and bypasses inhibition by bone morphogenetic protein 4 but not dominant negative beta-catenin. **7**, 67 (2009).
183 Mok, G. F. & Sweetman, D. Many routes to the same destination: lessons from skeletal muscle development. *Reproduction* **141**, 301-312, doi:10.1530/rep-10-0394 (2010).
184 Jin, G. P., Chang, Z. Y., Scholer, H. R. & Pei, D. Stem cell pluripotency and transcription factor Oct4. *Cell Res* **12**, 321-329 (2002).

185 Wang, X. & Dai, J. Concise Review: Isoforms of OCT4 Contribute to the Confusing Diversity in Stem Cell Biology. *STEM CELLS* **28**, 885-893, doi:10.1002/stem.419 (2010).
186 Le Grand, F., Jones, A. E., Seale, V., Scimè, A. & Rudnicki, M. A. Wnt7a Activates the Planar Cell Polarity Pathway to Drive the Symmetric Expansion of Satellite Stem Cells. *Cell Stem Cell* **4**, 535-547 (2009).
187 Ryan, T. *et al.* Retinoic Acid Enhances Skeletal Myogenesis in Human Embryonic Stem Cells by Expanding the Premyogenic Progenitor Population. *Stem Cell Reviews and Reports*, 1-12, doi:10.1007/s12015-011-9284-0 (2011).
188 Glowacki, J. & Mizuno, S. Collagen scaffolds for tissue engineering. *Biopolymers* **89**, 338-344, doi:10.1002/bip.20871 (2008).
189 Mauney, J. & Volloch, V. Collagen I matrix contributes to determination of adult human stem cell lineage via differential, structural conformation-specific elicitation of cellular stress response. *Matrix Biology* **28**, 251-262 (2009).
190 Li, Z., Leung, M., Hopper, R., Ellenbogen, R. & Zhang, M. Feeder-free self-renewal of human embryonic stem cells in 3D porous natural polymer scaffolds. *Biomaterials* **31**, 404-412, doi:10.1016/j.biomaterials.2009.09.070 (2010).
191 Lim, S. H. & Mao, H.-Q. Electrospun scaffolds for stem cell engineering. *Advanced Drug Delivery Reviews* **61**, 1084-1096, doi:10.1016/j.addr.2009.07.011 (2009).
192 Cooper, A., Jana, S., Bhattarai, N. & Zhang, M. Aligned chitosan-based nanofibers for enhanced myogenesis. *Journal of Materials Chemistry* (In press).
193 Cooper, A., Bhattarai, N. & Zhang, M. Fabrication and cellular compatibility of aligned chitosan–PCL fibers for nerve tissue regeneration. *Carbohydrate Polymers* **85**, 149-156, doi:10.1016/j.carbpol.2011.02.008 (2011).
194 Bhattarai, N. *et al.* Chitosan-based hydrogels for controlled, localized drug delivery. *Adv Drug Deliv Rev.* **21**, 2792-2797 (2010).
195 Cooper, A., Jana, S., Bhattarai, N. & Zhang, M. Aligned chitosan-based nanofibers for enhanced myogenesis. *Journal of Materials Chemistry* **20**, 8904, doi:10.1039/c0jm01841d (2010).
196 Ward, S. R., Loren, G. J., Lundberg, S. & Lieber, R. L. High Stiffness of Human Digital Flexor Tendons Is Suited for Precise Finger Positional Control. *Journal of Neurophysiology* **96**, 2815-2818, doi:10.1152/jn.00284.2006 (2006).
197 Docheva, D., Hunziker, E. B., Fassler, R. & Brandau, O. Tenomodulin Is Necessary for Tenocyte Proliferation and Tendon Maturation. *Molecular and Cellular Biology* **25**, 699-705, doi:10.1128/mcb.25.2.699-705.2005 (2005).
198 Chen, X. *et al.* Force and scleraxis synergistically promote the commitment of human ES cells derived MSCs to tenocytes. *Sci. Rep.* **2**, doi:http://www.nature.com/srep/2012/121214/srep00977/abs/srep00977.html#supplementary-information (2012).
199 Lui, P. P.-Y., Chan, L.-S., Lee, Y.-W., Fu, S. C. & Chan, K.-M. Sustained expression of proteoglycans and collagen type III/type I ratio in a calcified tendinopathy model. *Rheumatology* **49**, 231-239, doi:10.1093/rheumatology/kep384 (2010).
200 Dahlgren, L. A., Brower-Toland, B. D. & Nixon, A. J. Cloning and expression of type III collagen in normal and injured tendons of horses. *American Journal of Veterinary Research* **66**, 266-270, doi:10.2460/ajvr.2005.66.266 (2005).

201 Jones, K. H. & Senft, J. A. An improved method to determine cell viability by simultaneous staining with fluorescein diacetate-propidium iodide. *Journal of Histochemistry & Cytochemistry* **33**, 77-79, doi:10.1177/33.1.2578146 (1985).

202 Barber, J. G., Handorf, A. M., Allee, T. J. & Li, W. J. Braided Nanofibrous Scaffold for Tendon and Ligament Tissue Engineering. *Tissue Eng Part A*, doi:10.1089/ten.tea.2010.0538 (2011).

Appendix: Reprint Permissions

APPENDIX A

NATURE PUBLISHING GROUP LICENSE TERMS AND CONDITIONS

Aug 19, 2013

This is a License Agreement between Matthew Leung ("You") and Nature Publishing Group ("Nature Publishing Group") provided by Copyright Clearance Center ("CCC"). The license consists of your order details, the terms and conditions provided by Nature Publishing Group, and the payment terms and conditions.

All payments must be made in full to CCC. For payment instructions, please see information listed at the bottom of this form.

License Number	3212690336799
License date	Aug 19, 2013
Licensed content publisher	Nature Publishing Group
Licensed content publication	Nature Biotechnology
Licensed content title	Synthetic biomaterials as instructive extracellular microenvironments for morphogenesis in tissue engineering
Licensed content author	M P Lutolf and J A Hubbell
Licensed content date	Jan 6, 2005
Volume number	23
Issue number	1
Type of Use	reuse in a thesis/dissertation
Requestor type	academic/educational
Format	print and electronic
Portion	figures/tables/illustrations
Number of figures/tables/illustrations	1
High-res required	no
Figures	Figure 1: The behavior of individual cells and the dynamic state of multicellular tissues is regulated by intricate reciprocal molecular interactions between cells and their surroundings.
Author of this NPG article	no
Your reference number	Figure 1
Title of your thesis / dissertation	Chitosan Based Scaffolds for Stem Cell Renewal and Differentiation
Expected completion date	Aug 2013
Estimated size (number of pages)	130
Total	0.00 USD

Terms and Conditions

Terms and Conditions for Permissions

Nature Publishing Group hereby grants you a non-exclusive license to reproduce this material for this purpose, and for no other use,subject to the conditions below:

1. NPG warrants that it has, to the best of its knowledge, the rights to license reuse of this material. However, you should ensure that the material you are requesting is original to Nature Publishing Group and does not carry the copyright of another entity (as credited in the published version). If the credit line on any part of the material you have requested indicates that it was reprinted or adapted by NPG with permission from another source, then you should also seek permission from that source to reuse the material.

2. Permission granted free of charge for material in print is also usually granted for any electronic version of that work, provided that the material is incidental to the work as a whole and that the electronic version is essentially equivalent to, or substitutes for, the print version.Where print permission has been granted for a fee, separate permission must be obtained for any additional, electronic re-use (unless, as in the case of a full paper, this has already been accounted for during your initial request in the calculation of a print run).NB: In all cases, web-based use of full-text articles must be authorized separately through the 'Use on a Web Site' option when requesting permission.

3. Permission granted for a first edition does not apply to second and subsequent editions and for editions in other languages (except for signatories to the STM Permissions Guidelines, or where the first edition permission was granted for free).

4. Nature Publishing Group's permission must be acknowledged next to the figure, table or abstract in print. In electronic form, this acknowledgement must be visible at the same time as the figure/table/abstract, and must be hyperlinked to the journal's homepage.

5. The credit line should read:
   Reprinted by permission from Macmillan Publishers Ltd: [JOURNAL NAME] (reference citation), copyright (year of publication)
   For AOP papers, the credit line should read:
   Reprinted by permission from Macmillan Publishers Ltd: [JOURNAL NAME], advance online publication, day month year (doi: 10.1038/sj.[JOURNAL ACRONYM].XXXXX)

   Note: For republication from the *British Journal of Cancer*, the following credit lines apply.
   Reprinted by permission from Macmillan Publishers Ltd on behalf of Cancer Research UK: [JOURNAL NAME] (reference citation), copyright (year of publication)For AOP papers, the credit line should read:
   Reprinted by permission from Macmillan Publishers Ltd on behalf of Cancer Research UK: [JOURNAL NAME], advance online publication, day month year (doi: 10.1038/sj.[JOURNAL ACRONYM].XXXXX)

6. Adaptations of single figures do not require NPG approval. However, the adaptation should be credited as follows:

   Adapted by permission from Macmillan Publishers Ltd: [JOURNAL NAME] (reference citation), copyright (year of publication)

   Note: For adaptation from the *British Journal of Cancer*, the following credit line applies.
   Adapted by permission from Macmillan Publishers Ltd on behalf of Cancer Research UK: [JOURNAL NAME] (reference citation), copyright (year of publication)

7. Translations of 401 words up to a whole article require NPG approval. Please visit http://www.macmillanmedicalcommunications.com for more information.Translations of up to a 400 words do not require NPG approval. The translation should be credited as follows:

   Translated by permission from Macmillan Publishers Ltd: [JOURNAL NAME] (reference citation), copyright (year of publication).

   Note: For translation from the *British Journal of Cancer*, the following credit line applies.
   Translated by permission from Macmillan Publishers Ltd on behalf of Cancer Research UK: [JOURNAL NAME] (reference citation), copyright (year of publication)

We are certain that all parties will benefit from this agreement and wish you the best in the use of this material. Thank you.

Special Terms:

v1.1

If you would like to pay for this license now, please remit this license along with your payment made payable to "COPYRIGHT CLEARANCE CENTER" otherwise you will be invoiced within 48 hours of the license date. Payment should be in the form of a check or money order referencing your account number and this invoice number RLNK501093704. Once you receive your invoice for this order, you may pay your invoice by credit card. Please follow instructions provided at that time.

Make Payment To:
Copyright Clearance Center
Dept 001
P.O. Box 843006
Boston, MA 02284-3006

For suggestions or comments regarding this order, contact RightsLink Customer Support: customercare@copyright.com or +1-877-622-5543 (toll free in the US) or +1-978-646-2777.

Gratis licenses (referencing $0 in the Total field) are free. Please retain this printable license for your reference. No payment is required.

APPENDIX B

MDPI OPEN ACCESS

Title / Keyword Journal all Volume
Author Section — Issue Clear
Article Type all Special Issue — Page Search

MDPI Open Access Information and Policy

All articles published by MDPI are made immediately available worldwide under an open access license. This means:

everyone has free and unlimited access to the full-text of all articles published in MDPI journals, and
everyone is free to re-use the published material if proper accreditation/citation of the original publication is given.
open access publication is supported by the authors' institutes or research funding agencies by payment of a comparatively low Article Processing Charge (APC) for accepted articles.

External Open Access Resources

MDPI is a RoMEO green publisher — RoMEO is a database of Publishers' copyright and self-archiving policies hosted by the University of Nottingham

Those who are new to the concept of open access might find the following websites or 'Open Access 101' video informative:

Wikipedia article on 'Open Access'
Peter Suber's 'Open Access Overview'
Information Platform Open Access [in English, in German]
SHERPA's 'Authors and Open Access'

Meaning of Open Access

In accordance with major definitions of open access in scientific literature (namely the Budapest, Berlin, and Bethesda declarations), MDPI defines *open access* by the following conditions:

- peer-reviewed literature is freely available without subscription or price barriers,
- literature is immediately released in open access format (no embargo period), and
- published material can be re-used without obtaining permission as long as a correct citation to the original publication is given.

Until 2008, most articles published by MDPI contained the note: "© *year* by MDPI (http://www.mdpi.org). Reproduction is permitted for noncommercial purposes". During 2008, MDPI journals started to publish articles under the Creative Commons Attribution License. All articles published by MDPI before and during 2008 should now be considered as having been released under the post-2008 Creative Commons Attribution License.

SPARC Open Access 101 Video

This means that all articles published in MDPI journals, including data, graphics, and supplements, can be linked from external sources, scanned by search engines, re-used by text mining applications or websites, blogs, *etc.* free of charge under the sole condition of proper accreditation of the source and original publisher. MDPI believes that open access publishing fosters the exchange of research results amongst scientists from different disciplines, thus facilitating interdisciplinary research. Open access publishing also provides access to research results to researchers worldwide, including those from developing countries, and to an interested general public. Although MDPI publishes all of its journals under the open access model, we believe that open access is an enriching part of the scholarly communication process that can and should co-exist with other forms of communication and publication, such as society-based publishing and conferencing activities.

Important Note: some articles (especially *Reviews*) may contain figures, tables or text taken from other publications, for which MDPI does not hold the copyright or the right to re-license the published material. Please note that you should inquire with the original copyright holder (usually the original publisher or authors), whether or not this material can be re-used.

Advantages of Open Access for Authors

The High Availability and Visibility of our open access articles is guaranteed through the free and unlimited accessibility of the publication over the Internet. Everyone can freely access and download the full text of all articles published with MDPI: readers of open access journals, *i.e.*, mostly other researchers, do not need to pay any subscription or pay-per-view charges to read articles published by MDPI. Open access publications are also more likely to be included in search engines and indexing databases.

The Higher Citation Impact of open access articles results from their high publicity and availability. Open access publications are demonstrably more frequently cited [1,2].

Lower Publishing Costs: Open access publishers cover their costs for editorial handling and editing of a paper by charging authors' institutes or research funding agencies. The cost of handling and producing an article is covered through the one-time payment of an article processing charge (APC) for each accepted article. The APCs of open access publishers are only a fraction of the average income per paper earned by traditional, subscription-based publishers. MDPI's article processing charge (APC) is the same, irrespective of article length, because we wish to encourage publication of long papers with complete results and full experimental or computational details [3].

Faster Publication in MDPI's open access journals is achieved by online-only availability. Accepted articles are typically published online more rapidly in MDPI journals than those of traditional, subscription-based and printed journals are [4].

Links and Notes

1. Open access citation impact advantage: http://en.wikipedia.org/wiki/Open_access#Authors_and_researchers. For example, a standard research paper "Shutalev, A.D.; Kishko, E.A.; Sivova, N.V.; Kuznetsov, A.Y. *Molecules* **1998**, *3*, 100-106" has been cited 51 times, the highest number among all the papers published so far by the same author.
2. Lin, S.-K. *Editorial:* Non-Open Access and Its Adverse Impact on Molecules. *Molecules* **2007**, *12*, 1436-1437 (PDF format 16 K, HTML format).
3. Recently a research paper of 30 pages has been published: *Molecules* **2008**, *13*(5), 1081-1110.
4. Some well written papers have been peer reviewed and published in less than two weeks from manuscript submission, see e.g.: *Molecules* **2006**, *11*(4),

APPENDIX C

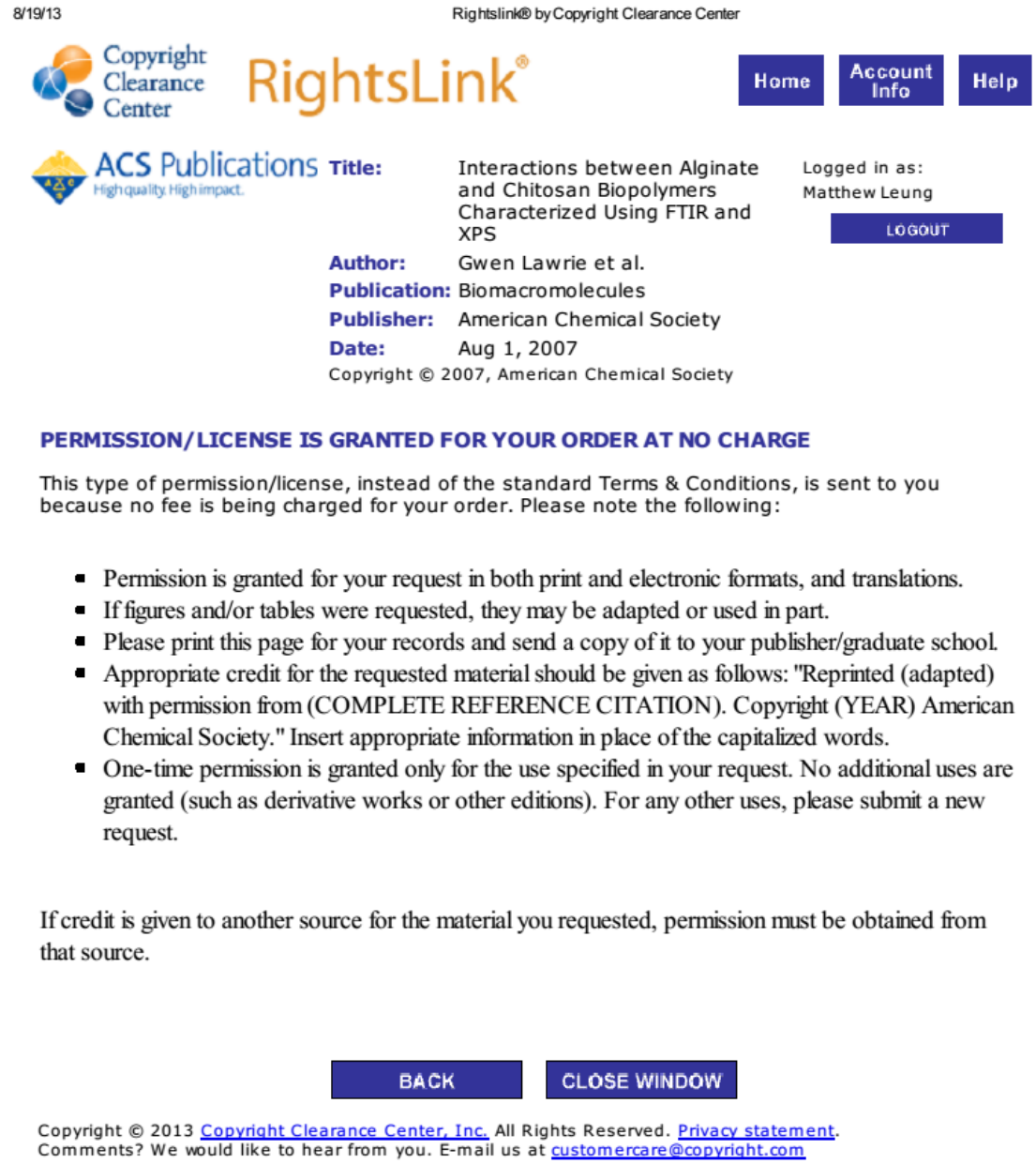

8/19/13 Rightslink® by Copyright Clearance Center

Copyright Clearance Center RightsLink®

Home | Account Info | Help

ACS Publications High quality. High impact.

Title: Interactions between Alginate and Chitosan Biopolymers Characterized Using FTIR and XPS

Logged in as: Matthew Leung

LOGOUT

Author: Gwen Lawrie et al.
Publication: Biomacromolecules
Publisher: American Chemical Society
Date: Aug 1, 2007
Copyright © 2007, American Chemical Society

PERMISSION/LICENSE IS GRANTED FOR YOUR ORDER AT NO CHARGE

This type of permission/license, instead of the standard Terms & Conditions, is sent to you because no fee is being charged for your order. Please note the following:

- Permission is granted for your request in both print and electronic formats, and translations.
- If figures and/or tables were requested, they may be adapted or used in part.
- Please print this page for your records and send a copy of it to your publisher/graduate school.
- Appropriate credit for the requested material should be given as follows: "Reprinted (adapted) with permission from (COMPLETE REFERENCE CITATION). Copyright (YEAR) American Chemical Society." Insert appropriate information in place of the capitalized words.
- One-time permission is granted only for the use specified in your request. No additional uses are granted (such as derivative works or other editions). For any other uses, please submit a new request.

If credit is given to another source for the material you requested, permission must be obtained from that source.

BACK | CLOSE WINDOW

Copyright © 2013 Copyright Clearance Center, Inc. All Rights Reserved. Privacy statement.
Comments? We would like to hear from you. E-mail us at customercare@copyright.com

APPENDIX D

J Tissue Eng. 2012; 3(1): 2041731412443530. PMCID: PMC3324843
Published online 2012 April
4. doi: 10.1177/2041731412443530

A short review: Recent advances in electrospinning for bone tissue regeneration

Song-Hee Shin,[1,2] Odnoo Purevdorj,[1,2] Oscar Castano,[3,4] Josep A Planell,[3,4,5] and Hae-Won Kim[1,2,6]

[1]Institute of Tissue Regeneration Engineering (ITREN), Dankook University, Cheonan, South Korea
[2]Department of Nanobiomedical Science and WCU Research Center, Dankook University, Cheonan, South Korea
[3]Biomaterials for Regenerative Therapies, Institute for Bioengineering of Catalonia (IBEC), Barcelona, Spain
[4]Centro de Investigación Biomédica en Red en Bioingeniería, Biomateriales y Nanomedicina (CIBER-BBN), Zaragoza, Spain
[5]Technical University of Catalonia (UPC), Barcelona, Spain
[6]Department of Biomaterials Science, School of Dentistry, Dankook University, Cheonan, South Korea
Corresponding author.
Hae-Won Kim Institute of Tissue Regeneration Engineering (ITREN) Dankook University Cheonan 330-714 South Korea
Email: kimhw@dku.edu

Author information ▼ Copyright and License information ▼

Abstract

Go to:

Nanofibrous structures developed by electrospinning technology provide attractive extracellular matrix conditions for the anchorage, migration, and differentiation of tissue cells, including those responsible for the regeneration of hard tissues. Together with the ease of set up and cost-effectiveness, the possibility to produce nanofibers with a wide range of compositions and morphologies is the merit of electrospinning. Significant efforts have exploited the development of bone regenerative nanofibers, which includes tailoring of composite/hybrid compositions that are bone mimicking and the surface functionalization such as mineralization. Moreover, by utilizing bioactive molecules such as adhesive proteins, growth factors, and chemical drugs, in concert with the nanofibrous matrices, it is possible to provide artificial materials with improved cellular responses and therapeutic efficacy. These studies have mainly focused on the regulation of stem cell behaviors for use in regenerative medicine and tissue engineering. While there are some challenges in achieving controllable delivery of bioactive molecules and complex-shaped three-dimensional scaffolds for tissue engineering, the electrospun nanofibrous matrices can still have a beneficial impact in the area of hard-tissue regeneration.

Keywords: Electrospinning, hard-tissue regeneration, composites, drug delivery, stem cells

APPENDIX E